CELLULAR AND MOLECULAR STUDIES OF *MYCOPLASMA PNEUMONIAE* ADHERENCE AND GLIDING MOTILITY

by

JARRAT LANCE JORDAN

(Under the Direction of DUNCAN CHARLES KRAUSE)

ABSTRACT

Mycoplasmas are cell wall-less prokaryotes considered to be among the simplest known microorganisms capable of self-replication. Several mycoplasma species are distinguished by the presence of a complex assemblage of proteins comprising a differentiated terminal organelle containing a Triton X-100 insoluble electron-dense core. This terminal organelle is an extension of the mycoplasma cell and is thought to function in cell division, host cell interactions, and gliding motility. Through mutant analysis, several proteins have been found to be required for cytadherence and are components of the terminal organelle including HMW1-HMW3, P1, B, C, and P30. Protein P30 consists of a predicted signal sequence, cytoplasmic domain, membrane-spanning region, and extracellular proline-rich C-terminal domain. Protein P65 localizes to the terminal organelle, yet its role in cytadherence is unknown as no mutant lacking only P65 has been reported. Upon analysis of previously isolated cytadherence mutants and P30 structure-function constructs created here and expressed in a P30 null mutant, we found that HMW1-HMW3, and P30 are required for P65 stability and in the case of P30, stabilization was mediated by the surface-exposed and not cytoplasmic domain. In contrast, P65 localization only required HMW1-HMW3 and not P30. We examined gliding motility of *M. pneumoniae* using two assays we developed and found that cytadherence mutants absent of electron-dense cores (HMW1-HMW2) were incapable of motility. Of the strains possessing electron-dense cores an intermediate level of gliding was seen in the absence of HMW3, and in strains having certain defects in the surface-exposed domain of P30. Despite the presence of electron-dense cores, no motility was seen in the absence of proteins B and C and in certain P30 mutants. P30 stability was most affected by deletion of a highly conserved region in the surface-exposed domain of P30 and although hemadsorption was the most sensitive phenotype to any alteration in the P30 sequence, a P30 revertant strain was isolated which exhibited wild-type levels of attachment to hamster respiratory epithelium yet only demonstrated an intermediate motility phenotype. Thus, this strain might be useful to determine if gliding motility is a virulence determinant for *M. pneumoniae* pathogenesis.

INDEX WORDS: *Mycoplasma pneumoniae,* P30, P65, cytadherence, gliding motility, green fluorescent protein, attachment organelle, cell division

CELLULAR AND MOLECULAR STUDIES OF *MYCOPLASMA PNEUMONIAE* ADHERENCE AND GLIDING MOTILITY

by

JARRAT LANCE JORDAN

B.S., Valdosta State University, 1996

A Dissertation Submitted to the Graduate Faculty of The University of Georgia in Partial Fulfillment of the Requirements for the Degree

DOCTOR OF PHILOSOPHY

ATHENS, GEORGIA

2003

CELLULAR AND MOLECULAR STUDIES OF *MYCOPLASMA PNEUMONIAE* ADHERENCE AND GLIDING MOTILITY

by

JARRAT LANCE JORDAN

Major Professor: Duncan C. Krause

Committee: Daniel G. Colley
Mark A. Farmer
Margie D. Lee
Robert J. Maier

Electronic Version Approved:

Maureen Grasso
Dean of the Graduate School
The University of Georgia
August 2003

DEDICATION

This work is dedicated to my parents, the best parents anyone could have ever asked for. Although my dad “Captain Jack” never completed this journey with me in the flesh, I know he is with me in spirit. I am extremely grateful for the emotional and financial support from my mom. I can truly say that without her encouragement I would never have completed this goal. I am blessed to have you both as parents. Thanks for feeding my interests in the sciences early.

ACKNOWLEDGEMENTS

I consider myself extremely lucky to get to work on such an interesting organism and to have the instruction of so many gifted people. I am exceedingly indebted for the mentorship of Dr. Duncan Charles Krause who took me into his lab, at a time when bench-space was at an absolute minimum. Thanks for sticking with me and as hard as it must have been, training me to think as a scientist. It was a privilege to be in your lab and your guidance will never be forgotten. I want to also thank Linda Buffington for being my second mom. Linda, you will always be family. You both have helped me more than you will ever know.

I would also like to thank my committee members. I thank Dr. Mark Farmer for his enthusiasm and giving me great advice for experiments, for his cutting-edge knowledge of imaging, and for letting me use all the cool microscopes at the center. I thank Dr. Margie Lee for her ‘straight up’ cut to the chase mindset, for introducing me to fruitful collaborations and for all the advice, time, and support for my research. I thank Dr. Robert Maier, for being very supportive and for balancing out my committee with his laid back, quiet personality with a Science paper to boot! And finally, I thank Dr. Daniel Colley, for giving me tremendous insight about future career decisions, and for letting me in on some intimate Shistosome encounters! Your enthusiasm for science is infectious. Being a late addition to my committee, it is extremely uplifting to see someone with as little free time as you go out of their way to talk and give advice.

I would also like to thank the past and present members of the Krause lab for making the valleys and peaks of mycoplasma research and graduate student life in general a whole lot more tolerable. Mitch Balish for being the best science writer I know, for some of the most stimulating scientific discussions I ever had, for his enthusiasm about science, and for all his help in my scientific training. I can't wait to read what will come next from Mitch. I thank Melisa Willby, who naturally performed the task of being the lab mom for a bunch of her helpless labmates. Thanks for helping me out when I needed it the most. Robert Waldo III, although we have a lot of differences in opinion, I'm glad to have you as a labmate. Thanks for all the helpful discussions about the data, for all the assistance with the computers and of course for coffee in the Cavendish. Stephanie Ross, for balancing out the lab with her refreshing perspectives. It's a delight to have you in the lab. I also thank the newest member and P30 philosopher of the Krause lab, Benjamin Hasselbring for his determination and enthusiasm. I expect great things from you, keep up the good work. To Kyungok Lee, for setting disorganized people like me straight while at the same time being such a kind-hearted person. To Ryan Santurri for all the great workouts, parties, and good times. I will never forget our experience at Bellmont! Also many thanks to my former labmates: Karen Berry, Tae-wook Hahn, Sondra Ricci, Makda Fisseha and Phillip Popham. You have all touched my life in many ways. Thanks for making the Krause lab a great home throughout the years. Last but not least, I would like to thank my girlfriend Andrea for knowing just the right thing to say at the right time, for being such a kind soul, and most importantly, not trying to change me. I am lucky to have you.

TABLE OF CONTENTS

LIST OF TABLES

Page

LIST OF FIGURES

Page

CHAPTER 1

INTRODUCTION

Mycoplasmas are successful eubacterial parasites of plants and animals, characterized by small genomes and the lack of a cell wall. Currently there are well over 170 known mycoplasmas species. Commenting on their ubiquitous distribution, it has been said that new mycoplasma discovery most likely depends on the effort the investigator is willing to expend to isolate and legitimize their taxonomic identity (Razin *et al.*, 1998). Mycoplasmas are members of the taxonomic class *Mollicutes* meaning "soft skin". Due to the lack of a cell wall, these bacteria are particularly pleomorphic and resistant to β-lactam antibiotics. Mycoplasmas are also unusual in the prokaryotic world in that they incorporate cholesterol into their cell membranes and use of the widespread stop codon UGA to encode tryptophan. The genomes of five species of *Mollicutes* have been fully sequenced: *Mycoplasma genitalium*, *Mycoplasma pneumoniae*, *Mycoplasma pulmonis*, *Mycoplasma penetrans*, and *Ureaplasma urealyticum* (Chambaud *et al.*, 2001; Fraser *et al.*, 1995; Glass *et al.*, 2000; Himmelreich *et al.*, 1996; Sasaki *et al.*, 2002). Three of these share in common a polar, differentiated terminal organelle and gliding motility (Kirchhoff, 1992), features thought to be important for successful host colonization.

An obligate parasite of humans, *M. pneumoniae* causes tracheobronchitis and atypical pneumonia. Adherence to host respiratory epithelium (cytadherence) is a prerequisite for colonization and pathogenesis (Hu *et al.*, 1976) and is mediated by the terminal organelle (Powell *et al.*, 1976). This structure is most commonly referred to as the attachment organelle in *M. pneumoniae*, the species for which the most detailed studies exist. This membrane-bound extension of the mycoplasma cell is distinguished ultrastructurally by an electron-dense core having a slightly enlarged terminal button (Biberfield and Biberfield, 1970), both of which are part of a Triton X-100 (TX)-insoluble cytoskeletal network [Triton shell; (Gobel *et al.*, 1981; Meng and Pfister, 1980)]. The attachment organelle is the leading end as cells move by gliding motility (Bredt, 1968; Kirchhoff, 1992), and its duplication is coordinated with cell division (Boatman, 1979; Krause and Balish, 2001; Seto *et al.*, 2001). Several cytadherence mutants have been isolated, resulting in the identification of proteins required for cytadherence. The primary adhesin protein P1, cytadherence-related proteins P30, and P65, as well as other cytadherence accessory proteins including HMW1, HMW2, and HMW3, have been localized to this organelle. Loss of any of these proteins has pleiotrophic affects on the mycoplasma, including the decreased stability of other cytadherence proteins, atypical cellular morphology, and cell development defects, demonstrating the interdependence of the components of the attachment organelle and the importance of this dynamic structure in many processes. This dissertation focuses in particular on *M. pneumoniae* cytadherence-related proteins P65 and P30.

Although there are no reported P65 mutants, this cytadherence-related protein is a component of the Triton shell, localizes to the attachment organelle, and is encoded in an

operon immediately preceding *hmw2*. Loss of HMW2 (mutant I-2), results in instability of many cytadherence proteins, including P65 (Jordan *et al.*, 2001) and P30 (Balish and Krause, 2002). Furthermore, HMW2 mutants lack the characteristic electron dense core seen in wild-type *M. pneumoniae*. Thus HMW2 is believed to be an essential component of the electron dense core (Seto and Miyata, 2003), which is a definitive feature of attachment organelles in thin sections examined by transmission electron microscopy (TEM).

Mutations in the cytadherence-related *p30* gene result in attachment organelle defects. A previously isolated, spontaneously arising P30 null mutant (II-3) was found to be avirulent (Krause *et al.*, 1982), morphologically branched, and unlike other tested adherence mutants, is capable of localizing major adhesin protein P1 to the attachment organelle (Romero-Arroyo *et al.*, 1999). Protein P30 is an integral membrane protein containing a predicted N-terminal signal sequence (Dallo *et al.*, 1990) followed by a cytoplasmic domain, transmembrane domain, and C-terminal extracellular domain consisting of several proline-rich repeats (Dallo *et al.*, 1996). In wild-type *M. pneumoniae* P30 localizes exclusively to the attachment organelle, and anti-P30 antibodies inhibit cytadherence (Dallo *et al.*, 1990). Closely related species *M. genitalium* and *M. gallisepticum* have homologs to P30 (Boguslavsky *et al.*, 2000; Hnatow *et al.*, 1998; Reddy *et al.*, 1995), and also exhibit gliding motility (Kirchhoff, 1992).

M. pneumoniae is somewhat paradoxical, exhibiting gliding motility and chemokinesis despite its limited genome size (816-kbp) and a lack of homologs to two-component systems and known gliding motility proteins in other organisms (Kirchhoff, 1992). *M. pneumoniae* cells localize at the base of cilia and microvilli of respiratory

epithelial cells as can be seen in sputum samples from patients with culturally verified infections and tracheal epithelium from experimentally infected hamsters by TEM (Collier and Clyde, 1974). In order to access this colonization site the mycoplasma presumably must traverse flowing mucous several microns in depth propelled by the vigorous beating of the cilia. This line of defense functions to keep bacterial and particulate insults from contacting and possibly damaging the delicate epithelium (Gabridge, 1983). Gliding motility of *M. pneumoniae* is thought to be helpful in allowing the mycoplasma to penetrate the respiratory mucosa to access the epithelial cell surface. However, the role of gliding motility in the virulence of *M. pneumoniae* infection remains untested, as there are no characterized motility mutants capable of cytadherence. Even now, more than half a century after *M. pulmonis* was first reported to exhibit gliding motility, and despite the completion of the genome sequences for three gliding mycoplasmas (*M. genitalium*, *M. pneumoniae*, and *M. pulmonis*), little is known about the mechanism of gliding in the mycoplasmas.

The objectives of this dissertation project were:

I. To address the stability and subcellular localization of P65 in wild-type and non-cytadhering mutant *M. pneumoniae*;

II. To develop a means to allow rapid screening for motility in wild-type and mutant *M. pneumoniae* strains. This objective includes the optimization of time-lapse microcinematography to record cellular motility of *M. pneumoniae*; and

III. To perform structure function analysis of protein P30 to correlate specific domains with cytadherence, morphology, gliding motility, P65 stability, and P30 localization. This

final objective includes the characterization of spontaneously arising P30 mutants and isolated revertants as well as the construction and characterization of a functional P30-GFP fusion.

CHAPTER 2

REVIEW OF THE LITERATURE

History of *M. pneumoniae*

Although *M. pneumoniae* is not the only mycoplasmal human pathogen, it has the distinction of being the first described (Krause and Taylor-Robinson, 1992). The discovery of *M. pneumoniae* began in the late 1930's when patients were found to have pneumonia with characteristics dissimilar from what were typically seen (Luby, 1991). With the coming of the Second World War, this form of pneumonia became increasingly more common and was coined primary atypical pneumonia (PAP). The crowded living conditions of military barracks contributed to an increased incidence of this disease due to enhanced transmission. The filterability of the agent initially suggested a viral origin. Eaton and colleagues isolated the microorganism, also known as Eaton's agent, from the lungs of patients with PAP using various animals as propagation hosts and were the first to cultivate the organism successfully in cell-free medium (Chanock *et al.*, 1962). Shortly thereafter, Eaton's agent was shown by Chanock in 1962 to be a mycoplasma and was officially named *M. pneumoniae* the following year (Chanock *et al.*, 1963).

Epidemiology and Clinical Features of *M. pneumoniae* Infection

M. pneumoniae is the most common etiologic agent of primary atypical pneumonia, which is a significant health problem generally affecting older children and

young adults. *M. pneumoniae* accounts for as many as 20% of all cases of pneumonia in humans (Foy, 1999). Occasionally fatal, an estimated 2 million cases occur annually in the United States alone, with up to 100,000 pneumonia-related hospitalizations (CDC, 2002). Currently there is no vaccine for the disease, and treatment usually involves erythromycin or tetracycline derivatives.

M. pneumoniae is transmitted by respiratory droplets through person-to-person contact or aerosolization. *M. pneumoniae* infections have a cosmopolitan distribution, with a higher prevalence during colder months. Generally affecting children from 5-9 years of age (Razin *et al.*, 1998), symptoms range from subclinical, to respiratory disease with or without pneumonia, with the most common clinical manifestation being tracheobronchitis (Krause and Taylor-Robinson, 1992).

After inhalation, *M. pneumoniae* reaches the trachea, bronchi, and bronchioles and an intractable nonproductive cough ensues; in about 10% of such cases radiologically confirmed pneumonia develops. Symptoms are chronic in onset and recovery and atypical for pneumonia, often flu-like, including general aches and pains, headaches, and chills (Krause and Taylor-Robinson, 1992). Sequelae from *M. pneumoniae* infections sometimes arise as a result of production of certain autoantibodies, including cold agglutinins reacting with the erythrocyte I antigen, or cross-reactive antibodies against lymphocytes, smooth muscle cells, brain, and lung antigens (Razin *et al.*, 1998). For example, the presence of anti-Gal-C antibodies cross-reactive with *M. pneumoniae* antigens were found in higher incidences in patients with Guillain-Barré syndrome (GBS) when there was a preceding *M. pneumoniae* infection (Ang *et al.*, 2002). Furthermore, anti-Gal-C activities in GBS patient antisera were inhibited by preincubation with *M.*

pneumoniae antigens (Kusunoki *et al.*, 2001). The authors suggested that this GalC cross-reactivity may be a form of molecular mimicry (Kusunoki *et al.*, 2001). Evidence of molecular mimicry in *M. pneumoniae* has been well documented with the primary adhesin P1, (see P1 section; (Jacobs *et al.*, 1995). The possible role anti-Gal-C antibodies may have in the pathogenesis of GBS is unclear, yet demyelinating features are found in the majority of GBS patients exhibiting GalC reactivity. Furthermore, rabbits hyperimmunized with purified Gal-C exhibited demyelinating neuropathies coincident with the production of anti-Gal-C antibodies, and anti-Gal-C antibodies have been shown to have a demyelinating effect *in vitro* (Ang *et al.*, 2002). Although uncommon, extra-pulmonary syndromes including cardiologic, neurologic, and dermatologic manifestations can develop from *M. pneumoniae* infections.

Phylogeny, Growth Requirements, and Characteristics of the Mycoplasmas

The ancestral Mollicute probably arose from Streptococcal lineages of the Gram-positive bacteria, diverging to form the AAP branch subsequent to the loss of some biosynthesis, cell-wall synthesis, and rRNA genes. Around the appearance of the first land plants, the Mollicutes split to form a second branch termed the SEM (Maniloff, 2002). The SEM branch later evolved to include a sterol-requiring branch which incorporates the Mycoplasmataceae. Soon after the appearance of the first mammals and other vertebrate groups a rapid period of evolution occurred in the Mycoplasmataceae, further partitioning the branch by taking advantage of the new hosts available.

Millions of years of evolution in the mycoplasmas have resulted in the loss of a plethora of genes including those involved in cell-wall and amino acid biosynthesis, as well as many involved in cofactor biosynthesis (Razin *et al.*, 1998). This genomic

streamlining has rendered the mycoplasmas strictly dependent on their hosts for sustenance. In addition to biosynthetic inadequacies, *M. pneumoniae* does not have the genetic complement to complete the Tricarboxylic Acid cycle, thereby relying on the very limited energy returns of substrate-level phosphorylation. However, due to their parasitic lifestyle, the large amount of energy needed for biosynthesis reactions is reduced.

The fastidiousness of *M. pneumoniae* is reflected by the media needed to support its growth *in vitro*. Mycoplasmas are unique among prokaryotes in that they require cholesterol for growth. Thus, *M. pneumoniae* requires a high concentration of serum in its growth media to supply cholesterol and fatty acids (Razin *et al.*, 1998). It is believed that the membrane incorporation of cholesterol supplied by the host enables the mycoplasma to alter its membrane fluidity without having to modify its fatty acid biosynthesis, a process severely stymied through genetic reduction. Mycoplasmas also lack genes and enzymes involved in purine and pyrimidine synthesis (Razin *et al.*, 1998). Genes for the salvage pathways utilizing purines and pyrimidines for the synthesis of ribonucleotides and their conversion to deoxyribonucleotides have been identified in the mycoplasmas (Razin *et al.*, 1998). Similar to the loss of biosynthetic genes, and likely coupled with the loss of cell wall genes, *M. pneumoniae* appears to lack many of the cell division proteins known in other prokaryotes (Himmelreich *et al.*, 1996). Importantly, *M. pneumoniae* does possess the gene and gene product for FtsZ (Himmelreich *et al.*, 1996) (Regula *et al.*, 2000) (Regula *et al.*, 2001), and recent evidence suggests also the gene encoding FtsA (M.F. Balish unpublished data).

Mycoplasma Genetics

Mycoplasma pneumoniae has not been shown to carry plasmids or viruses. Homologous recombination has also not been reported in *M. pneumoniae*, although the genome sequence revealed the existence of the *recA* gene (Himmelreich *et al.*, 1996). Encouragingly, a directed gene disruption mutant was created in the closely related *M. genitalium* (Dhandayuthapani *et al.*, 1999). Although no naturally occurring transposons have been found in *M. pneumoniae*, the *Staphylococcus aureus* transposon Tn*4001* has been used successfully and is currently the tool of choice for mutagenesis and genetic complementation experiments (Renaudin, 2002).

Mycoplasmas use the termination codon UGA to encode the amino acid tryptophan. Expression of mycoplasmal genes in *E. coli* can result in the premature termination of tryptophan-containing proteins, although some success has been achieved using opal suppressor strains (Muto and Ushida, 2002). While *Bacillus subtilis* uses UGA as a termination codon, this species also contains a tRNA that reads the UGA stop codon as tryptophan. *PrfB* mutants in *B. subtilis* have enhanced readthrough of UGA, allowing better expression of mycoplasma genes (Kannan and Baseman, 2000). In some cases, depending on the number of UGA codons, site-directed mutagenesis is the method of choice.

Morphology and Ultrastructure of *M. pneumoniae*

M. pneumoniae cells average from 0.19 to 0.22 μm in diameter and 2.2 μm in length and exhibit a capricious morphology. (Muse *et al.*, 1976). Although pleomorphic, these cells generally have a distinct elongated morphology which is also described as 'flask shaped' (Kirchhoff *et al.*, 1984). Phase-contrast images of *M. pneumoniae* mutants

deficient in attachment indicate an overall branched morphology different from the more elongated wild-type cells (Seto and Miyata, 2003), with wild-type morphology perhaps resulting from the stretching of attached cells exhibiting gliding motility. Due to their minute size, nuances in the morphology of adherence mutants must be determined by using electron microscopy. Morphological characteristics of wild-type organisms grown *in vitro* appear identical to those seen in infected hamster tracheal epithelium and sputum from infected patients (Collier and Clyde, 1974), revealing a polar attachment organelle or 'tip' having an electron-dense core terminating in a button at the distal end of the cell (Biberfield and Biberfield, 1970). Micrographs of TX treated *M. pneumoniae* cells reveal a complex network of proteins associated with the tip structure. This Triton-insoluble complex of proteins, often described as a cytoskeleton (Razin and Jacobs, 1992), cooperates structurally and functionally to localize and concentrate adhesin proteins to the tip structure (Baseman and Tully, 1997). Besides its role in adherence, the attachment organelle is also thought to function in cell division and gliding motility (Krause and Balish, 2001).

Pathogenesis

Human and animal mycoplasmas typically colonize the mucosal surface of the respiratory and urogenital tracts and the joints of some animals (Razin and Jacobs, 1992). Although humans are the only natural host for *M. pneumoniae*, hamsters and monkeys are alternative animal models for infection studies (Krause and Taylor-Robinson, 1992). In order to parasitize the human host successfully, *M. pneumoniae* must bind respiratory epithelium. Mutants unable to do so are incapable of causing significant pathology in experimentally infected hamsters (Krause *et al.*, 1982). The attachment organelle of wild-

type *M. pneumoniae* binds sialoglycoproteins and sulfated glycolipid receptors on tracheal epithelium (Razin and Jacobs, 1992). Neuraminidase is an enzyme that cleaves N-acetyl neuraminic acid (sialic acid) from a variety of glycoproteins. Neuraminidase treatment of hamster tracheal rings reduces the amount of attached mycoplasmas, demonstrating the importance of sialic acid moieties in attachment (Powell *et al.*, 1976). By chemically inducing a decrease in ciliation of tracheal epithelium through vitamin A starvation, it was shown that the number of attached mycoplasmas decreased; the authors thereby concluded that ciliated respiratory epithelium contains more sialic acid receptors than non-ciliated epithelium (Gabridge, 1979).

Hemadsorption

Although Mycoplasmas are not normally found in the blood, a correlation exists between hemadsorption and the ability to bind respiratory epithelium (Sobeslavsky *et al.*, 1968). Sialic acid-containing moieties like those on ciliated respiratory epithelium are also present on erythrocytes. Hemadsorption is regarded as a convenient method for screening mycoplasma colonies for attachment capabilities. Although hemadsorption and attachment to respiratory epithelium correlate, this association is not perfect. For example, a mutant produced from the chemical mutagenesis of wild-type *M. pneumoniae* exhibited a lack of hemadsorption yet retained a wild-type capacity to bind to a hamster lung cell line (Yayoshi, 1983). After intranasal infection of hamsters, it was noted upon lung lobe examination that this strain showed only mild pathological effects to the lungs in comparison to the wild-type strain. *In vitro* examination of ciliary activity of organ cultures infected with this strain revealed similar findings with the *in vivo* study. The reduced virulence of this isolate did not hinder the ability to culture it successfully from

infected hamster lung tissue, in contrast to the failure to recover a non-cytadherent mutant. Further illustrating the discrepancy between hemadsorption and attachment to respiratory epithelium, mutants lacking the P30 protein (designated mutant II-3) were likewise found to be incapable of hemadsorption yet were recovered from experimentally infected hamster lungs, albeit at much lower levels than wild-type *M. pneumoniae* (Krause *et al.*, 1982). It is noteworthy that the lungs of these infected hamsters exhibited little lung pathology. Pretreatment of tracheal rings with neuraminidase did not significantly affect attachment levels of the P30 mutant strain (Krause *et al.*, 1982), in contrast to the reduction observed with neuraminidase treated rings infected with wild-type *M. pneumoniae* (Collier and Baseman, 1973). The authors suggested the existence of one or more attachment mechanisms in addition to a sialic acid receptor/ligand interaction.

Cytotoxicity

Pathology caused by *M. pneumoniae* infection is believed to be due primarily to oxidative damage to the host cell caused by generation of peroxide and superoxide radicals (Razin and Jacobs, 1992). In the absence of genes encoding superoxide dismutase, catalase, and peroxidase, it is thought that *M. genitalium* and *M. pneumoniae* use the thioredoxin reductase system for protection from these reactive oxygen radicals (Razin *et al.*, 1998). Examination by TEM of thin sections from infected tracheal epithelium reveals an intimate association of the mycoplasma attachment organelle with the host cell membrane, in which some suggest a membrane fusion event occurs (Razin and Jacobs, 1992). Significantly, the ability of colonies to form hemolytic plaques was impaired in an avirulent *M. pneumoniae* mutant that was fully capable of attachment to a

hamster lung cell line (Yayoshi, 1983). It has also been suggested that decreased precursor transport might cause cellular damage to host cells due to the sheer number of attached mycoplasmas, resulting in loss of transport sites associated with the apical portion of the ciliated cells or perhaps a steric block of available transport sites by attached organisms (Muse *et al.*, 1976). Evidence that nutrient acquisition may be involved in *M. pneumoniae* pathogenicity comes from Gabridge and Stahl's findings that exogenous adenine provides some protection for cells, indicating that cells may lose their nutrients during *M. pneumoniae* infection (Gabridge and Stahl, 1978). Interestingly, purified *M. pneumoniae* membranes have also been shown capable of causing ciliostasis and ATP depletion in hamster tracheal organ culture, whereas infection with attenuated or nonvirulent mycoplasmas only caused negligible decreases in ciliary beat frequencies and no decreases in ATP levels (Gabridge and Polisky, 1977). In a later study, *M. pneumoniae* cell-free extract was found to decrease ciliary activity in tracheal explant culture. This ciliostatic response was dose-dependent, and the ciliostatic-inducing component(s) in the extract were resistant to trypsin and chymotrypsin, as well as to boiling for 10 min. Perhaps most significantly, when administered to hamsters the extract was capable of inducing similar histopathology as is seen when hamsters are infected with virulent *M. pneumoniae* (Chandler *et al.*, 1987).

Cytadherence - Associated Proteins

Proteins P1, A, B, C- After brief preincubation of radiolabeled mycoplasmas with trypsin, it was found that attachment to hamster tracheal epithelium was noticeably reduced, indicating a proteinaceous mediator of attachment. Comparison of SDS-PAGE profiles of protease treated and untreated mycoplasmas revealed that cleavage of a high

molecular weight protein designated P1 correlated with the reduction in attachment (Hu *et al.*, 1977). In this elegant work, Hu et al. showed that *M. pneumonaie* could regain the ability to attach with time after removing trypsin and reincubating in fresh medium, unless the protein synthesis inhibitor erythromycin was present. Protein P1 was later shown to be localized to the attachment organelle by using immunoelectron microscopy (Hu *et al.*, 1982), and shortly thereafter confirmed by immunofluorescence microscopy (Feldner *et al.*, 1982). The former study demonstrated P1 to be a major immunogen in natural human infections, hyperimmunized rabbits, and experimental infections in hamsters, and that antibodies against P1 inhibit attachment to tracheal epithelium (Hu *et al.*, 1982). The latter study similarly provided evidence that antibodies against protein P1 inhibit hemadsorption, attachment to glass and gliding motility (Feldner *et al.*, 1982). The role of P1 as an adhesin was established by Krause *et al*., who showed that anti-P1 Fab fragments likewise inhibit cytadsorption, thus reducing the possibility of steric effects, while also demonstrating that anti-P1 antibodies do not inhibit *M. pneumoniae* metabolism (Krause and Baseman, 1983).

The P1 adhesin is associated both with the TX-insoluble fraction (Triton shell) and the TX-soluble fraction (Kahane *et al.*, 1985; Layh-Schmitt and Harkenthal, 1999). The proteins forming the Triton shell must cooperate structurally and functionally to localize and concentrate adhesin proteins to the tip (Baseman and Tully, 1997). A spontaneously arising or chemically mutagenized mutant lacking only P1 has never been isolated. Only one non-cytadherent mutant (designated IV-22) lacking P1 is available for study. However, IV-22 contains a defect resulting in the loss of protein P1 as well as proteins A, B, and C (Krause *et al.*, 1982; Su *et al.*, 1989).

Proteins A, B, and C are also absent in cytadherence mutants III-4 (Krause *et al.*, 1982). The identity of protein A remains to be determined, while proteins B and C appear to correspond to the 90-kDa and 40-kDa cleavage products of a 130-kDa protein encoded by ORF6, which is located immediately downstream of the *p1* gene (Layh-Schmitt and Herrmann, 1992). Protein P1 is thought to be translationally coupled to the ORF6 product (Su *et al.*, 1989). In mutant III-4, the P1 adhesin was found only in the TX-soluble phase, demonstrating the importance of one or both of these proteins in anchoring P1 in the cytoskeleton (Layh-Schmitt and Harkenthal, 1999). Furthermore, chemical cross-linking studies have shown proteins B and C to be within 0.1 nm of each other and the P1 adhesin (Layh-Schmitt and Herrmann, 1994).

Native protein P1 is predicted to assume a conformation whereby regions of the N-terminus, C-terminus, and a central portion of the protein collectively are responsible for receptor binding, as deduced from epitope mapping, antibody competition assays, and attachment inhibition tests (Gerstenecker and Jacobs, 1990). In later studies it was found that antibody from convalescent sera derived from known human *M. pneumoniae* infections was reactive against a number of different octapeptides of P1, but none derived from receptor binding sequence (Jacobs *et al.*, 1995). Interestingly, some *M. pneumoniae* adherence-inhibiting antibodies made from the hyperimmunization of animals with various presentations of P1 were also cross-reactive with host-cell antigens, indicating that molecular mimicry may occur (Jacobs *et al.*, 1995).

HMW Proteins- The cytadherence-accessory proteins HMW1, HMW2, and HMW3 (high molecular weight proteins) are associated with the cytoskeleton (Stevens and Krause, 1991, 1992). Like proteins B and C, these proteins are not adhesins but are

ultimately required for the proper functioning of P1 (Razin and Jacobs, 1992). A mutant lacking HMW1 (designated M6) fails to localize P1 to the tip, as demonstrated by immunoelectron microscopy. P1 localization was subsequently restored in this mutant by complementation with the wild-type recombinant *hmw1* allele (Hahn *et al.*, 1998). Although debatable (Seto *et al.*, 2001), protein HMW1 unlike other known proteins involved in cytadherence, exhibits a bipolar localization, scattered on the leading and trailing end of the mycoplasma (Stevens and Krause, 1991). HMW1 contains a 31-amino acid (106-136) EAGR motif (enriched in aromatic and glycine residues). The EAGR motif precedes an acidic, proline-rich domain (APR) spanning residues 170-522 followed by two coiled-coil regions in the C-terminal portion of the 1,018 residue protein (Balish *et al.*, 2001). Loss of HMW1 results in a morphological change from the typical filamentous shape of wild-type cells to a more ovoid shape without a conspicuous attachment organelle (Hahn *et al.*, 1998). In wild-type *M. pneumoniae*, HMW1 is synthesized and translocated from a TX-soluble to a TX-insoluble pool (Triton shell) eventually reaching a predominantly cytoskeletal association on the cell surface (Balish *et al.*, 2001).

Cells of the spontaneously arising non-cytadherent mutant I-2 do not produce the structural protein HMW2 and lack the filamentous morphology of wild-type *M. pneumoniae* (Krause *et al.*, 1982; Seto and Miyata, 2003). Turnover of the cytadherence-accessory proteins HMW1, HMW3, and P65 is accelerated in this mutant (Jordan *et al.*, 2001; Popham *et al.*, 1997; Willby and Krause, 2002). Mutant I-2 cells regain a wild type phenotype when complemented with the recombinant wild-type *hmw2* allele. Thus HMW2 is necessary as a stabilizing factor for HMW1 and several other cytadherence-

accessory proteins. HMW2 is a TX-insoluble 216-kDa protein predicted to be primarily α-helical and containing discontinuous coiled coil regions throughout its length (Krause *et al.*, 1997). HMW2 was recently localized to the attachment organelle using a HMW2/ green fluorescent protein (GFP) sandwich fusion (Balish *et al.*, 2003). The recombinant sandwich fusion successfully complemented the *hmw2* mutant, thereby stabilizing proteins HMW1, HMW3, and P65. Hemadsorption by the complemented strain was likewise restored to a wild-type level, although cellular morphology was only partially restored. It was noted that these transformants exhibited a higher incidence of bifurcated terminal organelles. According to the current model, *M. pneumoniae* cell division begins with duplication of the attachment organelle (see below). The higher incidence of bifurcated tips in wild-type and mutant I-2 cells containing the HMW2/GFP fusion suggests that the fusion protein is interfering at least partially with the cell division process. It is hypothesized that HMW2 is a major component of the electron-dense core and is required at the beginning of the pathway for attachment organelle assembly based on the dependence of HMW1, HMW3, P30, and P65 on HMW2 for stability (Balish and Krause, 2002), the apparent absence of cores in this mutant (Seto and Miyata, 2003), and its localization to the terminal organelle (Balish *et al.*, 2003).

HMW3 exhibits reduced levels in mutants deficient in HMW1 (mutant M6), and HMW2 (mutant I-2) and has a predicted molecular weight of 73,725 (Krause, 1998; Ogle *et al.*, 1992; Popham *et al.*, 1997). Migrating at 140,000 by SDS-PAGE, it is thought that an APR domain spanning residues 88-488 contributes to this migration as other *M. pneumoniae* proteins containing APR domains migrate uncharacteristically (Dirksen *et al.*, 1996; Ogle *et al.*, 1992; Proft *et al.*, 1995; Proft *et al.*, 1996). In a recently discovered

non-adherent, *hmw3* transposon insertion mutant (Willby and Krause, 2002), only cytadherence accessory protein P65 exhibited reduced levels. Protein P65 also displayed a patchy distribution in this mutant, unlike the tip-clustered localization seen in wild-type cells. In some HMW3- cells adhesin protein P1 was localized to polar structures yet most often was found scattered along the rest of the cell. The inability to localize P1 to the attachment organelle like the wild-type strain could explain the intermediate level of hemadsorption and gliding motility observed in this mutant. The current data suggest that HMW3 stability depends on proteins HMW1 and HMW2, yet only protein P65 is affected by the absence of HMW3. Interestingly, 20% of cells in a given field of thin sections of the HMW3 mutant have a V shaped electron dense core with the vertex distally located (Willby and Krause, 2002). These altered electron-dense cores reveal that HMW3 may be needed to stabilize the core structure.

Protein P65- Like HMW1 and HMW3, protein P65 is a component of the Triton shell of *M. pneumoniae* and is found at significantly reduced levels in *hmw2* mutants. In the wild-type strain, protein P65 has been shown to partition with the Triton shell as well as the TX-soluble fraction. The cytoskeletal-associated P65 appears to be firmly associated with the Triton shell, unlike proteins P1 (Balish and Krause, 2002), and P30, which can be released from the TX-insoluble cytoskeleton after repeated fractionation (Waldo *et al.*, 2002). Furthermore, like HMW1, P65 is peripherally associated with the mycoplasma membrane. P65 contains an APR domain, which, unlike that of HMW1 and HMW3, is found at its N-terminus. The APR domain of P65 shares limited sequence similarity to that of HMW3. The gene encoding P65 is the first gene in the operon of the same name and immediately precedes the gene for HMW2; thus, P65 shares not only

structural similarity with HMW1 and HMW3, but also a functional association with HMW1, HMW2, and HMW3. Although these data imply a role in cytadherence, no P65 mutant has been isolated to date; hence the role of this protein in mycoplasma cytadherence is unclear.

Seto et al. localized P65 to the attachment organelle in wild-type *M. pneumoniae* by using immunofluorescence microscopy. However, P65 was not detected by this technique with several cytadherence mutants, despite its reported presence at wild-type levels in the mutants by Western immunoblotting. In a later study evaluating protein P65 further, reduced levels of P65 were demonstrated by both Western immunoblotting and immunofluorescence microscopy in some but not all cytadherence mutants tested (Jordan *et al.*, 2001).

Pulse-chase analysis established that P65 is subject to accelerated turnover in the same manner as HMW1 and HMW3 in *hmw2* mutants (Jordan *et al.*, 2001). The level of P65 in wild-type *M. pneumoniae* profiles remained stable throughout the 8-h chase. Furthermore, the amounts of P65 in the wild-type and mutant I-2 profiles were comparable at the 0-h time point. However, the level of P65 in the mutant decreased over the 8-h chase period, as was seen previously for HMW1 and HMW3. A similar pattern was observed with the *hmw2* transposon insertion mutant designated A3 (Jordan *et al.*, 2001). Analysis of the spent medium for wild-type and mutant cultures yielded no evidence of P65 release. Thus, like HMW1 and HMW3, P65 is lost post-translationally in the absence of HMW2, apparently due to accelerated turnover (Jordan *et al.*, 2001). Stability of P65 appears to be extremely sensitive to changes in the amounts of other cytadherence proteins. It is thought that P65 associates with the nascent tip after the other

cytadherence proteins have assembled, and this complex is necessary for the proper stability of P65 (Seto *et al.*, 2001). Interestingly, P65 localization was not affected by the absence of P1, A, B, C, or protein P30. Thus, only HMW1, HMW2, and HMW3 appear to be needed for efficient translocation of P65 to the tip.

Protein P30- P30 is a membrane protein encoded in the operon that also contains the genes for *hmw1* and *hmw3*, as well as several ORFs of unknown function. Through promoter deletion studies, it was found that a promoter directly upstream of *p21,* which immediately precedes *p30,* drives the transcription of *p30* and the adjacent downstream gene for *hmw3* (Figure 1) (Waldo *et al.*, 1999). Like the major adhesin P1, protein P30 (30-kDa) is found clustered at the attachment organelle and is essential for *M. pneumoniae* pathogenesis (Baseman *et al.*, 1987). Pleiotropic effects on colonization and virulence (Baseman *et al.*, 1987; Krause, 1998), and cellular morphology (Romero-Arroyo *et al.*, 1999) accompany the loss of P30. Reacquisition of P30 by complementation with the wild-type recombinant *p30* allele restores a wild-type phenotype (Romero-Arroyo *et al.*, 1999), demonstrating the importance of P30 in proper cell development and virulence. Antibodies against P30 inhibit hemadsorption (Baseman *et al.*, 1987), although the possibility of steric effects of the antibody on nearby proteins was not addressed.

The P30 protein contains a putative signal sequence of 33 residues (Dallo *et al.*, 1990; Romero-Arroyo *et al.*, 1999). The mature protein is predicted to have a cytoplasmic N-terminal domain (38 amino acids), a membrane-spanning domain (27 amino acids), and a surface-exposed C-terminal domain (176 amino acids; Figure 2). The C-terminus of P30 was determined to be surface-exposed based upon carboxypeptidase Y

Figure 1. **Map of the *hmw* gene cluster of *M. pneumoniae* modified from Waldo *et. al.* (Waldo *et al.*, 1999).** The number of the first nucleotide relative to the published genome sequence of *M. pneumoniae* (Himmelreich *et al.*, 1996) is given to the left and far right, and the scale in kilobase pairs is shown below the map. The genes for *p30*, *hmw3*, *hmw1*, and ORFs encoding predicted proteins of unknown function are indicated. The promoter-like sequences evaluated by primer extension are indicated by bent arrows. PromP21 has been shown by promoter deletion studies to drive transcription of both *p30* and *hmw3* (Waldo *et al.*, 1999).

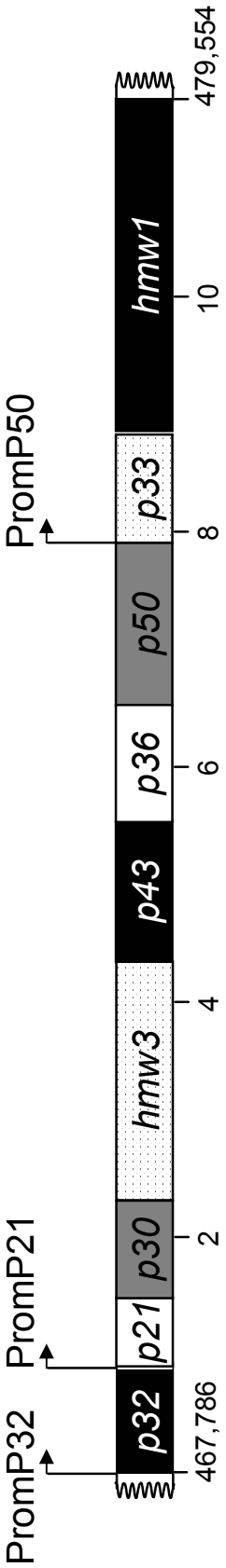
PromP32
PromP21
PromP50
p32
p21
p30
hmw3
p43
p36
p50
p33
hmw1
467,786
2
4
6
8
10
479,554

Figure 2. Predicted domains of protein P30. P30 is thought to be oriented with the N-terminus in the cell interior and the C-terminus on the cell surface, as indicated. Mutant II-3 does not produce detectable P30 due to a frameshift at the codon for residue 151 (Romero-Arroyo *et al.*, 1999). P30 mutant II-7 contains a deletion at the indicated residues (Dallo *et al.*, 1996), identical to that in M6 (Layh-Schmitt *et al.*, 1997).

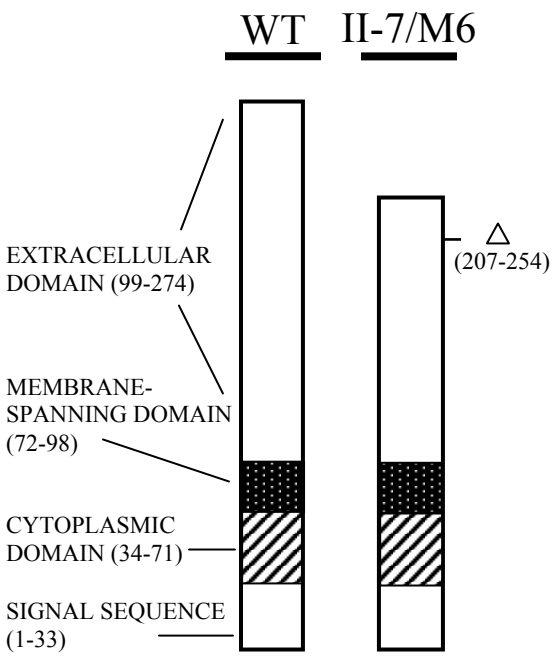
WT
II-7/M6
EXTRACELLULAR DOMAIN (99-274)
MEMBRANE-SPANNING DOMAIN (72-98)
CYTOPLASMIC DOMAIN (34-71)
SIGNAL SEQUENCE (1-33)
△ (207-254)

accessibility and radioimmunoprecipitation of P30 using intact cells (Dallo *et al.*, 1996; Layh-Schmitt *et al.*, 1997). The P30 C-terminal domain contains three different types of proline-rich, 6-amino-acid repeats. The first, designated A (PGMAPR), is repeated seven times, type B (PGMPPH), is repeated three times, and type C (PGFPPQ), is likewise repeated three times (Dallo *et al.*, 1996). The role of these proline repeats in P30 function is unknown. In-frame deletions within the C-terminal repeat region of P30 result in a cytadherence-negative phenotype (mutants II-7/M6,M7) (Dallo *et al.*, 1996; Layh-Schmitt *et al.*, 1997), and in the mutants tested (II-7/M6), decreased stability of protein P65 (Jordan *et al.*, 2001).

Not including homologs in the closely related species *M. genitalium* and *M. gallisepticum*, no significant homology exists between P30 and what is found in the current sequence database. *M. pneumoniae* protein P30 has one homolog in *M. genitalium* (P32) (Reddy *et al.*, 1995), and two in *M. gallisepticum* (MCG2, PvpA) (Boguslavsky *et al.*, 2000; Hnatow *et al.*, 1998) (Figure 3). The predicted membrane-spanning region and part of the surface-exposed domain are highly conserved in the P30 homolog P32 of closely related *M. genitalium* (94.4% identical and 96.3% similar) (Figure 4). *M. genitalium*, like *M. pneumoniae*, is a human pathogen that exhibits gliding motility, a similar flask-shaped morphology, and a polar attachment organelle (Razin and Jacobs, 1992). Interestingly, P32 is also encoded in an operon similar in organization to that of *M. pneumoniae*, which includes a homolog to *M. pneumoniae* cytadherence-related protein HMW3 (Reddy *et al.*, 1995).

Like P30 in *M. pneumoniae* and P32 in *M. genitalium*, MGC2 was localized to the attachment organelle equivalent in *M. gallisepticum*, as demonstrated by immunoelectron

Figure 3. Boxshade of *M. pneumonaie* protein P30 (MPN P30) (Baseman *et al.*, 1987), *M. genitalium* homolog P32 (MGN P32) (Reddy *et al.*, 1995), and *M. gallisepticum* homologs MGC2 (Hnatow *et al.*, 1998) and PvpA (Boguslavsky *et al.*, 2000). Black blocks indicate identity between all sequences, dark grey boxes indicate identity between at least 2 sequences, and light grey blocks indicate similarity. *M. pneumoniae* protein P30 is 49.8% identical and 54.5% similar to P32, 46.1% identical and 56.2% similar to MCG2, and 34.4% identical and 42% similar to PvpA, as analyzed by the GAP alignment program from the Sequence Analysis Software Package of the Genetics Computer Group.

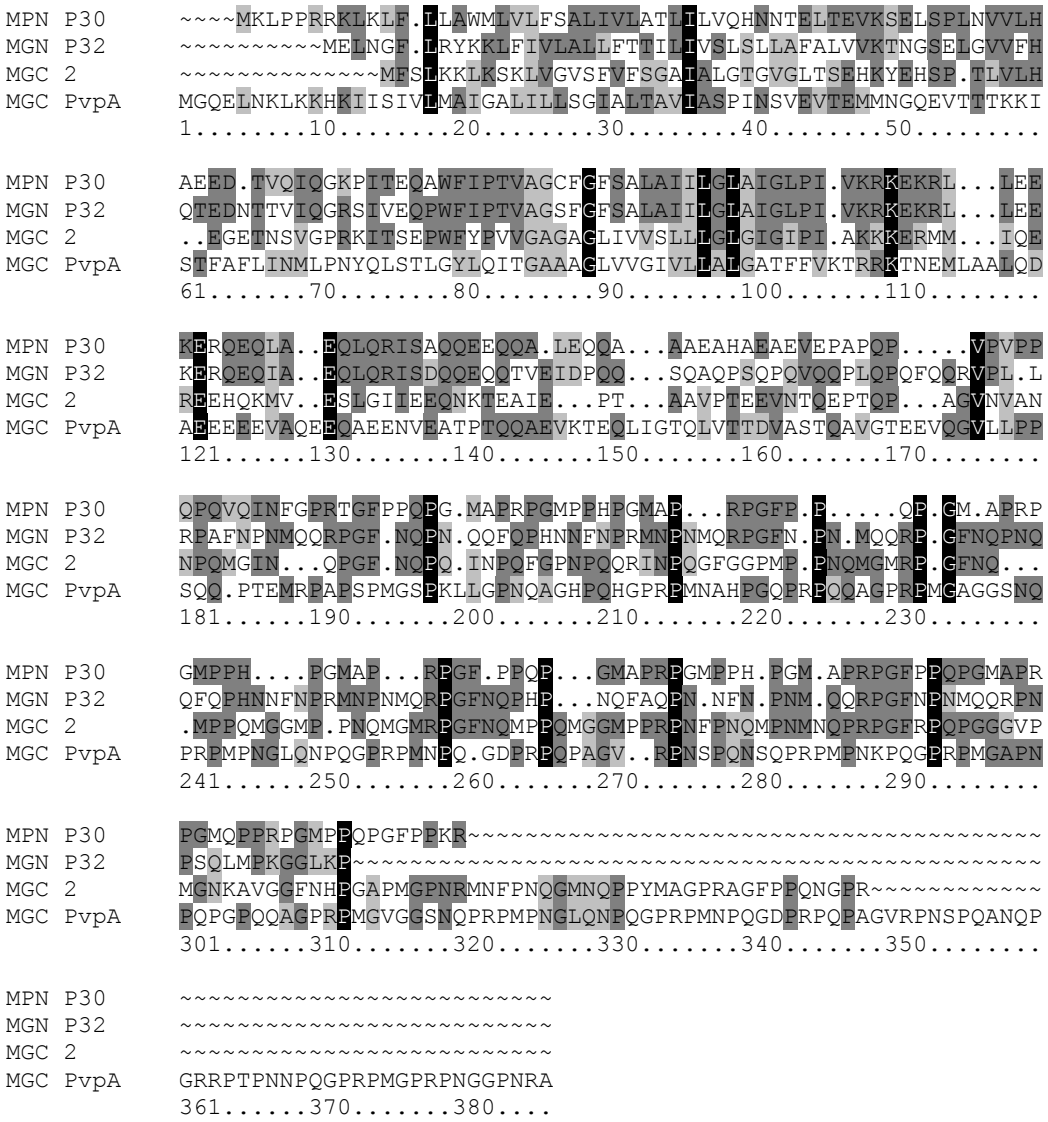
MPN P30
MGN P32
MGC 2
MGC PvpA
1.....10.....20.....30.....40.....50.....
61.....70.....80.....90.....100.....110.....
121.....130.....140.....150.....160.....170.....
181.....190.....200.....210.....220.....230.....
241.....250.....260.....270.....280.....290.....
301.....310.....320.....330.....340.....350.....
361.....370.....380....

Figure 4. Boxshade of *M. pneumonaie* protein P30 and *M. genitalium* homolog P32. Black blocks indicate identity, grey blocks indicate similarity. *M. pneumoniae* protein P30 is 49.8% identical and 54.5% similar to P32 over the entire protein and (96.2% identical, and 98.1% similar) in the predicted transmembrane domain and part of surface exposed domain (amino acids 73-125, indicate by bracket) as analyzed by the GAP alignment program from the Sequence Analysis Software Package of the Genetics Computer Group.

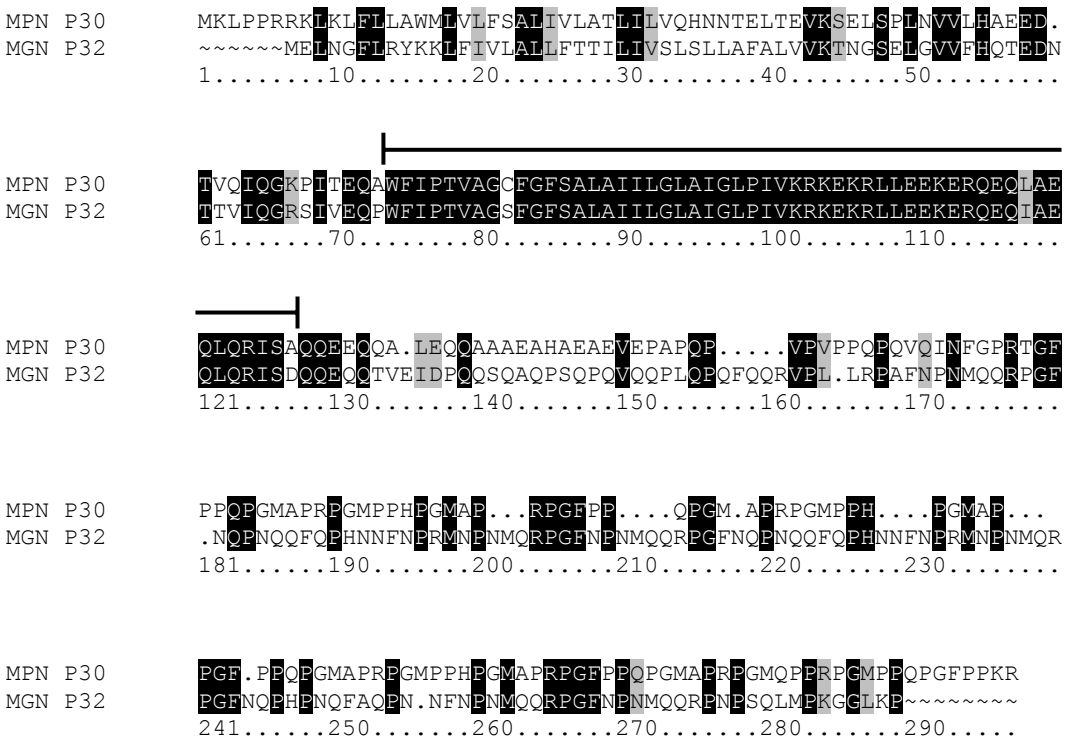
MPN P30 MKLPPRRKLKLFLLAWMLVLFSALIVLATLILVQHNNTELTEVKSELSPLNVVLHAEED.
MGN P32 ~~~~~~MELNGFLRYKKLFIVLALLFTTILIVSLSLLAFALVVKTNGSELGVVFHQTEDN
1.....10.....20.....30.....40.....50.....
MPN P30 TVQIQGKPITEQAWFIPTVAGCFGFSALAIILGLAIGLPIVKRKEKRLLEEKERQEQLAE
MGN P32 TTVIQGRSIVEQPWFIPTVAGSFGFSALAIILGLAIGLPIVKRKEKRLLEEKERQEQIAE
61.....70.....80.....90.....100.....110.....
MPN P30 QLQRISAQQEEQQA.LEQQAAAEAHAEAEVEPAPQP.....VPVPPQPQVQINFGPRTGF
MGN P32 QLQRISDQQEQQTVEIDPQQSQAQPSQPQVQQPLQPQFQQRVPL.LRPAFNPNMQQRPGF
121.....130.....140.....150.....160.....170.....
MPN P30 PPQPGMAPRPGMPPHPGMAP...RPGFPP....QPGM.APRPGMPPH....PGMAP...
MGN P32 .NQPNQQFQPHNNFNPRMNPNMQRPGFNPNMQQRPGFNQPNQQFQPHNNFNPRMNPNMQR
181.....190.....200.....210.....220.....230.....
MPN P30 PGF.PPQPGMAPRPGMPPHPGMAPRPGFPPQPGMAPRPGMQPPRPGMPPQPGFPPKR
MGN P32 PGFNQPHPNQFAQPN.NFNPNMQQRPGFNPNMQQRPNPSQLMPKGGLKP~~~~~~~~
241.....250.....260.....270.....280.....290.....

microscopy. Antiserum against MGC2 likewise inhibited attachment of *M. gallisepticum* to chicken embryo fibroblast cells (Hnatow *et al.*, 1998). PvpA, a second P30 homolog in *M. gallisepticum*, is localized to the terminal structure and has an extracellular exposed C-terminus (Boguslavsky *et al.*, 2000). PvpA was found to exhibit phase and antigenic variation with size variable mutants of PvpA resulting from deletions in the region encoding the proline-rich C-terminal region. Phase variation of PvpA was controlled at the translational level, as transcripts detected for *pvpA* were found in strains producing and lacking PvpA. A nonsense mutation resulting in premature termination at the N-terminal end of PvpA was found in the PvpA-negative isolates (Boguslavsky *et al.*, 2000). Possibly due to the mechanism of variation in the PvpA-negative isolates, no mutants where found containing reversible switching events, suggesting that the original switching was either irreversible or occurs at a low frequency (Boguslavsky *et al.*, 2000).

The spontaneously arising non-hemadsorbing mutants of *M. pneumoniae* designated: II-3, II-7, M6, and M7 (Dallo *et al.*, 1990; Dallo *et al.*, 1996; Layh-Schmitt *et al.*, 1997) lack P30 (mutant II-3), or produce a truncated, non-functional, P30 (Dallo *et al.*, 1996). Mutant II-3 was shown to contain a single nucleotide deletion at position 453 in the *p30* gene, resulting in a frameshift mutation (Romero-Arroyo *et al.*, 1999). Despite the change in reading frame, the altered *p30* gene in this mutant was predicted to yield a product only slightly shorter than the wild-type *p30* gene product. However, this modified P30 was not detected with antibodies generated against synthetic peptides from two different regions encoded by the altered reading frame (Romero-Arroyo *et al.*, 1999), suggesting that rapid turnover of this altered protein most likely occurs. Mutant II-3 exhibits a conspicuous, star-shaped morphology different from the typical flask-shaped

appearance of wild-type *M. pneumoniae* cells (Romero-Arroyo *et al.*, 1999). The P30 defect in mutant II-7 results from a 144-bp internal deletion near the 3' end of the *p30* gene. Mutant II-7 produces a stable 25-kDa truncated P30 (Dallo *et al.*, 1996). This mutant has a morphology similar to that of the II-3 mutant early in culture, but with time assumes a more wild-type appearance (Romero-Arroyo *et al.*, 1999). P30 mutant M6 contains an identical mutation to that in mutant II-7, in addition to a frameshift mutation in the gene encoding the cytadherence accessory protein HMW1 (Layh-Schmitt *et al.*, 1995). Mutant M7 produces a 22-kDa truncated P30, the result of a 216-nucleotide internal deletion near the 3' end of the *p30* gene (Layh-Schmitt *et al.*, 1997). Interestingly, all P30 mutants capable of producing P30 contain deletions terminating at nucleotide 764 of the 825 base-pair gene, suggesting that the C-terminal region of P30 may be important for its stability.

Like other cytadherence-related proteins, P30 localizes to the attachment organelle in wild-type *M. pneumoniae*. However, unlike non-cytadhering mutants lacking HMW1 (Hahn *et al.*, 1998; Seto and Miyata, 2003) or HMW3 (Willby and Krause, 2002), P30 does not appear to be necessary in the trafficking of P1 to the attachment organelle, as P1 localizes to a pole in mutant II-3 based on immunoelectron and immunofluorescent microscopy (Hahn *et al.*, 1998; Seto and Miyata, 2003). Additionally, a truncated P30 (mutant M7), did not affect the ability of P1 to associate with the Triton shell (Layh-Schmitt and Harkenthal, 1999). Protein P30 does appear to affect protein P65, the absence (mutant II-3) or truncation (mutant II-7) of P30 has downstream effects on P65 stability yet does not hinder its proper localization (Jordan *et al.*, 2001).

Cell Division

Observations of living cells growing in liquid culture media by using phase contrast microscopy substantiated previous experimental evidence for binary fission in *M. pneumoniae* (Furness, 1970) (Baseman and Tully, 1997). The doubling time of *M. pneumoniae* grown *in vitro* is highly variable, ranging from 3h (Bredt, 1968), 6.5h (Furness, 1970), and 19h (Smith, 1967). Differences between media components and methods of growth rate determination could explain the inconsistencies in those studies (Bredt, 1968). The current model of cell division in *M. pneumoniae* begins with the cessation of gliding motility (Bredt, 1968). Gliding motility is also suspended during cell division in *Flavobacterium johnsoniae* and several genera of myxobacteria (Kempf and McBride, 2000). Fields of cells from electron micrograph and epifluorescent images of fixed cells labeled with P1-specific antibodies to identify the attachment organelle suggest that the nascent tip forms adjacent to the existing tip and is translocated to the opposite pole of the dividing cell before cytokinesis occurs (Krause, 1998; Seto *et al.*, 2001). When the nascent tip encounters the trailing end of the mycoplasma, gliding motility resumes and cytokinesis occurs. Limitations arising from the minute size of *M. pneumoniae* cells have so far precluded visualization of nascent tip formation *in vivo*. Perhaps with GFP technology (Chalfie *et al.*, 1994), division of *M. pneumoniae* in living cells can be observed in the future. *M. gallisepticum* was also shown to divide by binary fission, and division was synchronous with DNA replication (Labarere, 1992). Like *M. genitalium* and *M. pneumoniae*, *M. gallisepticum* has a terminal structure. Furthermore, many of the genes encoding proteins involved in the proper functioning or formation of the tip in *M. pneumoniae*, including *p30*, have homologs in this species as well. There is

evidence that mycoplasma DNA is physically complexed with the specialized tip structure in *M. gallisepticum*, suggesting that membrane synthesis may be coordinated with segregation of the chromosome during division (Maniloff and Quinlan, 1974). With what is known about the coordination of the attachment organelle with DNA replication, this may indeed be the case with *M. pneumoniae*.

Relationship Between Tip Duplication and Cell Division- The coordination of DNA replication with tip duplication in *M. pneumoniae* was substantiated by Seto et al. (Seto *et al.*, 2001). In those studies, log phase wild-type *M. pneumoniae* cells were fixed and labeled with the DNA stain DAPI to identify the nucleoid, and anti-P1 antibodies to label the attachment organelle. DAPI fluorescence was then quantified for each cell. Chromosome equivalents (ranging from 1 to 2) were determined and each cell was classified as to which stage of cell division was occurring at the time of fixation. P1 fluorescence was also noted in these cells and correlated with chromosome equivalency. Cells with only one genome contained one P1 focus (attachment organelle). As DAPI fluorescence increased from 1 to 1.5 chromosome equivalents, two P1 foci were evident and located adjacent to each other. Cells containing the equivalent of 2 genomes contained two P1 foci located at opposite poles of the cell. In these cells, two distinct nucleoids were also seen in the images, indicative of the chromosome segregation point of cell division (Figure 5). It is not known if cessation of motility occurs strictly before chromosome segregation or throughout the whole cell division process including the initial duplication of the attachment organelle. Based on the phase-contrast studies of

Figure 5. Illustration of the coordination of tip duplication with DNA replication in *M. pneumoniae.* Figure modified from Seto et. al. (Seto *et al.*, 2001); Intensity of blue nucleoid correlates with genomic content.

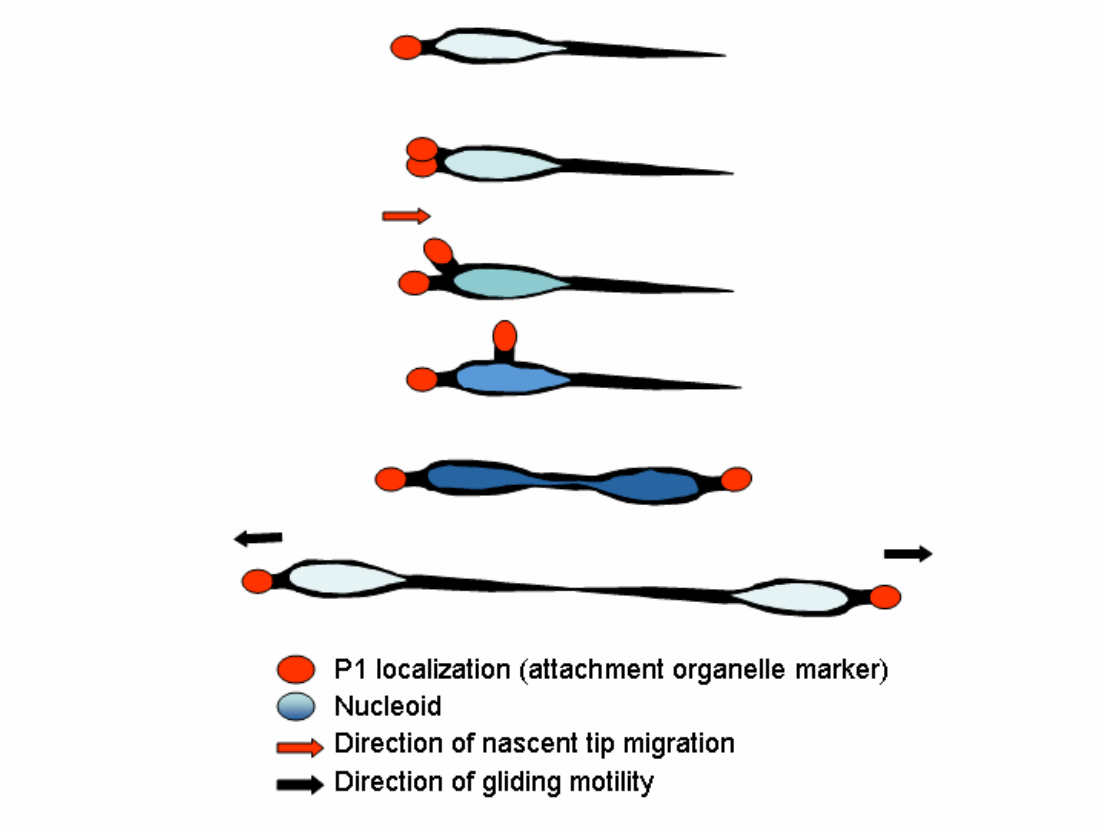
P1 localization (attachment organelle marker)
Nucleoid
Direction of nascent tip migration
Direction of gliding motility

Bredt (Bredt, 1968), at this point the dividing cell begins cytokinesis with the two daughter cells separating by gliding motility, with the tip being the leading end.

Due to the limitations in the resolution of phase-contrast microscopy, translocation of an unlabelled nascent tip to the opposite pole has not been visually documented in living cells. Seto's data substantiate a model previously formed by grouping scanning electron micrographs into morphologically similar phases. In these SEM images, nascent tips can be seen in various stages of translocation to the opposite pole of the cell (Boatman, 1979). Based on current data, as DNA replication begins a tip is likewise duplicated adjacent to the existing one. As the DNA replication process proceeds, the nascent tip translocates to the opposite pole of the cell (trailing end) (Figure 5). Protein P1 (Seto *et al.*, 2001), and HMW2 (Balish *et al.*, 2003) are components of the nascent attachment organelle during the process of translocation. It is not known if other tip-associated proteins are components of the tip before translocation to the opposite pole occurs.

Assembly of the Attachment Organelle - For *M. pneumoniae* cytadherence to take place a complex interaction of various adhesin and accessory proteins must occur (Figure 6). To illustrate the interdependence of the cytadherence proteins, absence or malfunction of any protein in this complex will affect either the stability, localization, or both of the other protein(s). Table 1 compares the steady state levels of various cytadherence proteins in the cytadherence mutants. Immunofluorescent microscopy (IFM) is the current methodology to determine the assembly order sequence of cytadherence proteins forming a functional attachment organelle in *M. pneumoniae*. Labeling wild-type and cytadherence mutant cells with anti-bodies against the various

Figure 6. Depiction of the location of cytadherence proteins in *M. pneumoniae*. Upper left panel is a TEM of the attachment organelle of *M. pneumoniae* parasitizing hamster tracheal epithelium, showing terminal button and electron dense core. Lower left cartoon represents the localization of several cytadherence proteins of *M. pneumoniae* modified from Balish and Krause (Balish and Krause, 2002). HMW2 is believed to be a component of the electron-dense core (Balish *et al.*, 2003), yet the exact spatial relationship between HMW2 and other cytadherence proteins in the attachment organelle is unclear. Scale bar is 250nm.

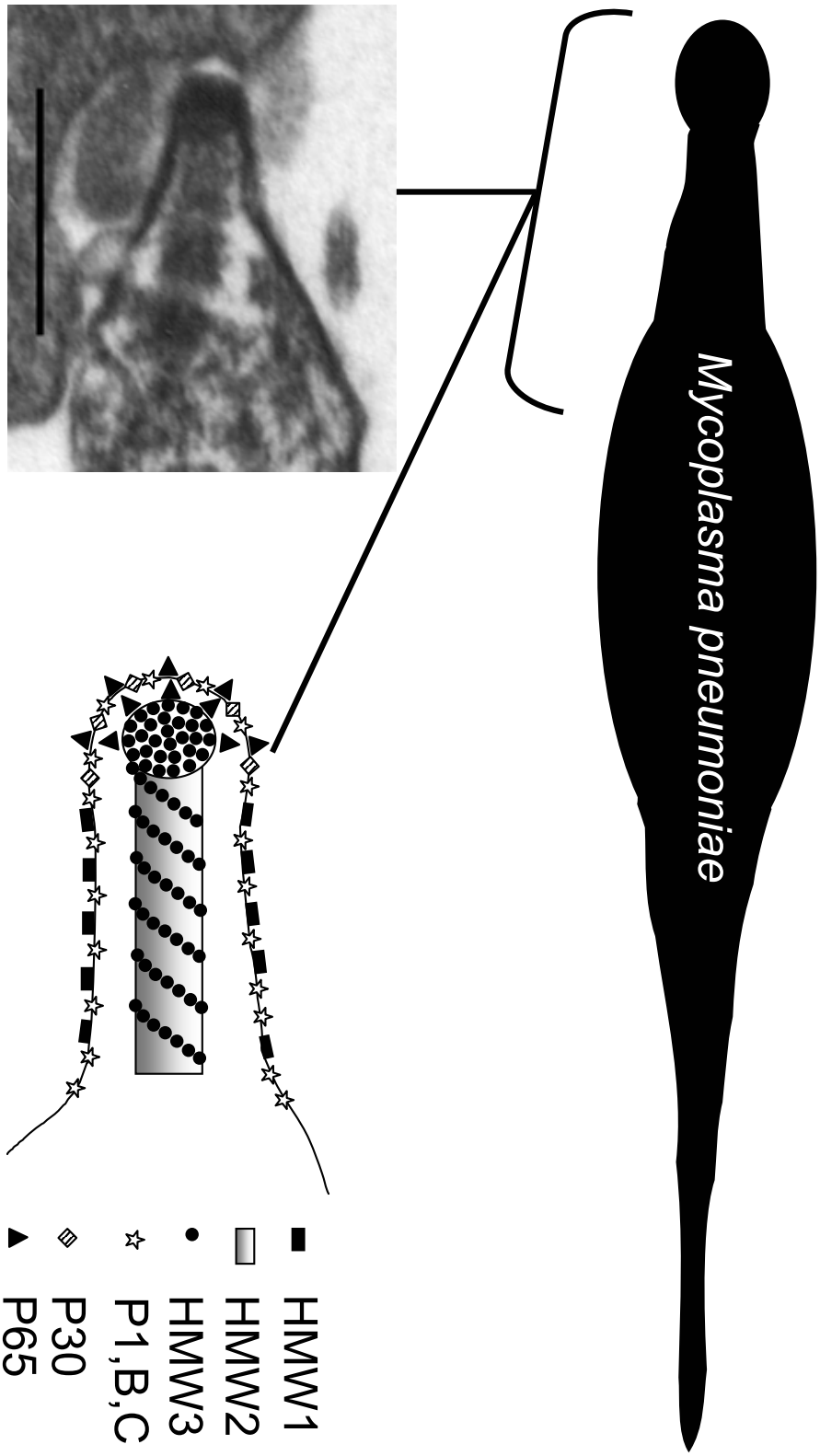
Mycoplasma pneumoniae
HMW1
HMW2
HMW3
P1,B,C
P30
P65

Table 1. Steady-state levels of cytadherence proteins in *M. pneumoniae* mutants.

	P1	B/C	P30	HMW1	HMW2	HMW3	P65
I-2	+++	+++	++	+	-	+	+
II-3	+++	+++	-	+++	+++	+++	++
II-7	+++	+++	++Δ	+++	+++	+++	++
III-4	+++	-	+++	+++	+++	+++	+++
IV-22	-	-	+++	+++	+++	+++	+++
M6	+++	+++	++Δ	-	+	+	+
hmw3-	+++	+++	+++	+++	+++	-	++

Modified from Balish and Krause (2002). +++ indicates wild-type levels, ++ indicates intermediate levels, + indicates low levels, - indicates none detected, Δ indicates a truncated P30.

cytadherence proteins has given insight as to which proteins are required for the subsequent proper localization of others. By using this approach the following model of tip assembly was proposed. HMW2 is not required for the proper localization of HMW1 and HMW3 although the stability of these proteins requires HMW2 (Seto and Miyata, 2003). P1 localization appears to be at least partly affected by the absence of HMW2, P1 staining was more diffuse in this mutant in comparison with the wild-type strain. Proteins B, C, P65, and P30 were faint to undetectable by IFM (Seto and Miyata, 2003). Proteins HMW1, HMW3, P1, P30, and P65 were localized in mutant III-4, which lacks proteins A, B, and C. This was in contrast to an earlier publication where P1 was found to be non-localized in mutant III-4 using immuno-electron microscopy (Baseman *et al.*, 1982). In mutant IV-22, which lacks A, B, C, and adhesin P1, proteins HMW1, HMW3, P30, and P65 were localized to a pole. Mutant M6 complemented with the wild-type *p30* allele, thus creating an HMW1 null mutant failed to localize HMW3, B, C, P30, P65, and P1 (Seto and Miyata, 2003). Localization of HMW2 has only been possible to date by GFP technology, which creates problems in maintaining selection of these constructs in mutants already supporting the Tn*4001* transposon. Although double transformation incorporating a cat derivative of Tn*4001* has been demonstrated (Hahn *et al.*, 1999)**,** the burden of multiple selection could potentially complicate interpretation of data. Electron-dense core formation appeared to be independent of proteins A, B, C, P1, P30, and P65 (Seto and Miyata, 2003). The absence of cores as visualized in thin sections of mutant M6, and I-2 cells by TEM indicates the importance of HMW1 and HMW2 for electron dense core formation (Seto and Miyata, 2003). HMW1 and HMW3 localization is independent of proteins HMW2, A, B, C, P1, P30, and P65. Additionally, spatial

differences were observed between the colocalized HMW1, and HMW3 proteins to that of P30, and P65 which also colocalized yet more distally noting that this distinction was more prominent in mutants lacking proteins A, B, and C (Seto and Miyata, 2003). A colocalization was also noted with proteins B, C, and adhesin P1; these were described as being more diffuse than HMW1, HMW3, P30, and P65, originating at the distal portion of the tip occupied by P30 and P65 and exceeding the entire length of the attachment organelle.

Gliding Motility

Gliding motility can be defined as locomotion across surfaces without the aid of flagella. Exhibited throughout many branches of the eubacterial phylogenetic tree (McBride, 2001), this poorly understood form of motility was first described in the mycoplasmas (*M. pulmonis*, a respiratory pathogen of mice and rats), in 1946 (Kirchhoff, 1992). Today the list of gliding mycoplasmas also includes: *M. pneumoniae*, *M. gallisepticum*, *M. genitalium*, and *M. mobile*. Interestingly, all mycoplasmas known to exhibit gliding motility possess a distinct terminal structure. This structure is conspicuously absent in all non-motile species with the exceptions of *Mycoplasma alvi*, *Mycoplasma sualvi*, and *Mycoplasma pirum* (Kirchhoff, 1992). This is quite remarkable considering that there are over 170 mycoplasmas so far discovered. Gliding motility studies in these species and mycoplasmas in general, however, have been historically lacking or preliminary at best. Inevitably, with more effort and technological advances being applied at reproducing the natural conditions where the mycoplasmas are found, more mycoplasmal species will likely be found capable of motility.

Although many eubacterial genera are capable of gliding (McBride, 2001), no homologs have been found to the known motility proteins in these organisms in the three sequenced gliding mycoplasmas (Miyata, 2002). In addition to the presumably novel mechanism of gliding in the mycoplasmas (Miyata, 2002), several differences exist between the gliding mycoplasmas. For example, motility in *M. pulmonis* was lost after the sixth passage *in vitro* while gliding in *M. pneumoniae* was found to be a more stable phenotype still evident after several hundred passages on artificial medium (Bredt, 1979). Gliding in *M. mobile* was also found to be considerably more stable than in *M. pulmonis*. The affects of passaging on motility of different mycoplasmal species is another variable to consider when analyzing isolates for this property.

Gliding motility only occurs on a solid-liquid interface and is oriented in the direction of the mycoplasma terminal structure (Kirchhoff, 1992). Excluding the putative fish pathogen *M. mobile*, there is a well-demarcated nap on the known gliding mycoplasmas. This surface layer is restricted to the terminal structure in *M. pneumoniae* and *M. genitalium* (Kirchhoff, 1992). A recent morphological study of three gliding mycoplasmas (*M. pneumoniae*, *M. gallisepticum*, and *M. mobile*) using the freeze-substitution technique indicated the presence of an outer layer of material in the terminal structure (head) of *M. mobile* (Shimizu and Miyata, 2002). This layer could be a functional homolog to the nap layer seen in the other gliding mycoplasmas. The role, if any, of the nap layer in gliding motility remains to be studied.

Optics- The extremely small size of this filterable organism makes study using light microscopy difficult. Most such studies have been performed using phase-contrast optics with oil immersion objectives. More recent motility studies with *M. mobile* were

performed using dark-field microscopy and long time exposures enabling the researchers to trace the motility tracks from the negative images and quantify motility path lengths and velocities (Rosengarten and Kirchhoff, 1987).

Characteristics- Published studies on gliding motility in *M. pneumoniae* were primarily performed prior to the 1980s, with all studies to date utilizing the FH wild-type strain, not the M129 wild-type strain for which genome sequence data are available and on which cytadherence research has mostly focused. Furthermore, the *M. pneumoniae* cytadherence mutants have not been evaluated comprehensively for motility. Motility studies of *M. pneumoniae* cells *in vitro* portray movement only in the direction of the attachment organelle (Bredt, 1968) in linear and circular patterns interrupted by resting periods of various times and frequencies (Radestock and Bredt, 1977). *M. pulmonis* cells were found to glide in a more linear fashion than *M. pneumonaie*, with a decreased percentage of resting periods and cells being generally more active than what has been observed with *M. pneumoniae* (Bredt, 1979). Resting periods where also observed in motility studies of *M. genitalium*, and *M. gallisepticum* (Kirchhoff, 1992). Unfortunately, the characterization of *M. genitalium* gliding is limited to information published from a poster abstract (Taylor-Robinson and Bredt, 1983). Resting periods, however, are absent in *M. mobile* (Miyata *et al.*, 2000), the fastest known mycoplasma glider. The mechanisms for motility are poorly understood for any gliding mycoplasma and it is possible that different mechanisms exist between the motile species of mycoplasma.

Chemotaxis and rheotaxis (response to chemical and flow velocity gradients, respectively) have been observed in *M. mobile* (Kirchhoff, 1992). Both *M. pneumoniae* and *M. pulmonis* have been demonstrated experimentally to employ chemotaxis, albeit

much less efficiently than *M. mobile*. It is thought that the slower average velocity of gliding in *M. pneumoniae* (0.03-0.4 μm/s) and *M. pulmonis* (0.4-0.7 μm/s) compared to an average velocity of 2.0-4.5 μm/s in *M. mobile*, could account for this (Kirchhoff, 1992). Rheotaxis has not been tested in any other motile mycoplasma besides *M. mobile*, probably owing to their slower velocities and the necessity of observing these strains in incubation chambers using time-lapse microcinematography. In recent rheotactic experiments, *M. mobile* was shown to achieve a gliding force of 26-28 pN, which is equivalent to five to seven times that of myosin and kinesin (Miyata *et al.*, 2002).

***In vitro* Conditions Conducive to Motility**- *M. mobile*, which is associated with the gills of a freshwater fish, is the fastest known glider of all mycoplasmas and can be studied at ambient temperature, unlike other pathogenic mycoplasmas (Kirchhoff, 1992). Motility in the gliding mycoplasmas is temperature-dependent requiring conditions close to their optimal growth temperatures. In *M. mobile*, velocity increases in a linear fashion with temperature up to 36.5°C, after which cell adherence is compromised. Interestingly, cells still capable of binding at higher temperatures exhibit increasing velocities, suggesting that the adhesion complex is more heat susceptible than the motility apparatus, although motility is dependent on adhesion (Miyata *et al.*, 2002).

The velocity of gliding motility in *M. gallisepticum*, *M. genitalium*, and *M. pneumoniae* observed *in vitro* is optimized with the addition of 1-3% gelatin to the medium. Quantitative motility observations in *M. pneumoniae* require the use of 1-3% gelatin to help facilitate attachment to the glass substrate (Bredt, 1979). Increasing the viscosity of the medium by the addition of gelatin at concentrations of 5% or greater, however, results in reductions in gliding velocity (Radestock and Bredt, 1977). Motility

studies in *M. pulmonis* do not require the addition of gelatin (Bredt, 1979). Similarly, motility of *M. mobile* was optimal in medium not containing gelatin, as increases in medium viscosity correlate with decreases in gliding velocity in this organism (Kirchhoff, 1992).

Inhibitory Agents- The molecular basis as well as the nature of energy supply for gliding motility in the mycoplasmas is unknown (Rosengarten and Kirchhoff, 1988). Gliding motility in *M. pneumoniae* and *M. mobile* is severely inhibited by the DNA cross-linking agent mitomycin C (MMC; 2.5 and 0.4 μg/ml respectively) (Kirchhoff, 1992). *M. pneumoniae* has been shown to cease gliding motility during cell division (Bredt, 1968), thus the affect of MMC treatment is not surprising, as this would delay the process to complete DNA replication. Inhibition of motility in *M. pneumoniae* and *M. mobile* is also observed upon treatment with the protein thiol modifying agent *ρ*-chloromercuribenzoate (PCMB; 0.5 mM and 30 μg/ml respectively). Iodoacetate treatment of *M. pneumoniae* and *M. mobile* (2.5 mM and 2 μg/ml respectively) also result in motility inhibition in these species. Interestingly, both of these agents are thiol-reactive and inhibit gliding at inhibitory and sub-inhibitory concentrations (Bredt, 1979). The role of sulfhydryl-containing proteins in gliding motility, however, is unknown. Depending on the concentration, antiserum against whole cell antigen has also been shown to reversibly inhibit gliding in *M. pneumoniae* and *M. mobile* (Kirchhoff, 1992). These data should be interpreted cautiously, however, as indirect affects on metabolism as well as the possibility of preventing or occluding proper attachment of the mycoplasma could be a factor in motility inhibition.

Motility Mutants- In many gliding bacteria, motility has also been visualized as satellite growth on a solid medium with a low agar concentration, and the colonial morphology generally correlates with cellular motility (Burchard, 1981). Evidence of satellite growth has also been demonstrated in *Spiroplasma* and *M. mobile* (Miyata *et al.*, 2000). Although no motility mutants in *M. pneumoniae*, *M. genitalium*, *M. pulmonis* or *M. gallisepticum* have been characterized, several UV-generated motility mutants in *M. mobile* have been isolated and partially characterized (Miyata *et al.*, 2000). The motility mutants were screened by colonial morphology differences in soft agar. The partial characterization of these motility mutants revealed a positive correlation between gliding motility and the ability to hemadsorb. For example, in one mutant designated m6, the velocity of gliding was determined to be 50% that of wild-type, while hemadsorption and binding to glass were 24% and 54% respectively. Mutants found to have higher relative gliding speeds than wild-type were also noted to have a higher hemadsorption activity. Interestingly, *M. mobile* motility mutants with a rounded cellular morphology were found to have higher relative gliding speeds than the flask-shaped wild-type strain (Miyata *et al.*, 2000). Although binding to glass seems to be dependent on a 349-kDa acidic protein (Miyata *et al.*, 2002), little is known about the molecular defects in these non-motile mutants, as they are products of UV mutagenesis and further characterization for possible secondary mutations has been lacking.

Soft agar screening for motility mutants has also been used to isolate a motility mutant of *Spiroplasma citri* (Jacob *et al.*, 1997). A member of the class *Mollicutes*, *S. citri* is motile by rotation and undulation in a highly viscous medium. The *scm1* gene was identified in *S. citri* by transposon mutagenesis. Motility in the *scm1* insertion mutant was

complemented by transformation with the wild-type recombinant *scm1* gene. Not surprisingly, no homology is found to this gene in *M. pneumoniae* or *M. genitalium*, as gliding motility and the rotatory and flexional movements in this helical species of *Mollicutes* are clearly different.

In the host, motility presumably helps *M. pneumoniae* to overcome mucociliary clearance and reach the base of the cilia and microvilli, where they have been shown to colonize. It is tempting to speculate that gliding is a virulence determinant, but without a motility mutant still capable of cytadherence, this hypothesis will remain untested.

M. pneumoniae Infection Studies

Animal Studies- Although some studies have been done using human tracheal tissue, infections involving hamster tracheal epithelium with *M. pneumoniae* parallel one another in the onset, nature, duration, and resolution of respiratory disease (Cimolai *et al.*, 1992). Localization and morphology of mycoplasmas is also consistent between naturally and experimentally infected tissue (Collier and Clyde, 1974). Importantly, some differences were observed with the localization of mycoplasma receptors between hamster and human respiratory epithelium (Loveless *et al.*, 1992).

Tracheal Epithelium- The pseudostratified columnar ciliated epithelium rests on a basement membrane and two rows of basal cells in hamsters with two or more layers of nuclei evident in human respiratory epithelium (Becci *et al.*, 1978). In general, there are at least 3 distinct cellular types composing tracheal epithelium. Ascendant to the basement membrane is a layer of basal cells. In basal cells, the nucleus occupies a voluminous portion of the total cellular volume (Rhodin, 1966). Basal cells represent a poorly differentiated cell; healthy respiratory epithelium is constantly being renewed as

old epithelial cells dislodge themselves and are replaced by newly differentiated cells arising from the basal layer (Yayoshi, 1983). Goblet cells represent the mucous-producing cell of the epithelium and span the basement membrane to the epithelial surface. The base of the goblet cells tapers off considerably and appears to be more elongated elsewhere, perhaps due to the depth of the epithelium to the basement membrane. Swelling of these cells due to accumulations of mucous granules towards the luminal surface give these cells their characteristic goblet shape. After fusion of the mucin granules, discharge occurs by expulsion of the content of the goblet. Mucous disgorged by the goblet cells is drawn out into strands by the beating cilia (Sleigh, 1981). However, Mucous secretion in the human trachea is mostly due to the activity of the submucosal glands with a lesser contribution from goblet cells (Rhodin, 1966). In contrast, the scarcity of glands in hamster tracheal epithelium requires the vast majority of mucin to be produced by goblet cells.

Hamster tracheal epithelium is ≥ 50% ciliated (Gabridge, 1983; Sleigh, 1981);(Becci *et al.*, 1978), consisting of cilia 4.5 to 5 μm in length and 0.25 μm in diameter (Gabridge, 1983; Sleigh, 1981). The ciliated cells generally span from the luminal surface to the basement membrane and are intermingled with microvillus projections of 0.150 μm in diameter and from 0.2 to 0.6 μm in length. Non-ciliated cells appear dome-shaped and contain microvilli of 0.350 μm in diameter by 0.4 μm in length. After fixation of tracheal rings from organ culture, only thin strands of mucus can be seen, as opposed to the thick mucousal blanket seen with fixed *in situ* hamster tracheal epithelium (Muse *et al.*, 1976).

Presumably, *M. pneumoniae* cells must traverse several μm of flowing mucous and percilliary fluid and withstand the steady, coordinated beating of cilia at a rate of 1200 beats per minute in order to colonize the host successfully (Gabridge, 1983). Only the tip of the cilia (0.5μm) contacts the mucous and is responsible for net movement (Sleigh, 1981). The remaining depth of the cilia is bathed in the perciliary fluid lying beneath the mucus layer (Figure 7). Depending on the species, host, and the inoculum, mycoplasmas can be seen along the membrane, between cilia, and even attached to ciliary tips of tracheal tissue (Gabridge, 1986). Wild-type *M. pneumoniae* observed on tracheal monolayers did not have a preferential distribution along any given cell. In this culture system they attached to host cells via the attachment organelle and in regions of few cilia or microvilli, they were also seen oriented horizontally along the membrane (Gabridge, 1983).

Infected hamster tracheal epithelium generally shows signs of pathology within 24-48 hours *in vitro*. This was determined by loss of cilia and the existence of extruded fragments of host epithelial cells (Muse *et al.*, 1976). Collier showed by various forms of microscopy that after 24 hours post-infection of hamster tracheal rings *in vitro*, that little changes were evident in ciliary activity and only a minute level of bound mycoplasma could be resolved by immunofluorescence (Collier *et al.*, 1971). By 48 hours post-infection, ciliary activity was slowed and the luminal surface of the tracheal ring exhibited a high presence of mycoplasma as determined by immunofluorescence microscopy (Collier *et al.*, 1971). In a separate study using TEM, numerous mycoplasmas were found among the cilia, covering the base of the cilia, microvilli, and luminal border at 48 hours (Collier *et al.*, 1971), with as many as 11 organisms attached at the base of

Figure 7. Localization of wild-type *M. pneumoniae* on respiratory epithelium. It is thought that gliding motility in *M. pneumoniae* facilitates the colonization of respiratory epithelium. The top cartoon represents the different components of healthy respiratory epithelium. After inhalation, *M. pneumoniae* is faced with the turbulent environment of the respiratory mucosa which is constantly being propelled upwards toward the larynx (mucociliary escalator). Gliding motility may help *M. pneumoniae* translocate through the mucosa eventually reaching the tips of cilia. After attachment to the cilia, the organism is thought to glide down the ciliary shaft in the perciliary fluid eventually occupying the base of ciliated epithelial cells where they are found to be heavily colonized in experimental and natural infections. Panels 1-6 illustrate what is thought to occur during the initial colonization process.

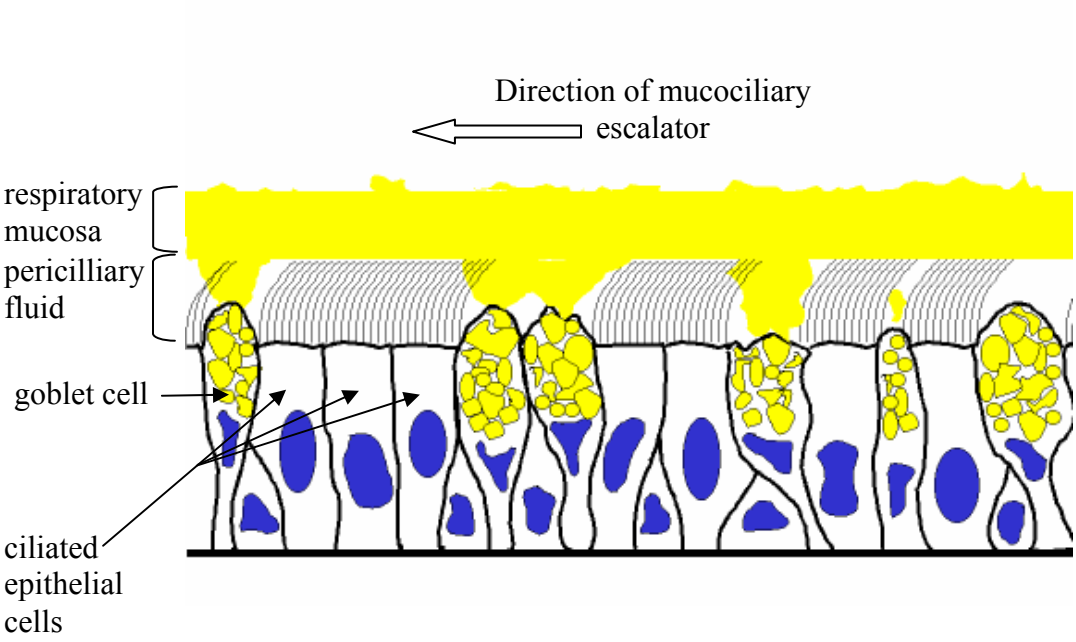
Direction of mucociliary escalator
respiratory mucosa
pericilliary fluid
goblet cell
ciliated epithelial cells

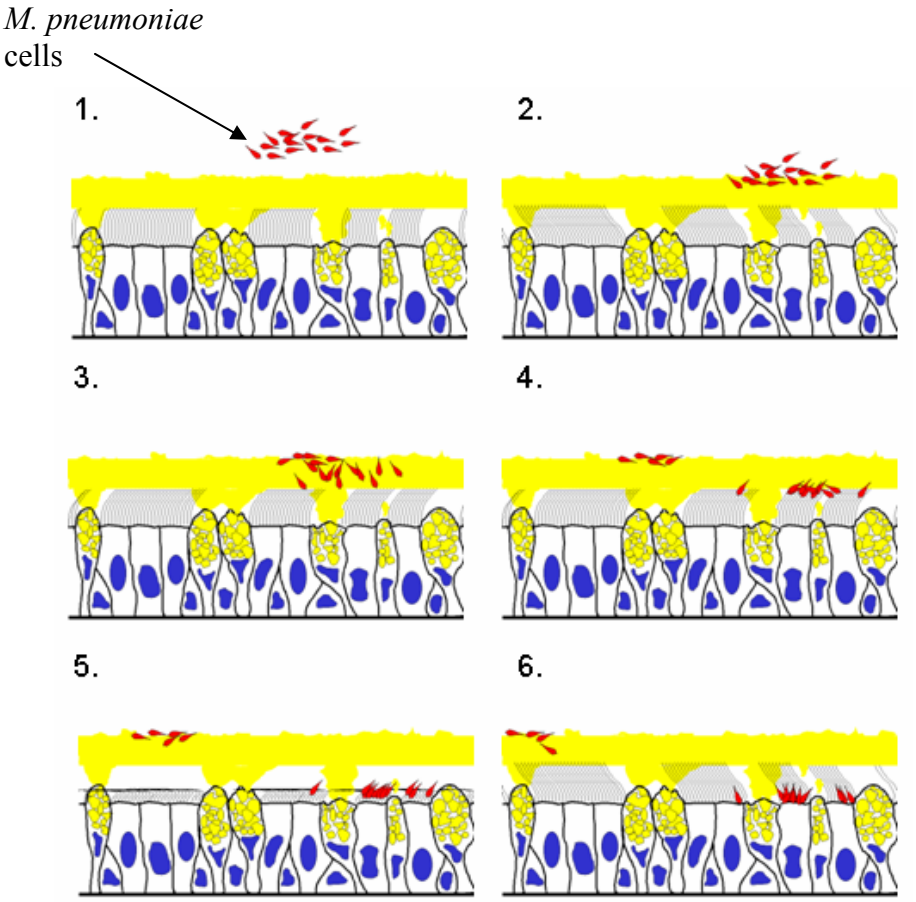
M. pneumoniae cells
1.
2.
3.
4.
5.
6.

the cilia spanning a single epithelial cell (Collier and Clyde, 1971). After 72 hours post-infection *in vitro*, wild-type *M. pneumoniae* cells were found in the junctional space between adjacent epithelial cells, with the attachment organelle oriented towards the epithelial surface (Collier and Baseman, 1973). Interestingly, localization of wild-type *M. pneumoniae* cells between the tight junctions of host cells was not seen in human tracheal rings (Collier and Baseman, 1973). By 72 hours post-infection tracheal rings showed progressive loss of cilia and sloughing of cells, with attached mycoplasmas being readily visible by scanning electron microscopy (SEM) (Muse *et al.*, 1976). TEM images revealed mycoplasmas between adjacent epithelial cells, and between the epithelium and the basement membrane (Collier *et al.*, 1971). In all TEM studies, no intracellular mycoplasmas were seen.

SEM Analysis- Structures recognizable as surface-attached mycoplasmas were not observed at either 24 or 48 hours post-infection when examined by SEM (Muse *et al.*, 1976). After 72h, mycoplasmas were seen at the base of cilia and on non-ciliated cells. There was an accumulation over the intercellular junctions with a scarcity of cells bound to the central region. By 96 hours post-infection, only sparse regions of ciliated cells were present, with non-ciliated microvilli-coated surfaces covered densely by *M. pneumoniae* predominating. At 96 hours much of the epithelial cell layer was lost, and localization of mycoplasmas was complicated. In another study, 96 hours post-infection the entire epithelium took on a squamous appearance with loss of organization and polarity of individual cells (Collier and Clyde, 1971). The uninfected tracheal ring epithelial surface, however, was well ciliated after 96 hours.

***In vivo* Infection Studies-** Infections with *M. gallisepticum* in chickens in vivo show similar responses as those seen in vitro, except that reduced production of mucous and an absence of an immunologic response are observed. It was noted in these studies that tracheal ring organ cultures were a reliable test system for the response of tracheal epithelium to *Mycoplasma* (Dykstra *et al.*, 1985). In *M. pneumoniae in vitro* infection studies, it was also noted that the destructive effects of the organism for tracheal cells are probably modified by the normal defenses of the intact host (Collier and Clyde, 1971). Tracheal rings *in vitro* show similar changes to those seen *in vivo*, except that exfoliation is more severe and occurs earlier. The subsequent changes to tracheal epithelium after infection with mycoplasma include release of mucous granules followed by exfoliation of ciliated and non-ciliated epithelial cells. Epithelial cells typically lose their intercellular connections, rounded, exfoliated, and then lysed, giving rise to a population of cellular organelles, such as mitochondria and cilia intermixed with mucous to form the exudate found within the tracheal lumen. Repair of the epithelial surface was effected by basilar epithelial cells differentiating and filling the spaces formed by exfoliated cells (Dykstra *et al.*, 1985).

GFP in mycoplasmas

First isolated from the jellyfish *Aequorea victoria* in 1971, (GFP) has become an important tool in studying protein localization and dynamics in prokaryotes (Margolin, 2000). Although sizeable (27-kDa) in comparison to common epitope tags, GFP requires only molecular oxygen to assume a fluorescence-competent conformation (Sullivan and Kay, 1998). Several mutant GFP forms have been derived from the original cloned gene, increasing the versatility of this protein (Margolin, 2000). For example, mutations with

direct effects on the fluorophore structure have resulted in fluorescent proteins with different spectral qualities (Sullivan and Kay, 1998). GFP mutants have also been obtained which have greater heat stability as well as increased brightness (Margolin, 2000). One such commercially available variant is EGFP, which fluoresces 35 times greater than wild-type GFP (GFPmut1;8-9) (Haas *et al.*, 1996). EGFP has a slightly red-shifted maximum excitation of 488 nm, while the maximum emission is 507 nm. Common fluorescein isothiocyanate (FITC) filter sets can be used to observe GFP and EGFP, making its use as a reporter protein accessible to many researchers (Margolin, 2000).

Until recently, GFP has not been used as a reporter in the mycoplasmas. In *M. pneumoniae*, a sandwich fusion of GFP and HMW2 was instrumental in localizing this cytadherence protein, as previous immunocytochemical methods were ineffective (Balish *et al.*, 2003). Expression of a non-translational GFP fusion in *M. pneumoniae* resulted in a diffuse signal consistent with a non-targeted protein (Ricci and University of Georgia., 1999). The construction and use of GFP reporter constructs to other *M. pneumoniae* cytadherence proteins should greatly facilitate our understanding of attachment organelle assembly and dynamics.

CHAPTER 3

MATERIALS AND METHODS

General Methods

Mycoplasma Strains and Culture Conditions- Wild-type, virulent *M. pneumoniae* strain M129 (Lipman and Clyde, 1969), broth passage 18, and derivatives thereof, were used in these studies including the spontaneously arising non-hemadsorbing mutants I-2, II-3, II-7, III-4, IV-22 (Krause *et al.*, 1982), *hmw3*:Tn*4001* (HMW3-) (Willby and Krause, 2002), and mutant M6 (Layh-Schmitt *et al.*, 1995). The hemadsorption-positive revertant II-3R, and mutant II-3 complemented with the recombinant wild-type *p30* allele, were described previously (Romero-Arroyo *et al.*, 1999), as was mutant I-2 complemented with the recombinant wild-type *hmw2* allele (Fisseha *et al.*, 1999). Mycoplasmas were cultured in Hayflick medium (Hayflick, 1965) with or without gentamicin (18 μg /ml) as required for selection and maintenance of Tn*4001* derivatives. Mycoplasma cells were harvested after incubation for approximately 72 h at 37˚C, when the phenol red pH indicator was orange (Stevens and Krause, 1992). All reagents used in these studies were purchased from Sigma Chemical Co., (St. Louis, Mo.) unless otherwise stated.

Analysis of Protein Profiles- *M. pneumoniae* cells were harvested by centrifugation for 15m at 20,000 x g at 4° C, washed three times with cold PBS [145.4

mM NaCl, 2.8 mM $NaH_2PO_4 \cdot H_2O$, 7.2 mM $Na_2HPO_4 \cdot 7H_2O$, pH-7.4], then suspended in PBS. Protein was quantitated using the bicinchoninic acid protein assay (Pierce, Rockford Ill). After quantification, the remainder of the mycoplasma cell suspension was added to an equal volume of 2x SDS-PAGE sample buffer [2% SDS, 20% glycerol, 4% β-mercaptoethanol, 0.2% bromophenol blue], and heated at 95° C for 10 min. Protein profiles were examined by discontinuous sodium dodecyl sulfate-polyacylamide gel electrophoresis (SDS-PAGE) (Laemmli, 1970) and Western immunoblotting (Towbin *et al.*, 1979) as described previously (Krause *et al.*, 1997). Stacking and separating gels were 3% and 12% polyacrylamide, respectively. One hundred μg of protein lysate was loaded per well. Proteins were transferred to nitrocellulose membranes for immunoblotting and stained briefly with Ponceau S, then probed with anti-P30 (1:3000) (Romero-Arroyo *et al.*, 1999), anti-C (1:1000), anti-P65 (1:7500) (Proft and Herrmann, 1994; Proft *et al.*, 1995), or anti-FtsH (1:500) (Balish *et al.*, 2001) polyclonal serum, followed by alkaline phosphatase-conjugated goat anti-rabbit IgG (Promega, Madison, Wis.). Protein bands were visualized using nitro blue tetrazolium and 5-brom-4-chloro-3-indoyl phosphate (Promega) according to the manufacturer's protocol.

Qualitative Hemadsorption- Colonies were examined microscopically for hemadsorption using chicken or sheep erythrocytes as described previously (Krause and Baseman, 1983). Briefly, cells were diluted and plated on Hayflick agar plates, then incubated for 5-7 days at 37° C. 1 ml of chicken or sheep blood (Gibson Labs, Lexington, KY) diluted 1:100 in PBS was added to each plate and incubated for 30min at 37° C. Plates were then washed gently 3 times with 1ml PBS (pH 7.2). Colonies where photographed using a Nikon Diaphot-TMD inverted microscope with phase-contrast

optics or a Leica DMIRB microscope (Leica Corp, Bannockburn, Il). Images where digitized using SNAPPY video snapshot software (Gryphon Software, Rancho, Calif.) or an ATI All-In-Wonder frame grabber (ATI, Ontario, CN) and captured through a Sony DXC-107A color CCD (Sony Corp., Tokyo, Japan).

Quantitative Hemadsorption- Hemadsorption was analyzed quantitatively using [^{3}H]-thymidine radiolabeled mycoplasmas, and chicken erythrocytes in suspension, essentially as described previously (Fisseha *et al.*, 1999). Cultures were incubated in 15 ml Hayflick medium containing 200 μCi [^{3}H]-thymidine (6.7 Ci/mmol; NEN, Boston, MA) for 72 hours at 37° C. Cells were washed three times in cold PBS (pH 7.2), suspended in 3 ml Hayflick medium, passed 7X through a 25-gauge needle, then centrifuged for 5 min at 123 x g in a clinical centrifuge (International Equipment Co., Needham Heights, MA). 150 μl aliquots were incubated at 4°C or 37°C for 30 min, during which time chicken blood < 2 weeks old, previously collected in Alsevers solution at a 1:1 mixture, was washed three times in cold PBS and suspended to a 4% (vol/vol) concentration in PBS. Fifty μl of the 4% chicken blood solution was added to tubes and incubated for another 30 min at 4°C or 37°C. One hundred fifty μl of the mycoplasma/chicken blood suspension was overlaid onto 150 μl of 40% sucrose, then centrifuged for 90 sec at 1690 x g in an Eppendorf 5417C microcentrifuge (Brinkmann Instruments, Westbury, NY) fitted with a swinging bucket rotor. The resulting blood cell pellet was suspended in 100 μl of PBS, and 10 μl of 10% SDS was added per sample. After samples were incubated overnight at room temperature, 5 μl of 30% H_2O_2 was added, and the suspension was incubated at 37°C for 2 h. The suspension was transferred to scintillation vials, and 5 ml Scintiverse scintillation fluid (Fisher) was added per vial.

After repeated inversion of samples, radioactivity was analyzed by liquid scintillation spectrometry on an LS 6500 scintillation counter (Beckman Instruments, Fullerton, CA).

Attachment to Glass- Mycoplasmas radiolabeled with [^{3}H]-thymidine and suspended in fresh Hayflick medium were added to sterile 18-mm glass coverslips in 24-well tissue culture plates (Costar, Corning, NY). After incubating 2 h at 37°C or 4°C, the coverslips were washed by immersing 3X in PBS, air-dried, and measured for radioactivity.

Attachment to Hamster Tracheal Rings- Hamster tracheal rings were prepared for organ culture as described elsewhere (Collier and Baseman, 1973). After sectioning, tracheal rings where incubated in Dulbecco's Modified Eagle Medium (DMEM) (GibcoBRL, Grand Island, NY) supplemented with 10% heat-inactivated fetal bovine serum. The antibiotics penicillin and streptomycin were included at 1000 U/ml, and 100 µg/ml respectively, to inhibit bacterial contamination. After an overnight incubation in a 5.0% CO_2 atmosphere at 37ºC, individual rings were examined for vigor of ciliary beat using a Nikon Diaphot-TMD inverted microscope with phase-contrast optics. Tracheal rings with beating cilia and of similar quality were transferred to individual wells of flat-bottomed 96-well microtiter plates (Corning, Corning, NY) containing heat-inactivated Hayflick medium buffered with 0.05 M HEPES (*N*-2 hydroxyethylpiperazine-*N'*-2-ethanesulfonic acid), pH 7.3.

Tracheal ring attachment was quantitated using [^{3}H]-thymidine-labeled mycoplasmas as described previously, with some modifications (Collier and Baseman, 1973; Krause *et al.*, 1982). Briefly, 15 ml cultures of radiolabeled mycoplasmas were harvested when the phenol red indicator turned slightly orange. Cultures were centrifuged

at 17,000 x g at 4ºC and washed 2X with 10 mls of HEPES-buffered Hayflick medium. After the final wash, the mycoplasma pellets were suspended in 3 ml HEPES-buffered Hayflick, as described in the quantitative hemadsorption assay. After passing the suspension 7X through a 25-gauge needle, the samples were then centrifuged for 5 min at 123 x g in a clinical centrifuge (International Equipment Co., Needham Heights, MA). Tracheal rings were washed twice in HEPES-buffered Hayflick medium, and 100 µl of the mycoplasma suspension was added per ring in a flat-bottomed 96-well microtiter plate and incubated for 3.5 h at 37 ºC or 4ºC. Tracheal rings were then submerged in PBS and blotted onto Kimwipes (Kimberly Clark, Dallas TX) 3X, and added to scintillation vials containing 100 µl of 1% SDS and incubated overnight. The following day, 3 ml of Scintiverse scintillation fluid (Fisher) was added per ring, and vials were agitated thoroughly to mix. Scintillation vials were then analyzed by liquid scintillation spectrometry on a Beckman LS 6500 scintillation counter (Beckman Instruments, Fullerton, CA).

Visualization of Infected and Uninfected Hamster Tracheal Epithelium- Tracheal rings exhibiting vigorous ciliary activity were placed in 24-well dishes containing 900 µl of HEPES-buffered Hayflick medium and infected with 100 µl of log phase cultures of wild-type, mutant, and revertant *M. pneumoniae* as described above. After 3.5 h of incubation, the tracheal rings were removed, washed 2x in PBS, blotted on Kimwipes and some were processed for microscopy while others were placed in fresh HEPES-buffered Hayflick for continued incubation at 37°C.

Laser Scanning Confocal Microscopy (LSCM)- Infected and uninfected control tracheal rings were washed 2x in PBS, blotted onto Kimwipes and transferred to wells

containing PBS-3% paraformaldehyde (v/v) for fixation at ambient temperature for 15 min followed by further incubation at 4°C for 45 min. Fixed rings were washed 2x5 min in PBS followed by a 5 min permeablization step in PBS-0.1% TX-100 (v/v). Permeabilized tracheal rings were further washed 2x5 min in PBS and quick frozen in Tissue-Tek O.C.T. compound (Miles Scientific, Naperville, IL) on stubs within a Reichert-Jung/Leica 2800 Frigocut E cryostat for thick sectioning. Sections were collected on Fisherbrand SuperFrost/Plus microscope slides, air-dried for 15 min, and blocked 1.5 h at room temperature or overnight at 4ºC in PBS-5% BSA (w/v). Tissue-containing slides were then placed in a primary antibody solution containing mouse anti-tubulin (1:5) and rabbit anti-*M. pneumoniae* (1:250) in PBS-1% BSA (w/v) overnight at 4ºC. Slides were washed 4X5 min in PBS and transferred to a secondary staining solution containing FITC conjugated anti-mouse (1:128), and Cy3 conjugated anti-rabbit (1:75) in PBS-1% BSA (w/v) and incubated for 1h at room temperature. Slides were then washed 4x5 min in PBS and briefly washed in tap water. After excess water was wicked away, 10 µl of Citifluor antifade (Ted Pella, Inc., Redding, CA) was applied and a no.1½, 22 mm square coverslip placed over the mounted tracheal rings and sealed with nail polish for later viewing. Optical sections of FITC and Cy3 fluorescence were scanned and stacked for image reconstruction using a Leica TCS SP2 Spectral Confocal Microscope and later merged in Adobe Photoshop (Adobe Systems, Mountain View, Calif.).

TEM Analysis- Infected and control tracheal rings were briefly washed in PBS and fixed in a (0.2% glutaraldehyde -0.2% paraformaldehyde -0.2% picric acid) solution in 0.1M Cacodylate-HCl buffer pH 7.0-7.3 overnight. Rings were then rinsed for 15 min at least three times in 0.1M Cacodylate-HCl buffer. Post-fixation was performed in 0.1%

OsO_4/0.1 M Cacodylate-HCl buffer for 1 hr. Tracheal rings were rinsed 4x 10 min each in deionized water, stained with 0.5% Uranyl Acetate (aqueous) for 1 hr followed by 3x 10 min washes in deionized water, and dehydrated by transfer through a series of ethanol concentrations (50, and 75%) for 1x 10 min, and (95, and 100%) 2x 15 min followed by a transfer to 100% acetone (2x 15 min), and 100% propylene oxide (2x 10 min). Samples were then incubated in a mixture of 50% Epon-Araldite in 100% propylene oxide overnight followed by 2x 1h incubations in 100% Epon-Araldite. Tracheal rings were then transferred to embedding molds containing fresh 100% Epon-Araldite and polymerized at 75ºC at least 24 h. Thin sections were cut with a diamond knife and collected on Formvar-coated nickel grids for examination.

Examination of Cellular Motility- Frozen stocks of mycoplasmas stored at -80˚C were thawed and passed at least 7X through a 25-gauge needle to disperse possible aggregates, then inoculated directly into untreated 4-well coverglass chambers (Nalge/Nunc, Naperville, Ill.) with 900 µl of phenol-red free Hayflick medium containing 4% gelatin (w/v) (Difco) per chamber. After 2 h and in some cases 24 h of incubation at 37 °C, the medium was removed, chambers were washed 1X with 1 ml of fresh pre-warmed medium, and 200 µl phenol-red free Hayflick medium containing 4% gelatin was added per chamber. After a 10-min incubation at 37 ºC, live mycoplasma cultures were examined by using phase-contrast optics (100X, N.A.= 1.4) on a Leica DMIRB microscope. Temperature was maintained at 37 °C using a Minitüb HT 50 control unit (Minitüb, Tiefenbach, Germany) coupled to a Leica DMIRB custom heating stage insert. Images were initially captured every 10 min for 2 h by an ORCA-ER CCD camera (Hamamatsu, Bridgewater, N.J.) and digitized with Openlab 3.0 (Improvision, Lexington,

MA). After this preliminary screening for motility, the more motile strains were imaged every 2 s for 5-20 min maintaining a 37ºC environment by heating the room. In all cases, digital images were stacked for animation using Scion image software (Scion Corporation, Frederick, Maryland) and manipulated using Adobe Photoshop version 7.0.

Colony Morphology- Mycoplasmas where plated on PPLO agar (Difco Laboratories, Detroit, Mich.) substituting 0.5% Noble agar (Difco) for the 1.5% standard agar. After overnight incubation at 37°C, Hayflick medium was gently applied to the agar surface and maintained throughout the incubation at 37˚ C in sealed plastic containers in a humid environment. Colony morphology was examined after 6-9 d using a Nikon Diaphot-TMD inverted scope with phase-contrast optics or a Leica DMIRB microscope. Colony morphology images were digitized using SNAPPY video snapshot software or an ATI All-In-Wonder frame grabber and captured through a DXC-107A color CCD.

Scanning Electron Microscopy- Frozen stocks of wild-type, mutant, and transformant *M. pneumoniae* cells were thawed and passed 4X through a 25-gauge needle to disrupt aggregates. Cell suspensions were added drop-wise directly to individual wells of 24-well tissue culture plates containing 1 ml Hayflick medium and 18-mm round glass coverslips pretreated with poly-L-lysine (0.01%). The seeded cover slips were incubated at 37°C for 2 h, after which an 8% glutaraldehyde solution was added to the Hayflick medium to achieve a final concentration of 2% and incubated for 45 min at 4°C. Samples were then washed 4X with 1 ml of PBS. Washed coverslips were dehydrated in a graded series of ethanol, critical point dried, and coated with chromium for examination on a LEO982 scanning electron microscope.

Isolation of a Mutant II-3 Revertant (II-3R)- A revertant of the non-cytadhering mutant II-3 was isolated by repeated enrichment for attachment to plastic. Dilutions of mutant II-3 were plated on PPLO agar, and three hemadsorption-negative colonies were transferred separately into 25cm^2 tissue culture flasks (Costar, Corning, NY) containing 5 ml of Hayflicks media. After an orange-red color change, the medium was removed and the flask washed 3X with 3 ml PBS. 500 µl Hayflick medium was added per flask, and adherent cells were dislodged by using a tissue culture flask scraper. Each suspension was then used to inoculate a 25 cm^2 flask containing 5 ml fresh Hayflick medium. The plastic enrichment process was repeated until a monolayer of mycoplasma cells was formed. The cells were then dislodged from the flask by scraping and diluted for plating. Several hemadsorption-positive colonies were picked, expanded, and PCR amplified *p30* alleles sequenced by the chain termination method, using custom synthesized primers, dye terminators, and an Applied Biosystems (Foster City, Calif.) model 373A automated sequencer according to the manufacturer's instructions.

Immunofluorescence (anti-P65)- Frozen stocks of mycoplasmas stored at -80°C in Hayflick broth were thawed, passed through a 25-gauge needle 5X to disperse aggregates, inoculated into 500 µl Hayflick medium in 24-well dishes containing glass cover slips which had been treated with poly-L-lysine, and incubated for 2 h at 37°C. Pretreatment with poly-L-lysine was included to enhance attachment of the non-cytadhering mutants to the glass surface. Cells were fixed with 3.4% paraformaldehyde (vol/vol) in Hayflick medium for 15 min at room temperature and 45 min at 4°C. The cover slips were removed and rinsed 4X for 5 min each with PBS, then treated for 5 min at room temperature in PBS-0.1% Triton X-100 (vol/vol) for permeabilization, as

described by Seto et al. (Seto *et al.*, 2001). Mycoplasmas were again washed 4X for 5 min each in PBS, then incubated for 1 h in a blocking solution of PBS-5% (wt/vol) bovine serum albumin (BSA) at room temperature to limit nonspecific labeling, and probed with either rabbit anti-P65 or rabbit anti-FtsH (Balish *et al.*, 2001) serum diluted 1:100 in PBS-1% BSA overnight at 4°C in a moisture chamber. After rinsing in PBS four times for 5 min each, the cover slips were incubated for 1 h at room temperature with indocarbocyanine (Cy3)-conjugated donkey anti-rabbit immunoglobulin G antibody (Jackson ImmunoResearch Laboratories, West Grove, Pa.) diluted 1:75 in PBS-1% BSA, then rinsed four times for 5 min each in PBS and once in distilled H_2O and mounted on microscope slides using Prolong Antifade.

Cells were examined using a Nikon TE300 epifluorescence microscope with a tetramethyl rhodamine isothiocyanate filter cube (528 to 552 nm) and equipped with phase-contrast optics. Samples were viewed using a 100× objective, and images were digitized using a Micromax CCD camera. The CCD exposure time was set at 0.6 s for fluorescence. Digital images were false colorized and superimposed using Adobe Photoshop version 5.0. Phase-contrast images were placed in the green channel, while the corresponding fluorescence images were placed in the red channel. The brightness and contrast of the blue channel were adjusted to give a black image.

Immunofluorescence (anti-P30, anti-P65)- Frozen stocks of mycoplasmas stored at -80°C in Hayflick broth were thawed, passed through a 25-gauge needle 5X to disperse aggregates, inoculated in 24-well dishes containing round sterile 18mm poly-L-lysine treated glass cover slips. 900 µl of Hayflick medium containing 4% gelatin (w/v) was then added to each inoculated well and incubated for 2 h and in some cases at 37°C.

Coverslips where then immersed 3X in PBS and placed in a fixative solution of 0.2% glutaraldehyde, 2% para-formaldehyde in PBS containing 0.02% NaN_3. After 15 min of fixation at room temperature, the fixative-submerged coverslips were placed at 4ºC for an additional 45 min and where then washed 2X 5min in IF-WASH [PBS with 0.05% Tween, and 0.02% NaN_3, pH-7.2] and permeabilized in PBS-0.1% TX-100 solution for 5 min. Coverslips where then washed 2X 5 min in IF-WASH and placed in IF-BLOCK [PBS containing: 0.05% Tween, 5% powdered milk (w/v), and 0.02% NaN_3] 1h at room temp or 4ºC overnight. Coverslips were probed with monoclonal anti-P30 antisera (1:50) or rabbit polyclonal anti-P65 antisera (1:300) in IF-DIL [PBS with 0.05% Tween, 2% powdered milk, and 0.02% NaN_3] at 4ºC overnight. After washing 4X 5 min in IF-WASH the coverslips were incubated 1h at room temperature in (Cy3)-conjugated donkey anti-mouse or anti-rabbit immunoglobulin G antibody (Jackson ImmunoResearch Laoratories) diluted 1:100 in IF-DIL. After incubation, coverslips were washed 4X 5min in IF-WASH and transferred to wells containing 1 μg/ml DAPI [4', 6-diamidino-2-phenylindole] in PBS and incubated at room temperature for 30 min. Stained cover slips were immersed 5X in tap water, wicked dry with filter paper, and inverted on precleaned microscope slides over a suspension of Citifluor antifade (Ted Pella, Inc., Redding, CA). Slides were examined immediately, or in some cases stored at 4°C overnight for later observation. Mycoplasmas were visualized using a Leica DMIRB microscope equipped with a 1.4 numerical aperture 100x objective lens. Specific fluorescence of P65 or P30 was accomplished using a TRITC (tetramethyl rhodamine isothiocyanate) filter cube set. Nucleoid fluorescence was attained with a DAPI filter cube set (excitation 372 nm, emission 456 nm). Images were captured by an ORCA-ER CCD camera and digitized

with Openlab 3.0. Digitized images were superimposed and false-colorized using Adobe Photoshop version 6.0. In pseudo-colorized images the nucleoid image was assigned to the blue channel and P30 or P65 fluorescence to the red channel.

GFP Visualization- Frozen stocks of mycoplasmas stored at -80˚C were thawed and passed at least 4X through a 25-gauge needle to disperse possible aggregates, then inoculated directly into 300 µl of Hayflick medium in 4-well coverglass chambers (Nalge/Nunc, Naperville, Ill.), untreated or pretreated with 0.1% poly-L-lysine as described elsewhere (Stevens and Krause, 1992). After a 2-h incubation at 37°C, live mycoplasma cultures were examined by using phase-contrast optics (100X oil-immersion objective) on a Leica DMIRB microscope and maintained at 37°C using a Minitüb HT 50 control unit (Minitüb, Tiefenbach, Germany) and a Leica DMIRB custom heating stage insert. Images were captured by an ORCA-ER CCD camera (Hamamatsu) and digitized with Openlab 3.0 (Improvision). A 31001 Chroma FITC (fluorescein isothiocynate) filter cube set (excitation 456-495 nm, emission 515-555 nm) was used for the illumination of GFP.

Structure-Function Analysis of Protein P30

Overview- The wild-type *p30* allele was cloned and modified by a series of deletions. Each mutated *p30* allele, or the wild-type allele as a control, was cloned into the modified Tn*4001* transposon (Hedreyda *et al.*, 1993) and subsequently transformed by electroporation into the P30 null mutant (II-3) background. Standard protocols were used for all DNA manipulations and electroporation of *M. pneumoniae* cells, as described in detail previously (Fisseha *et al.*, 1999). Transformants were sequenced through the entire *p30* gene by the chain termination method, using custom synthesized primers, dye

terminators, and an Applied Biosystems model 373A automated sequencer (Foster City, Calif.) according to the manufacturer's instructions. Two separate primers, one annealing upstream of the *p30* gene and one within the *p30* gene, were utilized to ensure fidelity of the sequence data (Table 2A). Multiple transformants were isolated and characterized in each case to control for possible positional effects of transposon insertion.

Previous studies demonstrated that recombinant P30 can be made at wild-type levels in *M. pneumoniae* transformants following transposon delivery (Romero-Arroyo *et al.*, 1999). These earlier genetic complementation studies with mutant II-3 incorporated a large region upstream of *p30* which included the genes for *p32* and *p21*. There is no apparent promoter directly upstream of the *p30* gene, and it has been demonstrated that the promoter for *p21* also drives transcription of *p30* (Waldo *et al.*, 1999). Although the transposon vector used contains a promoter that can drive transcription, the promoter upstream of *p21* was incorporated into all *p30* constructs in the studies described herein in hopes of achieving wild-type production of P30. Preliminary data from immunoblots using P21 specific antiserum also indicate that the *p21* gene product is produced at wild-type levels in mutant II-3 (data not shown), and that complementation of this mutant with the *Eco*RI - *Bam*HI fragment cloned from II-3 does not restore P30 production (Romero-Arroyo *et al.*, 1999).

Cloning of Wild-Type and II-3R *p30*- The wild-type and revertant *p30* alleles, including the upstream region encoding P21 and the PromP21 promoter sequence (Waldo *et al.*, 1999), were amplified by PCR and cloned into the *Eco*RI and *Bam*HI sites of the modified Tn*4001* in pKV74; (Figure 8) (Hahn *et al.*, 1998). An *Eco*RI site was engineered in the upstream primer (Eco21+) to facilitate this cloning (Figure 8,

Table 2. Description of primers used for sequencing (A), construction of P30 deletion derivatives (B), and a P30-GFP fusion (C).

A

Primer name	Primer 5' annealing position relative to *p30* ATG	Strand	Sequence 5'-3'
SEQP30POS1	- 61	+	GATTACTACTATGATGAAGC
SEQP30POS2	+435	+	GCGGAAGTTGAACCAGC

B

Primer name	Primer 5' annealing position relative to *p30* ATG	Strand	Sequence 5'-3'
ECO21+	- 763	+	GTAGCTTCATG/AATTCGGTCT
P30ECORVNEG	+ 120	-	CAGTTCGAT/ATCGTTGTGCTGTA
SCA982	+ 195	+	CAAGCCGAGT/ACTGAGCAAGCAT
NRU1NEG	+ 311	-	TCCTCG/CGATTCACAATTGG
XMN1POS	+351	+	AGCGGAACA/GCTTCAACGCA
TRUNCATEDP30	+ 761	-	CGAG/GATCCATACCGGG**TTA**A GGTGGGAAACCAGGTCTTGG
NCOP30NEG Q2155	+ 822	-	GATCC/CATGGTGCGTTTTGGTGG
HMW3NH3-	+ 1070	-	CAAAGCTAATTGGTTCATCACTGTC

C

Primer name	Primer 5' annealing position relative to *egfp* ATG	Strand	Sequence 5'-3'
GFPPOS	- 9	+	GTCGCCAC/CATGGTGAGCAAG
NEWGFPNEGBAM	+ 731	-	CGCG/GATCCGTCGCGGCCGCT TTACTTGTACAGCTCG

Underlined sequences represent consensuses sequences of restriction enzymes. Enzyme cleavage site is indicated by slash mark. Engineered stop codon is in bold.

Figure 8. Recombinant transposon construction for complementation. Primers used to amplify wild-type and revertant *p30* alleles. A 1,802-bp PCR product containing the wild-type or revertant *p30* allele was cloned into the *Eco*RI (E) and *Bam*HI (B) sites of previously modified Tn*4001*mod (Hahn *et al.*, 1998). PromP21 (open arrow) is an apparent promoter region for the operon (Waldo *et al.*, 1999). The genes encoding P32, P21, P30, and HMW3 are indicated.

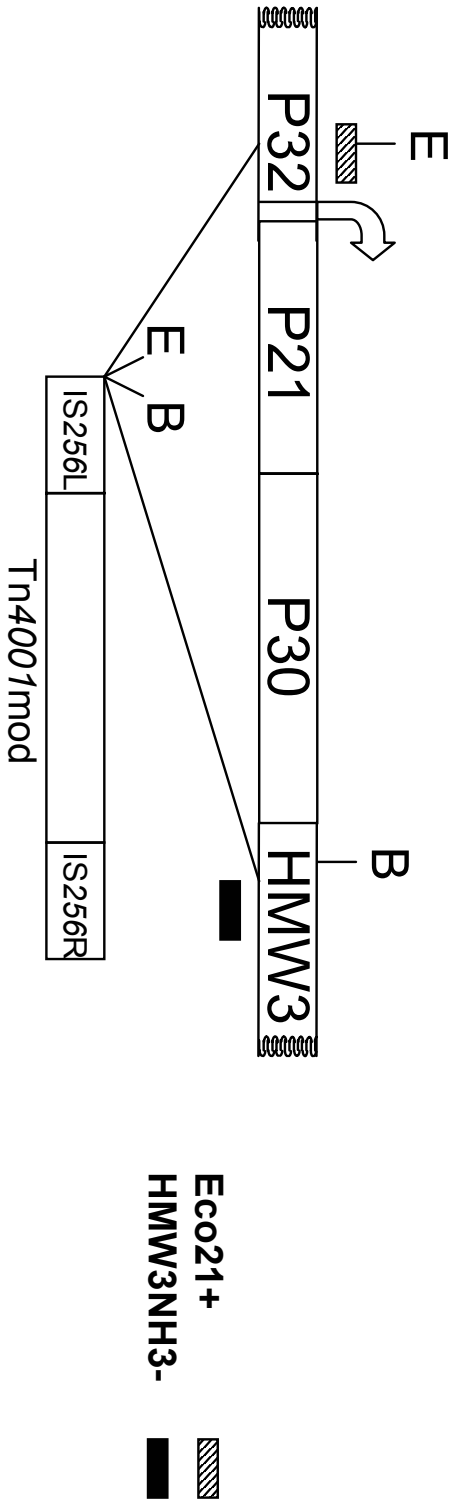
P32
P21
P30
HMW3
E
B
E
B
IS256L
Tn4001mod
IS256R
Eco21+
HMW3NH3-

underlined). An *Eco*RI site was engineered in the upstream primer (Eco21+) to facilitate this cloning (Figure 8, underlined). Minus strand primer HMW3NH3- was used with Eco21+, and the corresponding PCR products from wild-type and II-3R contained a *Bam*HI site downstream of *p30*, within the gene encoding HMW3. The resulting 1,833 bp products (wild-type and revertant) were digested with *Eco*RI and *Bam*HI and cloned separately into pKV74. Wild-type *p30* cloned into pKV74 was designated **(pKV 236/ KGA 433)**, and II-3 revertant *p30* cloned into pKV74 was designated **(pKV 237/ KGA 434)**.

Construction of P30 Cytoplasmic Domain Deletion Mutant (P30 ΔI)- Wild-type P30 consists of a putative signal sequence, cytoplasmic domain, transmembrane domain, and proline-rich surface-exposed domain (Figure 9). Using pKV 236 as template, an 833-bp fragment containing the entire *p21* and the *p30* region encoding the signal sequence was amplified by PCR using primers ECO21+ and P30ECORVNEG respectively. In addition a second PCR reaction using primers SCA982 and HMW3NH3- amplified an 875-bp region encoding the membrane-spanning domain as well as the remainder of the *p30* gene and the N-terminal coding region of *hmw3* (Figure 10). The 3' primer P30ECORVNEG used in the first reaction contained an engineered *Eco*RV restriction site within the primer sequence. The 5' primer of the second reaction (SCA982) contained a *Sca*I restriction site within the primer sequence (Table 2B). Both PCR products were digested, with either *Eco*RV or *Sca*I as appropriate, and the corresponding products were ligated, creating a 1,758-bp fragment. This product was subsequently used as PCR template and amplified using primers ECO21+ and HMW3NH3-.

Figure 9. Predicted domains of wild-type P30.

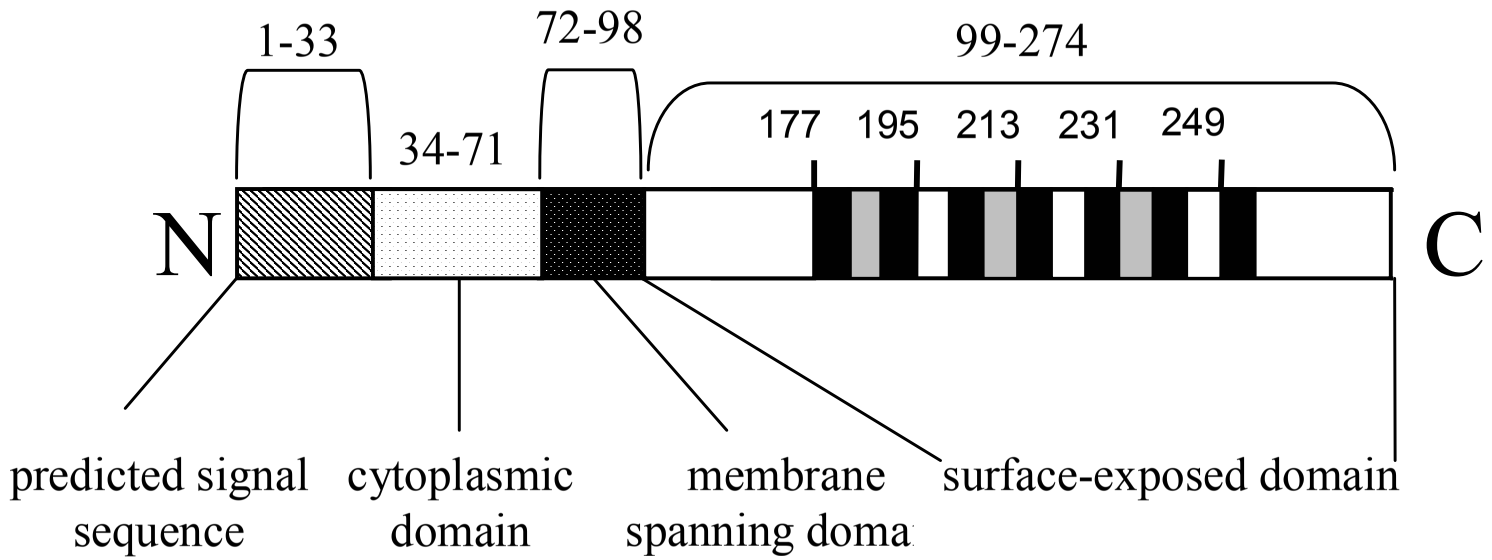

Proline-Rich Repeats

A		PGMAPR
B		PGMPPH
C		PGFPPQ

Figure 10. Construction of P30 cytoplasmic domain deletion mutant P30ΔI. Two PCR products were amplified using the wild-type *p30* allele as template. The 3' end of the first PCR product contained an *Eco*RV restriction site, while the 5' end of the second product contained a *Sca*I site. These blunt ended sites were ligated together creating a modified *p30* allele lacking of a significant portion (30 out of 38 aa) of the encoded cytoplasmic domain. The ligated PCR products were then used as template for another PCR reaction using the 5' primer from the first reaction (ECO21+) and the 3' primer from the second reaction (HMW3NH3-). This cloning technique was also used for construction of the P30 conserved region deletion derivative P30ΔII removing 19 out of 175 aa of the extracellular domain.

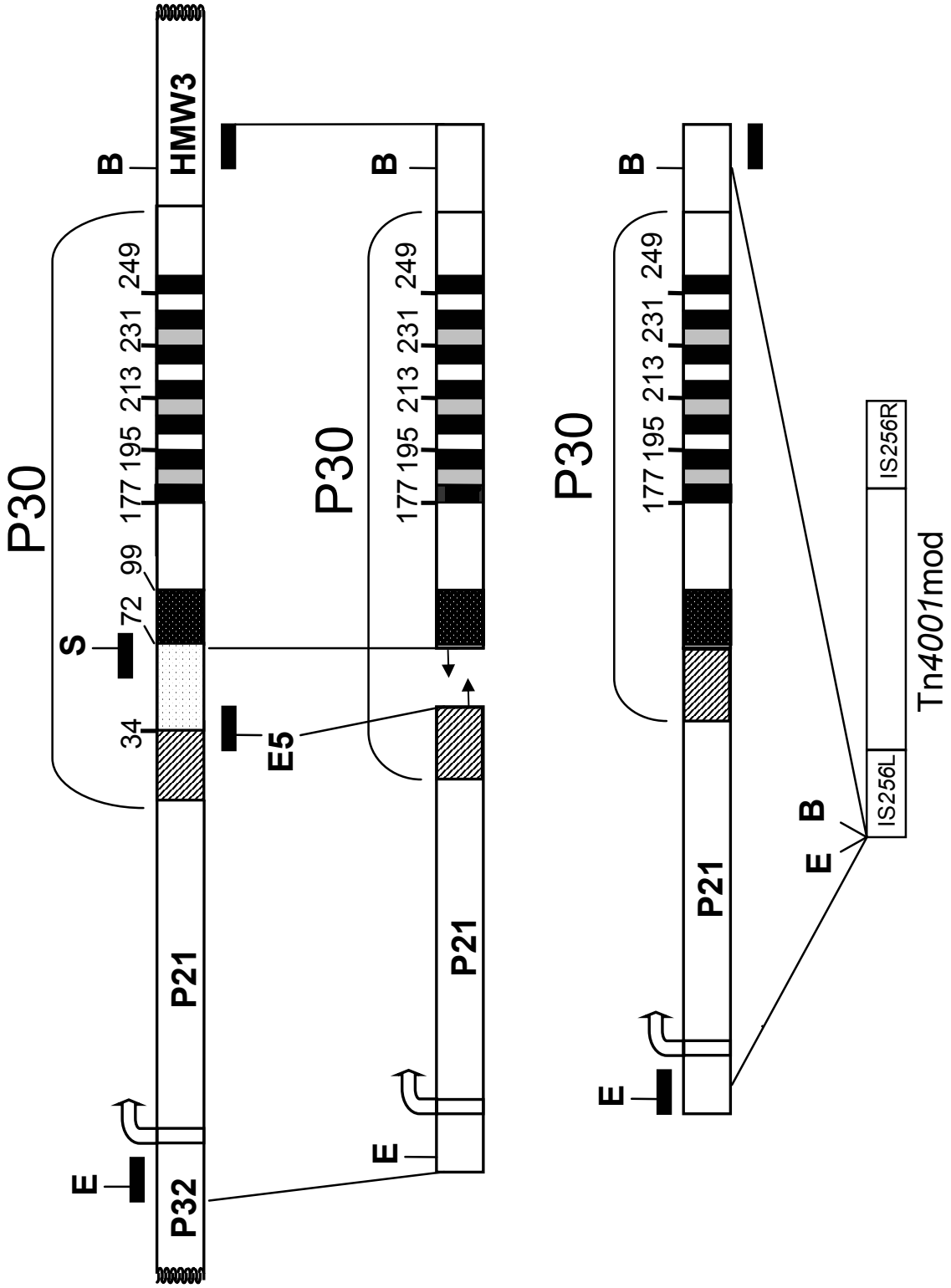
P30
B
HMW3
249
231
213
195
177
99
72
S
34
P21
E
P32
E5
P30
B
249
231
213
195
177
P21
E
P30
B
249
231
213
195
177
P21
E
B
IS256L
IS256R
Tn4001mod

Primer ECO21+ contained an *Eco*RI restriction site within the primer sequence, while a *Bam*HI site exists downstream of the coding sequence of *p30* encompassed by the PCR product (Table 2B). The PCR product was digested with *Eco*RI and *Bam*HI and cloned into the corresponding sites of Tn*4001*mod in pKV74, generating **pKV 238/ KGA 435.**

Construction of P30 Conserved Domain Deletion Mutant (P30 ΔII)- Using pKV 236 as template, a 1,074-bp product containing upstream gene *p21* and promoter prom21 and the *p30* gene encoding the signal sequence, cytoplasmic domain and membrane-spanning domain was amplified by PCR using primers ECO21+ and NRU1NEG. In addition, a second PCR reaction using primer XMN1POS and HMW3NH3- amplified a 719-bp region encoding the majority of the surface-exposed domain of *p30* and the N-terminal coding region of *hmw3*. The minus strand primer for reaction one (NRU1NEG) contained an engineered blunt-end restriction site *Nru*I. The positive strand primer for the second reaction (XMN1POS) likewise contained an engineered blunt-ended restriction site, but in this case *Xmn*I (Table 2B). The PCR products were digested with *Nru*I and *Xmn*I respectively, and then ligated, creating a 1,793-bp product removing coding sequence for 20 out of 176 aa of the surface-exposed domain which became the template for a subsequent round of PCR using primers ECO21+ and HMW3NH3- (similar procedure as depicted in Figure 10). Primer ECO21+ contained an *Eco*RI restriction site within the primer sequence, while a *Bam*HI site existed downstream of the coding sequence of *p30* encompassed by the PCR product. The PCR product was digested with *Eco*RI and *Bam*HI and cloned into the corresponding sites of Tn*4001*mod in pKV74, generating **pKV 239/ KGA 436.**

Construction of P30 C-Terminal Domain Deletion Mutants (P30 ΔIII-A,-B, and -C)- To construct a P30 mutant with a truncated C-terminus, a primer (TRUNCATEDP30) (Table 2B) containing a termination codon as well as a *Bam*HI site was designed to anneal just upstream of the last proline repeat in the *p30* gene. Using pKV 236 as template, a 1,524-bp fragment containing the entire *p21* and the *p30* gene excluding the coding region for 27 residues of the very C-terminus of *p30* was amplified by PCR using primers ECO21+ and TRUNCATEDP30. The *Eco*RI restriction site incorporated into the plus strand primer ECO21+, and the *Bam*HI site in the minus strand primer TRUNCATEDP30 (Figure 11), allowed the subsequent digestion and cloning of this insert into the *Eco*RI and *Bam*HI sites of pKV74, generating (P30ΔIIIA) **pKV 240/ KGA 437**. Due to the repetitive nature of the C-terminal region of P30, several different PCR products were generated using this primer combination, including two other novel P30 C-terminal deletion mutants designated (P30ΔIIIB) **pKV 241/ KGA 438**, and (P30ΔIIIC) **pKV 242/ KGA 439** truncating the P30 protein to 199, and 175 out of 274 residues respectively.

Construction of P30Cys81Ser- To determine if disulfide-bond mediated protein-protein interactions occurred with P30, the sole cysteine at residue 81 in P30 was mutated to a serine residue using primer (30CYSSECONDPOS)-5' AGTTGCTGGTAGCTTTGGTTT 3' and the Altered Sites Mutagenesis kit as recommended by the manufacturer (Promega, Madison, WI). The resulting plasmid was designated **pKV 243/ KGA 440**.

Figure 11. Construction of P30 truncation mutants P30ΔIII-A,-B, and -C. PCR was used to amplify the wild-type *p30* allele. The 3' primer (TRUNCATED P30) contained a stop codon and a *Bam*HI restriction site. The PCR product was digested with *Eco*RI and *Bam*HI and cloned into Tn*4001*mod. Due to the repetitive regions in the surface-exposed domain two additional truncation mutants where constructed with this primer combination, each containing truncations further upstream than the planned mutant.

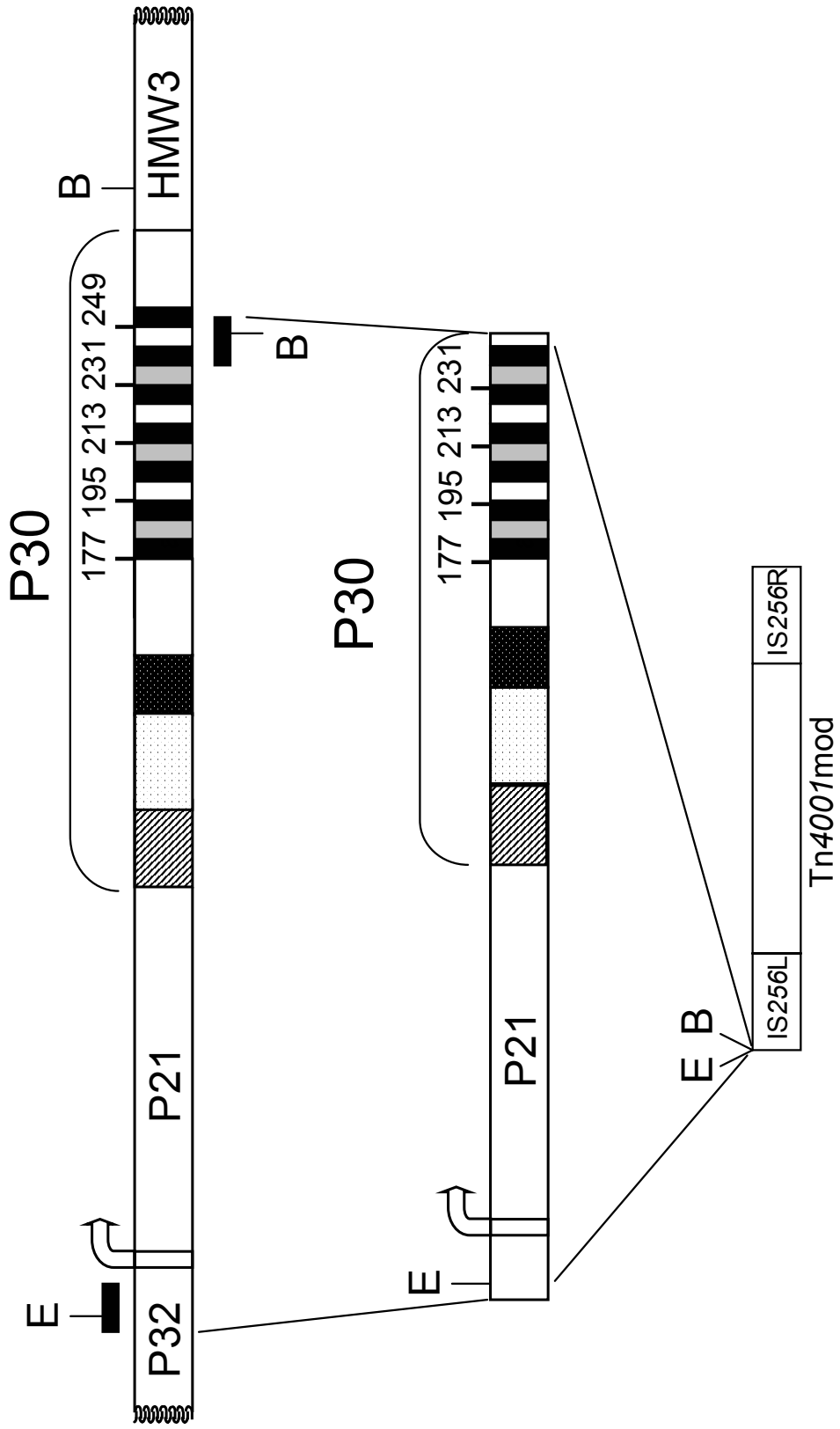
P30
177 195 213 231 249
B
HMW3
P32
P21
E
B
P30
177 195 213 231
P21
E
E B
IS256L
IS256R
Tn4001mod

Construction of P30-GFP- To localize P30 using time-lapse microscopy of living *M. pneumoniae* cells, a P30-GFP fusion was constructed. To facilitate this cloning, PCR was performed using pKV 236 as template. Positive strand primer ECO21+ was used with a negative strand primer synthesized corresponding to the very 3' end of *p30*. The latter primer, 30NCO, contained *Nco*I restriction site and was used in conjunction with ECO21+ to generate a 1,596-bp product (Table 2B). The gene encoding the mutationally enhanced green fluorescent protein (GFP) was also amplified using PCR using the 5' primer (Gfpplus) and 3' primer (NEWGFPNEGBAM) (Table 2C). The restriction site *Nco*I is found at the N-terminal methionine of GFP. Both products were digested with *Nco*I, then ligated and used as template for a subsequent round of PCR using primers ECO21+ and HMW3NH3- (Figure 12). Primer ECO21+ contained an *Eco*RI site within the primer sequence while a *Bam*HI site existed downstream of the coding sequence of *p30* encompassed by the PCR product. The PCR product was digested with *Eco*RI and *Bam*HI and cloned into the corresponding sites of Tn*4001*mod in pKV74 and designated (P30-GFP) **pKV 244/ KGA 441**.

Figure 12. Construction of a P30-GFP fusion. Two PCR products were amplified using the wild-type *p30* allele and the *gfp* allele as template. The 3' end of the first product and the 5' end of the second product contained an *Nco*I restriction sites which were engineered within the primer sequences. These products were digested with *Nco*I and ligated together creating a *p30-gfp* fusion. The ligated PCR product was then used as template for another PCR reaction using the 5' primer from the first reaction (ECO21+) and the 3' primer from the second reaction (NCOP30NEG).

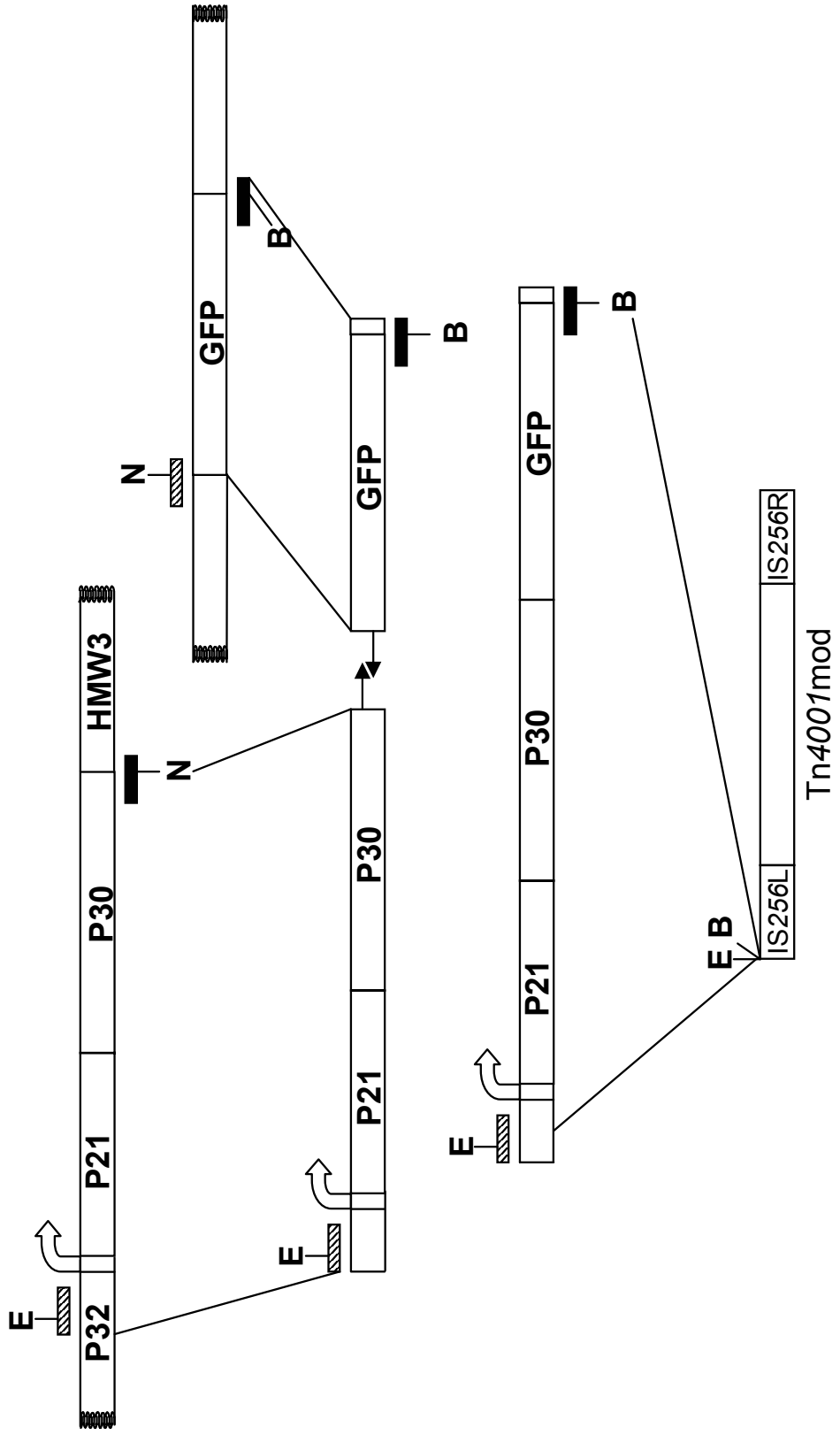
GFP
B
B
N
GFP
HMW3
N
P30
P21
E
P32
E
P30
P21
E
GFP
B
B
P30
P21
E
E B
IS256R
IS256L
Tn4001mod

CHAPTER 4

RESULTS

Stability and Subcellular Localization of Protein P65 in Wild-Type and Cytadherence Mutants of *M. pneumoniae*

Due to the hierarchal and complex interdependence of cytadherence proteins for stability and/or proper localization, and a general lack of knowledge about the role of protein P65 in these processes, effects of loss of other cytadherence-associated proteins on P65 was examined. Steady state levels of P65 were compared between wild-type *M. pneumoniae* and several cytadherence mutants by western-immunoblotting using P65-specific antiserum (Figure 13). Of the strains tested, mutants III-4 and IV-22, had levels of P65 comparable to that in wild-type. The loss of P30 (II-3), or an internal in-frame deletion in P30 (II-7), resulted in reduced levels of P65, while loss of HMW2 (I-2), or HMW1 in addition to an internal truncation of P30 (M6), resulted in scarcely detectable levels of P65 (Figure 13 and data not shown).

For mutant I-2 this reduction in steady state P65 was shown to be due to accelerated turnover (Jordan *et al.*, 2001). In wild-type *M. pneumoniae*, P65 was previously localized exclusively to the attachment organelle (Seto *et al.*, 2001). We observed the same here (Figure 14A). To clarify if P65 localization, like that of P1 (Hahn *et al.*, 1998), likewise depends on other cytadherence proteins, immunolocalization of

Figure 13. Analysis of P65 levels in wild-type and mutant *M. pneumoniae*. Western immunoblotting analysis of P65 in wild-type (WT) *M. pneumoniae* and noncytadhering mutants I-2, II-3, II-7, III-4, IV-22, and M6, as indicated (50 μg of protein per lane). Anti-P65 serum was used at a dilution of 1:7,500. The position of the 66 kDa protein size standard is shown on the left.

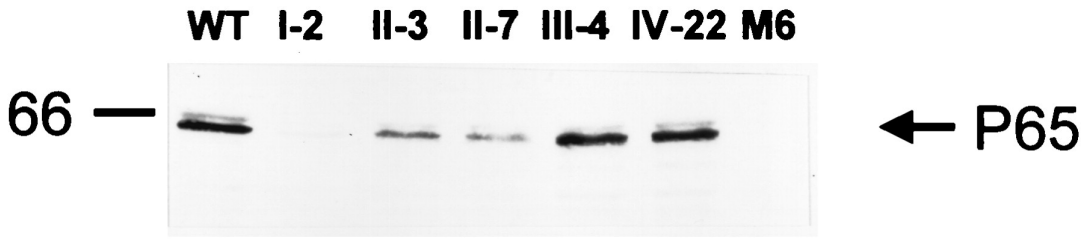
WT
I-2
II-3
II-7
III-4
IV-22
M6
66
P65

Figure 14. P65 and FtsH immunolocalization in *M. pneumoniae*. (A) Analysis of P65 and FtsH distribution in wild-type *M. pneumoniae*. **(B)** P65 localization in noncytadhering mutants I-2, II-3, II-7, III-4, IV-22, and M6. The first panel for each is the merged fluorescent and phase-contrast images of individual cells. The second panel is the fluorescent image from each composite. Bar: 2.0 μm (same for panels **A** and **B**).

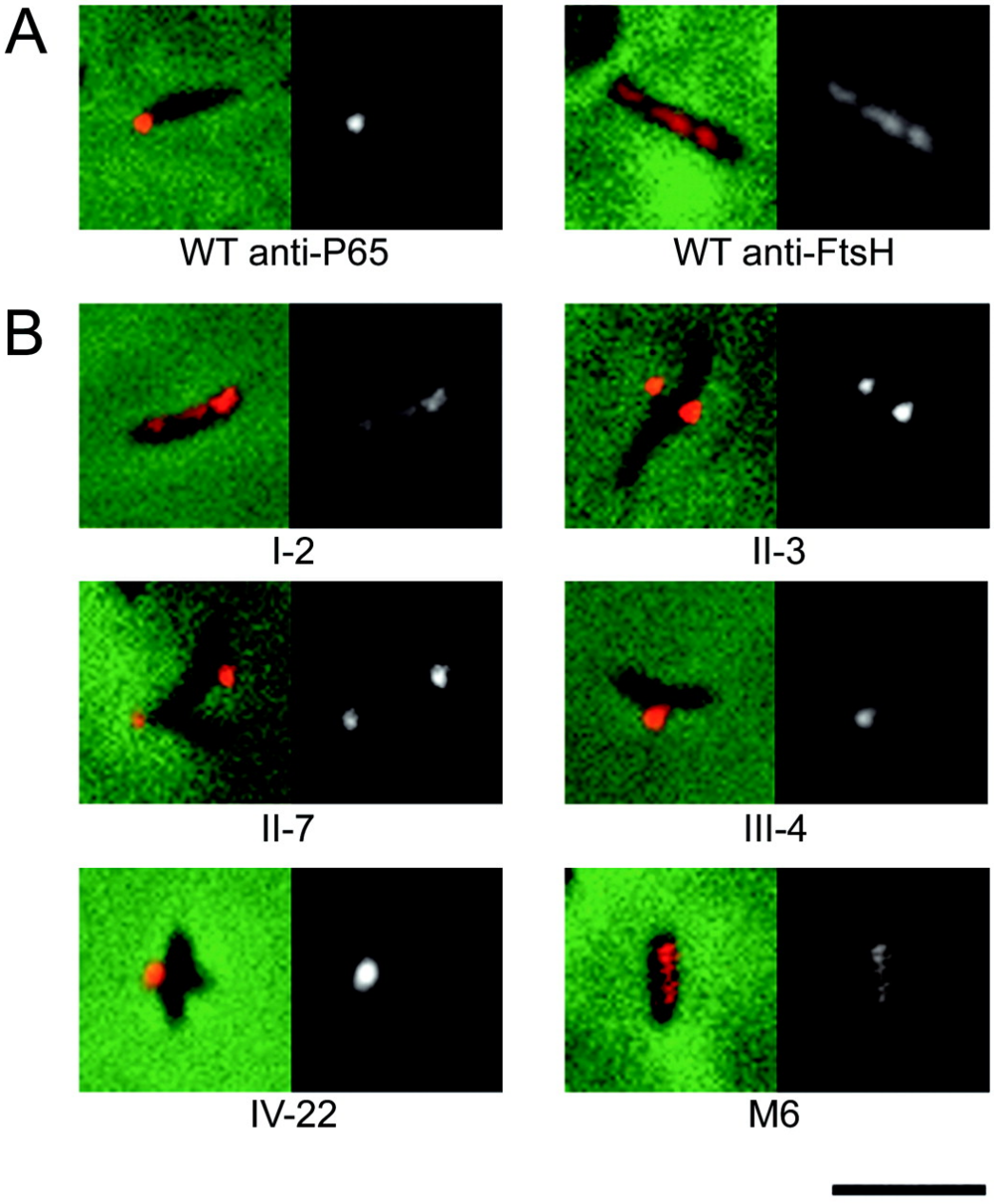
A
WT anti-P65
WT anti-FtsH
B
I-2
II-3
II-7
III-4
IV-22
M6

P65 in *M. pneumoniae* mutant cells was performed (Figure 14B). In those mutants having the lowest steady-state levels of P65 as determined by immunoblotting (mutants I-2 and M6), the P65 detected by immunofluorescence was diffusely scattered throughout the cells in a patchy distribution. As a presumably non-localized control, the membrane-bound protease FtsH was also examined in the wild-type background by immunofluorescence (Figure 14A). Fluorescence patterns of anti-FtsH labeled cells were similar in appearance to P65 localization in mutants I-2, and M-6. In mutants II-3, II-7, III-4, and IV-22, protein P65 was localized to a polar focus or to multiple foci (Figure 14B).

Characterization of *p30* in Mutant II-3

Naturally occurring P30 mutants can be grouped into two classes: those which contain in-frame internal deletions producing stable P30 variants (II-7, M6, and M7), and those lacking detectable P30 (II-3). A previous study reported no nucleotide sequence differences between II-3 *p30* and the wild-type *p30* allele (Dallo *et al.*, 1990). However, we later identified an adenine deletion at nucleotide 453 (Figure 15A) (Romero-Arroyo *et al.*, 1999). Despite the frameshift mutation, an open reading frame was maintained that would yield an altered P30 of nearly the same length and mass as wild-type P30 (Figure 15B). To determine if the altered P30 was actually stable in mutant II-3, two peptides were synthesized corresponding to regions predicted to be antigenic in the II-3 P30 sequence in the region of the deduced protein downstream of the frameshift. Western immunoblotting using antisera produced against these two peptide conjugates failed to react to protein in II-3 lysates while showing reactivity to there respective antigen used for immunization (data not shown).

Figure 15. Genetic characterization of *p30* reversion in II-3R. (A) Nucleotide sequence comparison of the indicated portion of the *p30* gene of wild-type *M. pneumoniae*, the HA^- mutant II-3, and an HA^+ revertant of II-3 (II-3R). The adenine nucleotide present in the wild-type sequence but absent from the II-3 sequence is shown in bold, as is the cytosine nucleotide absent from the wild-type and II-3 sequences but present in the revertant. Numbers correspond to nucleotide positions relative to the beginning of the *p30* ORF. **(B)** Comparison of the deduced amino acid sequence of the indicated portions of P30 from wild-type, II-3, and II-3R *M. pneumoniae*. The sequence altered as a result of the second-site mutation is underlined. Numbers indicate amino acid positions from the deduced N terminus of P30. Accession no. AF090171 and AF090172 have been assigned to the mutant and revertant *M. pneumoniae* sequences shown in Fig. 15B.

A

```
wild-type 401   TAGA.ACAACAAGCAGCTGCTGAAGCCCATGCTGAAGCGGAAGTTGAACCAGCACCACAACCA
                |||| |||||||||||||||||||||||||||||||||||||||||||||| |||||||||
II-3            TAGA.ACAACAAGCAGCTGCTGAAGCCCATGCTGAAGCGGAAGTTGAACCAGC.CCACAACCA
                |||| |||||||||||||||||||||||||||||||||||||||||||||| |||||||||
II-3R           TAGACACAACAAGCAGCTGCTGAAGCCCATGCTGAAGCGGAAGTTGAACCAGC.CCACAACCA
```

B

```
                                .         .         .         .         .         .         .
wild-type  130 EQQALEQQAAAEAHAEAEVEPAPQPVPVPPQPQVQINFGPRTGFPPQPGMAPRPGMPPHPGMAPRPGFPPQPGMAPRPGM
II-3           EQQALEQQAAAEAHAEAEVEPAHNQYQYHLNPKSKLTSVPVLVSHLNPVWRLVQVCRHTPVWLQDLVSHLNPVWRLVQVC
II-3R          EQQALDTTSSCWSPCWSGSWTSPQPVPVPPQPQVQINFGPRTGFPPQPGMAPRPGMPPHPGMAPRPGFPPQPGMAPRPGM

                          .         .         .         .         .         .
wild-type  221 PPHPGMAPRPGFPPQPGMAPRPGMPPHPGMAPRPGFPPQPGMAPRPGMQPPRPGMPPQPGFPPKR.
II-3           RHTPVWLQDLVSHLNPVWRLVQACRHTPVWLQDLVSHLNPVWRLVPECNHHVLACHPNPVFHQNAN.
II-3R          PPHPGMAPRPGFPPQPGMAPRPGMPPHPGMAPRPGFPPQPGMAPRPGMQPPRPGMPPQPGFPPKR.
```

Isolation of a II-3 Revertant

Attachment to inert surfaces is a common property of wild-type *M. pneumoniae* and lacking in many cytadherence mutants, including II-3. I isolated P30 revertants from mutant II-3 after repeated enrichment for attachment to plastic. Several independent isolates revealed an identical reversion resulting from a second-site mutation, specifically the addition of a cytosine (nt 405) to restore the P30 reading frame (Figure 15A). The deduced protein sequence of the II-3 revertant (II-3R) indicated a 17-residue region (135-151) distinct from wild-type P30 (Figure 15B). Western immunoblot analysis of II-3R using P30 specific antiserum revealed a major band of approximately 28,500 and minor bands 58,000 and 114,000 relative molecular weights (Figure 16A). To establish that the altered phenotype of II-3R was indeed due to the 17-amino acid difference in the P30 primary sequence, the recombinant *p30* gene from wild-type and revertant II-3R *M. pneumoniae* was amplified by PCR and cloned into a modified Tn*4001* for transpositional insertion in mutant II-3. Transformant protein profiles were examined by western immunoblotting to confirm the presence of the recombinant wild-type and II-3R P30. As demonstrated previously, P30-specific antibodies reacted with a protein band of the expected size (32,000 relative molecular weight) in wild-type *M. pneumoniae* and mutant II-3 transformed with the recombinant wild-type *p30* allele (Romero-Arroyo *et al.*, 1999). Revertant II-3R and mutant II-3 transformed with the revertant *p30* allele exhibited a distinctly different pattern from wild-type (Figure 16A, and data not shown). Protein P65 levels were indistinguishable between wild-type and revertant II-3R, unlike the reduced levels seen in mutant II-3 (Figure 16B).

Figure 16. Production of P65 and P30 in *M. pneumoniae* revertant II-3R. (A) Immunoblot analysis for production of P30. Molecular mass markers (kDa) are shown to the left, while arrows indicate migration of II-3R P30 and apparent multimers thereof. **(B)** Immunoblot analysis for production of P65. The 66 kDa molecular mass marker is indicated to the left.

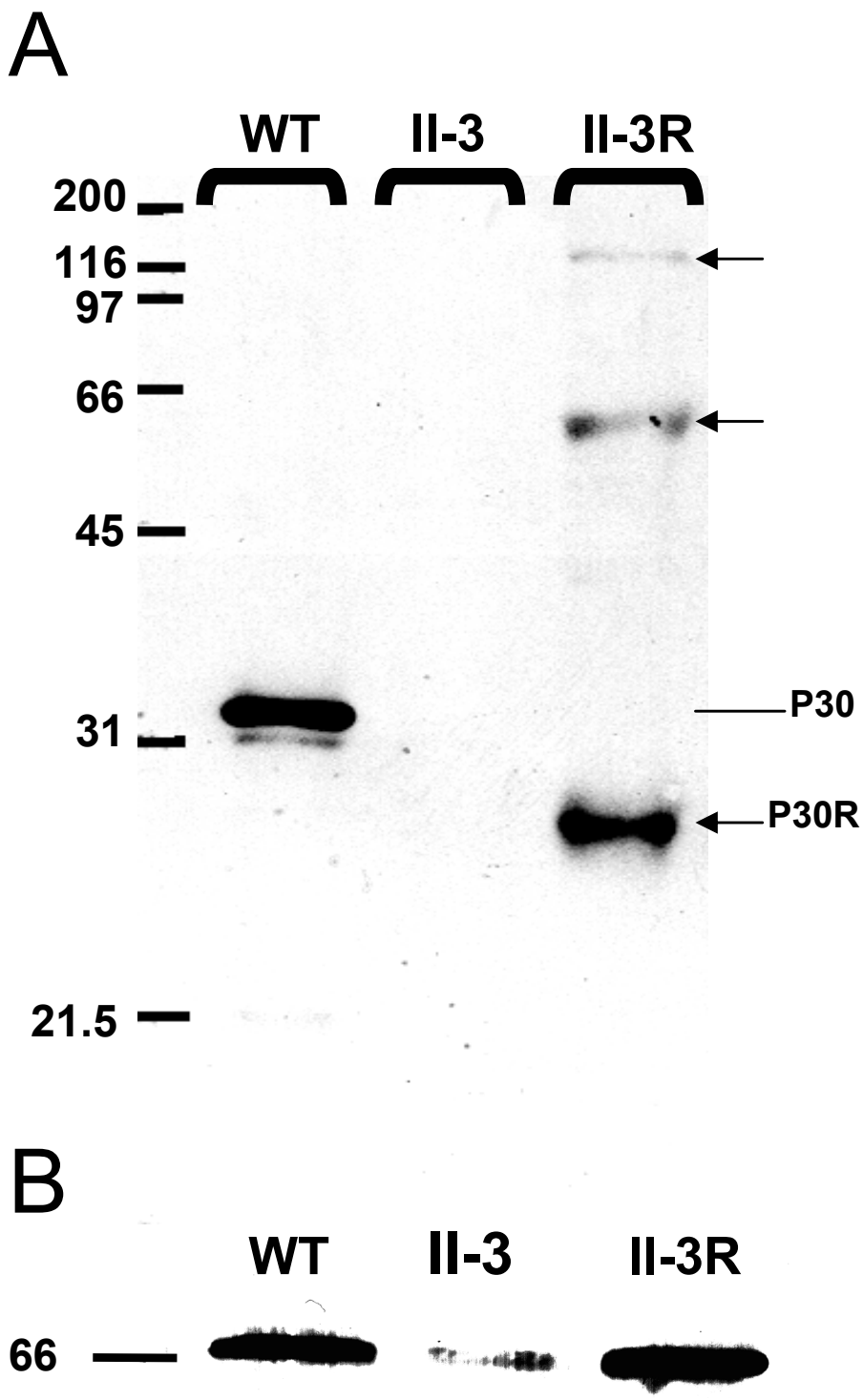
A
WT
II-3
II-3R
200
116
97
66
45
31
21.5
P30
P30R
B
WT
II-3
II-3R
66

Morphological Analysis of II-3R- Mutant II-3 exhibits a branched morphology (Romero-Arroyo *et al.*, 1999; Seto and Miyata, 2003), while complementation of II-3 with the recombinant wild-type *p30* allele restores cellular morphology to wild-type (Romero-Arroyo *et al.*, 1999). Phase-contrast and SEM images of II-3R revealed no morphological differences from the II-3 parental strain, with the predominant morphology being branched (Figure 17). Interestingly, upon addition of 4% gelatin to the growth medium II-3R but not II-3 assumed a more wild-type appearance when examined by phase-contrast microscopy (Figure 18). This morphological change was also noted with mutant II-7, with cells grown in medium containing 4% gelatin appearing indistinguishable from wild-type (data not shown).

Assessment of II-3R Adherence to Inert Surfaces, Erythrocytes, and Respiratory Epithelium- Revertant II-3R was isolated following enrichment by attachment to plastic and appeared HA-positive by qualitative screening of mycoplasma colonies (Romero-Arroyo *et al.*, 1999). When evaluated quantitatively for HA, revertant II-3R attached at a level that was only approximately 50% of that of wild-type *M. pneumoniae* but five-fold higher than the minimal cytadherence observed with mutant II-3 (Figure 19A). Furthermore, a similar pattern was observed for attachment to glass, with near background levels observed for mutant II-3, while revertant II-3R attached at a level approximately half of that seen with wild-type *M. pneumoniae* (data not shown). Upon re-examination of qualitative HA we noted a variable patchy pattern of erythrocyte attachment (Figure 19B), with many colonies fully covered with erythrocytes but others only partially covered. Sectoring was not apparent within colonies, and no consistent pattern to the location of erythrocyte attachment on the colonies was evident.

Figure 17. Morphology of wild-type (WT) *M. pneumoniae* cells, mutant II-3, II-3 complemented with wild-type P30 (II-3 + P30), and the revertant II-3R. Scanning electron micrographs of mycoplasmas grown for 2 hours on poly-L-lys-coated glass coverslips in Hayflick medium. The large central regions in the WT and II-3 + P30 panels are microcolonies; individual mycoplasmas can be seen around this region. Bar: 2 μm

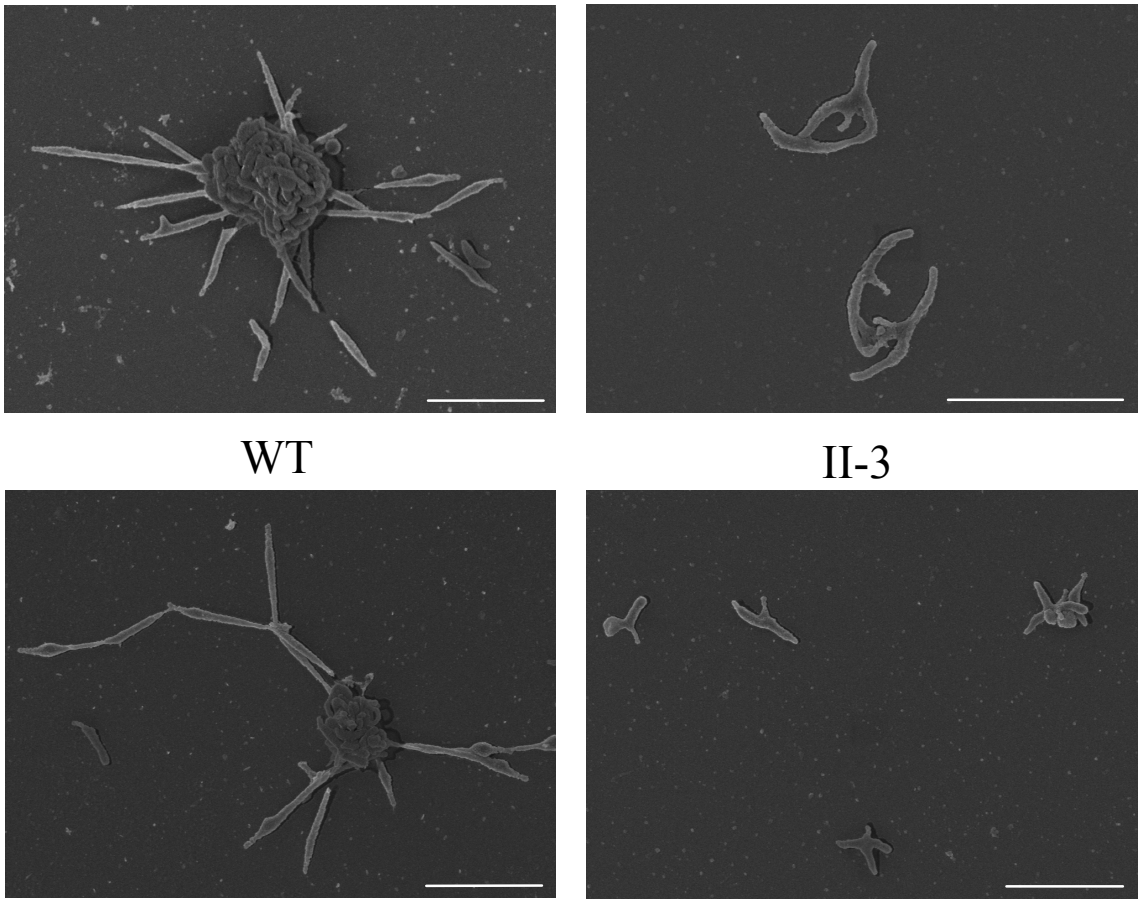

WT

II-3

II-3 + P30

II-3R

Figure 18. Morphology of WT, II-3, and II-3R *M. pneumonaie* cells in the presence (+) or absence (-) of 4% gelatin. Mycoplasma strains were grown in Hayflick medium for 2h on glass coverslips in the presence or absence of 4% gelatin (w/v) prior to fixation and DAPI staining. Scale bar: 2μm.

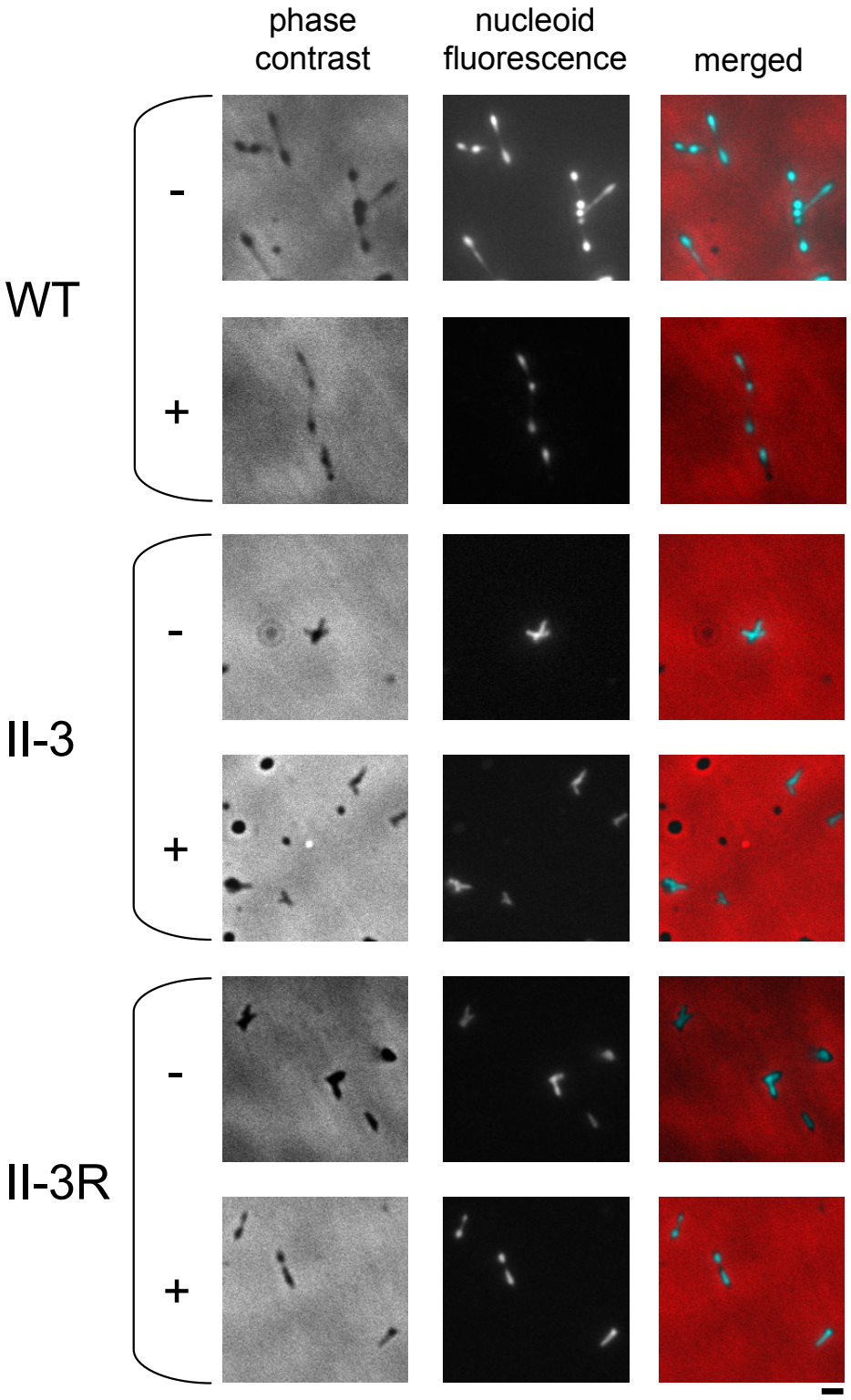
phase contrast
nucleoid fluorescence
merged
WT
II-3
II-3R
-
+
-
+
-
+

Figure 19. Adherence capacity of *M. pneumoniae* revertant II-3R and parent strains. Quantitative and qualitative hemadsorption (**A** and **B**, respectively), and quantitative attachment to hamster tracheal rings in organ culture **(C)**. Quantitative hemadsorption data **(A)** were from a single experiment and are representative of three separate experiments. Results in panel **C** were based upon two separate experiments, as indicated in the legend. Error bars denote positive standard deviations. Scale bar in panel **B**: 50 μm.

A

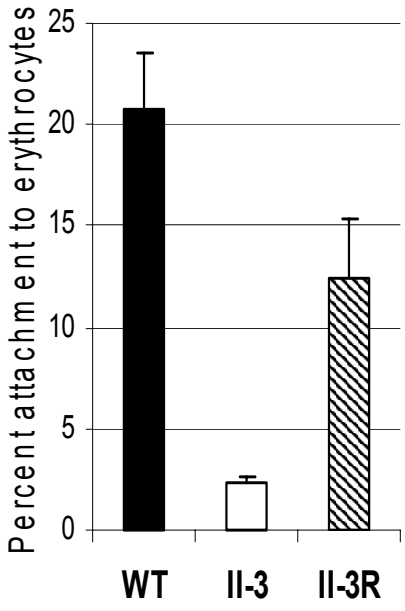
Percent attachment to erythrocytes
25
20
15
10
5
0
WT
II-3
II-3R

B

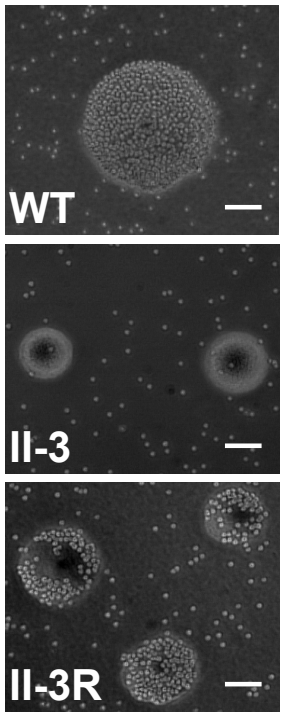
WT
II-3
II-3R

C

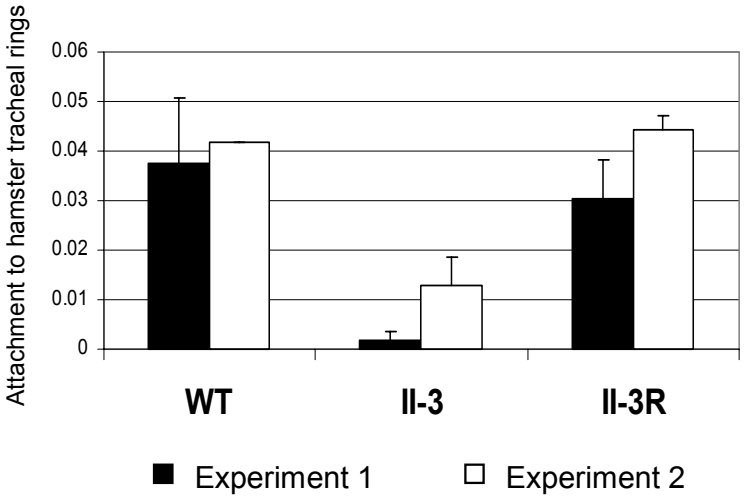
Attachment to hamster tracheal rings
0.06
0.05
0.04
0.03
0.02
0.01
0
WT
II-3
II-3R
Experiment 1
Experiment 2

While transformants of mutant II-3 producing recombinant wild-type P30 were fully HA positive, transformants producing recombinant revertant II-3R P30 exhibited the same patchy pattern of hemadsorption described above for II-3R (data not shown). Finally, we evaluated the attachment of revertant II-3R to respiratory epithelium, using as a model hamster tracheal rings in organ culture (Collier and Baseman, 1973; Krause *et al.*, 1982). In contrast to the intermediate level of adherence seen above with erythrocytes, II-3R attached at wild-type levels to hamster tracheal rings in organ culture (Figure 19C). Infected tracheal rings where additionally analyzed by TEM and laser scanning confocal microscopy (LSCM) using antibodies against *M. pneumoniae* and tubulin to visualize the mycoplasmas and ciliated epithelium, respectively (Figure 20). Mycoplasmas were not detected in uninfected tracheal rings in LSCM and TEM thin section images (Figure 20A, E). In infected tracheal rings, wild-type *M. pneumoniae* was preferentially localized to ciliated epithelial cells (Figure 20B). As cell numbers increased, mycoplasmas were also visualized in the junctions between adjacent non-ciliated cells (Figure 20C, F). Mutant II-3 is avirulent in the hamster model (Krause *et al.*, 1982), yet surprisingly LSCM images of tracheal epithelium infected with II-3 appeared identical to wild-type infected tissue (Figure 20D). LSCM images of II-3R infected tracheal rings likewise appeared identical to images of wild-type infections with mycoplasma cells localizing to ciliated epithelium and non-ciliated epithelial cell borders (data not shown). In TEM thin sections electron-dense cores were visualized in wild-type, II-3, and II-3R cells (Figure 20G). TEM images of mutant II-3 and revertant II-3R substantiated LSCM images showing similar attachment to hamster tracheal epithelium as the wild-type strain. Like wild-type *M. pneumoniae*, attachment of mutant II-3 to tracheal epithelium appeared to be mediated by

Figure 20. Localization of wild-type and mutant *M. pneumoniae* on hamster tracheal epithelium. The color composite images were generated from anti-*M. pneumoniae* (red) and anti-Tubulin (green) LSCM z-stacks to localize mycoplasma in relation to tracheal epithelial cilia. **(A)** LSCM image showing the luminal surface of uninfected hamster tracheal epithelium. **(B, C)** LSCM images of the luminal surface of hamster tracheal epithelium infected with wild-type *M. pneumoniae*. **(D)** LSCM image of the luminal surface of hamster tracheal epithelium infected with mutant II-3 *M. pneumoniae*. **(E)** TEM thin section of uninfected hamster tracheal epithelium. ci= cilia, mv= microvilli, cc= ciliated cell, gc= goblet cell. **(F)** TEM thin section of hamster tracheal epithelium infected with wild-type *M. pneumoniae*. myc= mycoplasma. **(G)** Thin section TEM images of wild-type, II-3, and II-3R infected hamster tracheal epithelium. Arrow points indicate electron-dense cores. Scale bars: 250 nm unless indicated otherwise.

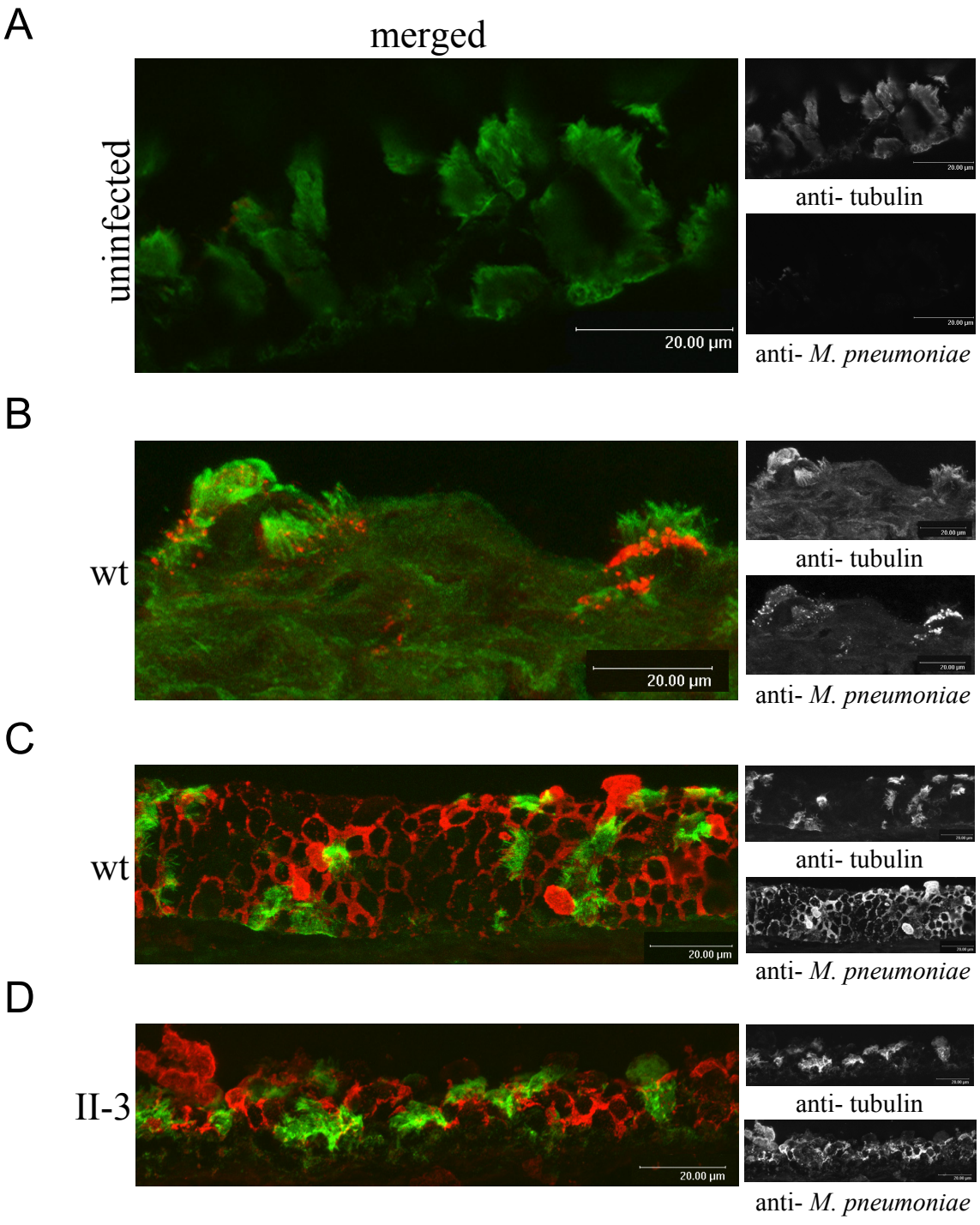
A
merged
uninfected
20.00 µm
anti- tubulin
anti- M. pneumoniae
B
wt
20.00 µm
anti- tubulin
anti- M. pneumoniae
C
wt
20.00 µm
anti- tubulin
anti- M. pneumoniae
D
II-3
20.00 µm
anti- tubulin
anti- M. pneumoniae

E

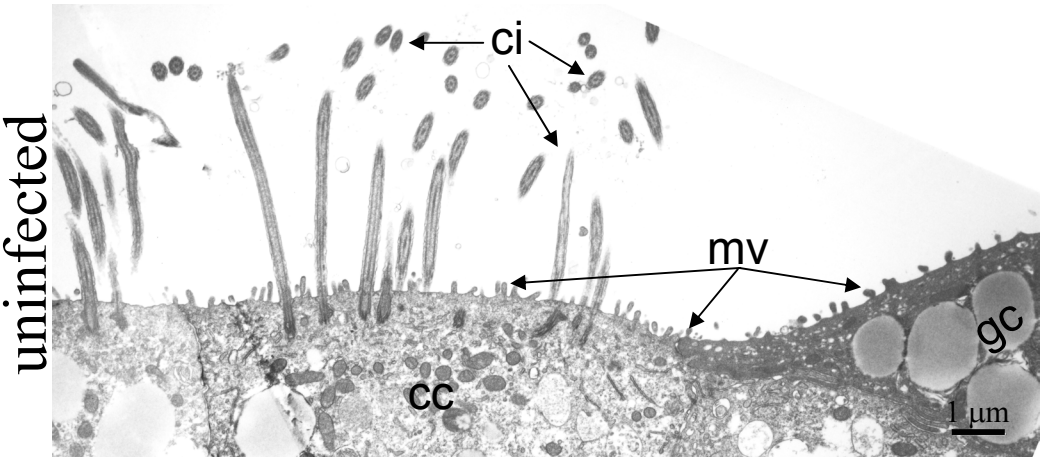

F

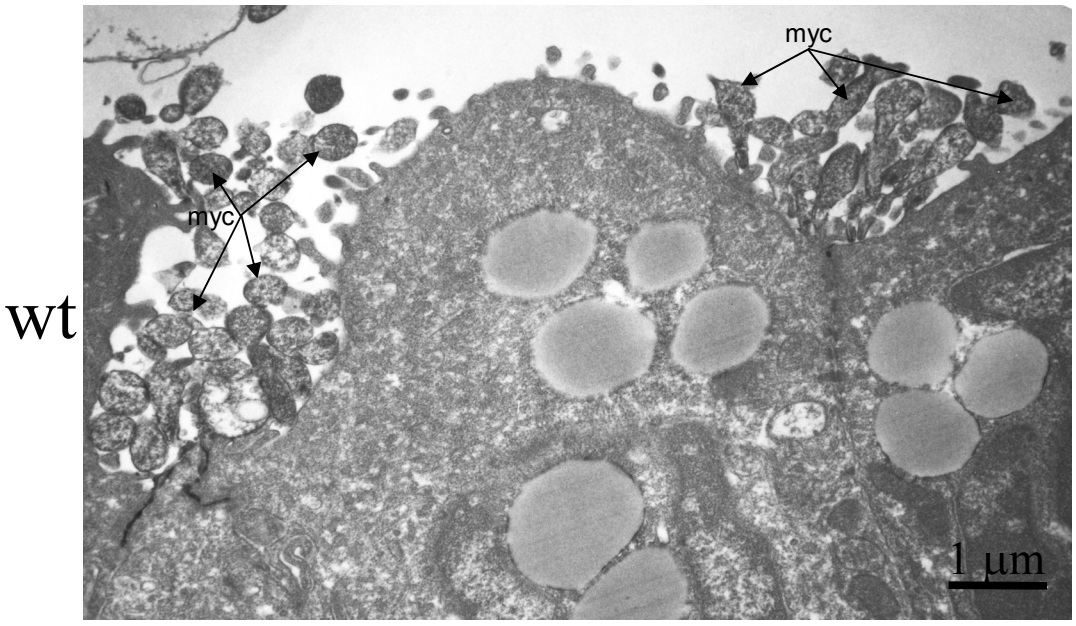

G

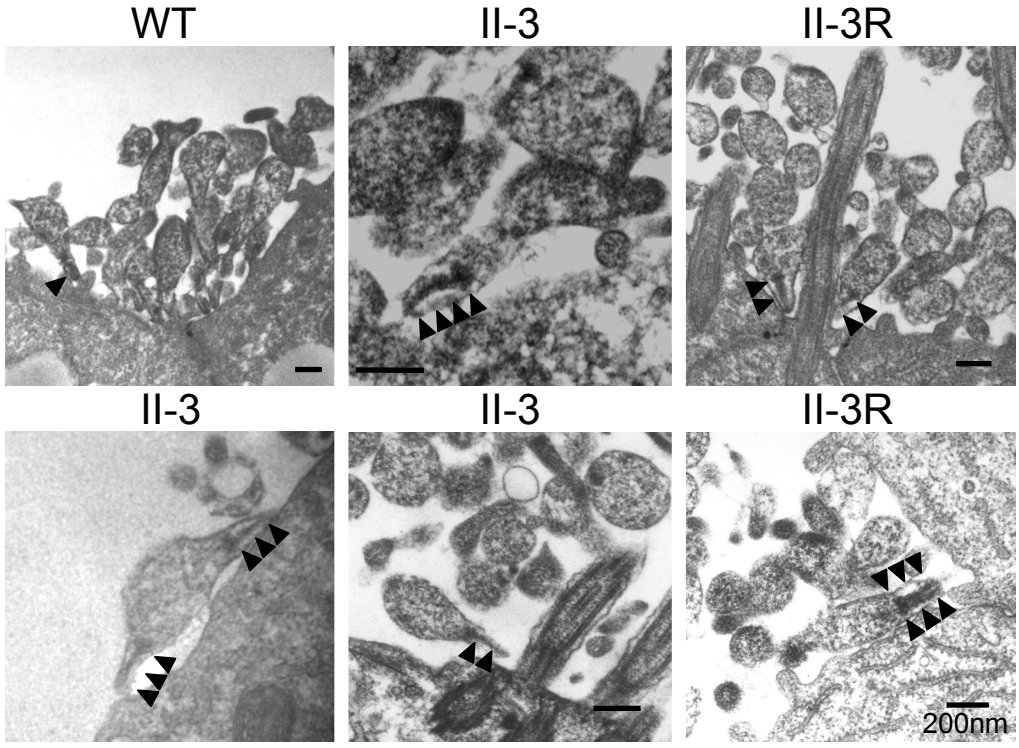

the attachment organelle and in some cases two electron dense cores were seen in individual II-3 cells.

Structure-Function Analysis of Protein P30

Due to a lack of mutants with defects in these regions, functional domains of P30 were analyzed by creating in-frame deletions of the predicted cytoplasmic domain (P30ΔI: 38-68), and a conserved region of the extracellular domain (P30ΔII: 101-120) (Figure 21A). Consecutive truncations of the extreme C-terminus of P30 where also created resulting in three P30 variants (P30ΔIII-A,-B, and -C) truncating P30 at residue 247, 199, and 175 of the 274-residue protein, respectively (Figure 21B). Additionally, the single cysteine in P30 (Cys 81) was mutagenized to a serine creating P30Cys81Ser. Altered *p30* alleles from all constructs were cloned into Tn*4001* and transformed into mutant II-3, and multiple transformants were analyzed.

P30 Detection in Deletion Derivatives- Western immunoblots were performed on P30 deletion constructs to confirm recombinant P30 production. P30 was detected in all deletion derivatives with the exception of mutants P30ΔII, and P30ΔIII-C (Figure 22). P30 in P30ΔI had a predicted molecular mass of 26.34 kDa and migrated aberrantly at 35 kDa on 12% SDS-PAGE gels. P30 in P30ΔIII-A had a predicted mass of 26.85 kDa and migrated at 29 kDa on 12% SDS-PAGE gels. P30ΔIII-B P30 had a predicted mass of 21.93 kDa and migrated at 25 kDa on 12% SDS-PAGE gels. P30 in P30Cys81Ser migrates identically to wild-type P30 at 32 kDa on 12% SDS-PAGE gels. For the C-terminal deletion derivatives, P30 levels decreased proportionally with each successive deletion, with P30ΔIII-A >> P30ΔIII-B >> P30ΔIII-C.

Figure 21. P30 deletion-derivatives for structure-function analysis. P30 consists of a predicted signal sequence (black), cytoplasmic domain (light blue), membrane-spanning region (yellow), and extracellular (red) proline-rich C-terminal domain. **(A)** The wild-type *p30* allele was modified by PCR to create in-frame deletions of the predicted cytoplasmic domain and a conserved region in the surface-exposed domain (P30ΔI, and P30ΔII, respectively). The wild-type *p30* allele was also modified by site-directed mutagenesis to substitute a serine codon for a cysteine (P30Cys81Ser). **(B)** II-7 and M6 are spontaneously arising P30 mutants containing identical in-frame mutations within the proline-repeat encoding region. Mutant M6 contains a second mutation in the cytadherence-accessory protein HMW1. To create C-terminal deletion mutants, PCR was performed using a 3' primer homologous to the *p30* region encoding the proline repeats also incorporating a stop codon. Three C-terminal truncation mutants were created using this technique (P30 ΔIII-A,-B, and-C). All modified recombinant *p30* alleles were cloned into Tn*4001*mod and transformed into P30 null mutant II-3.

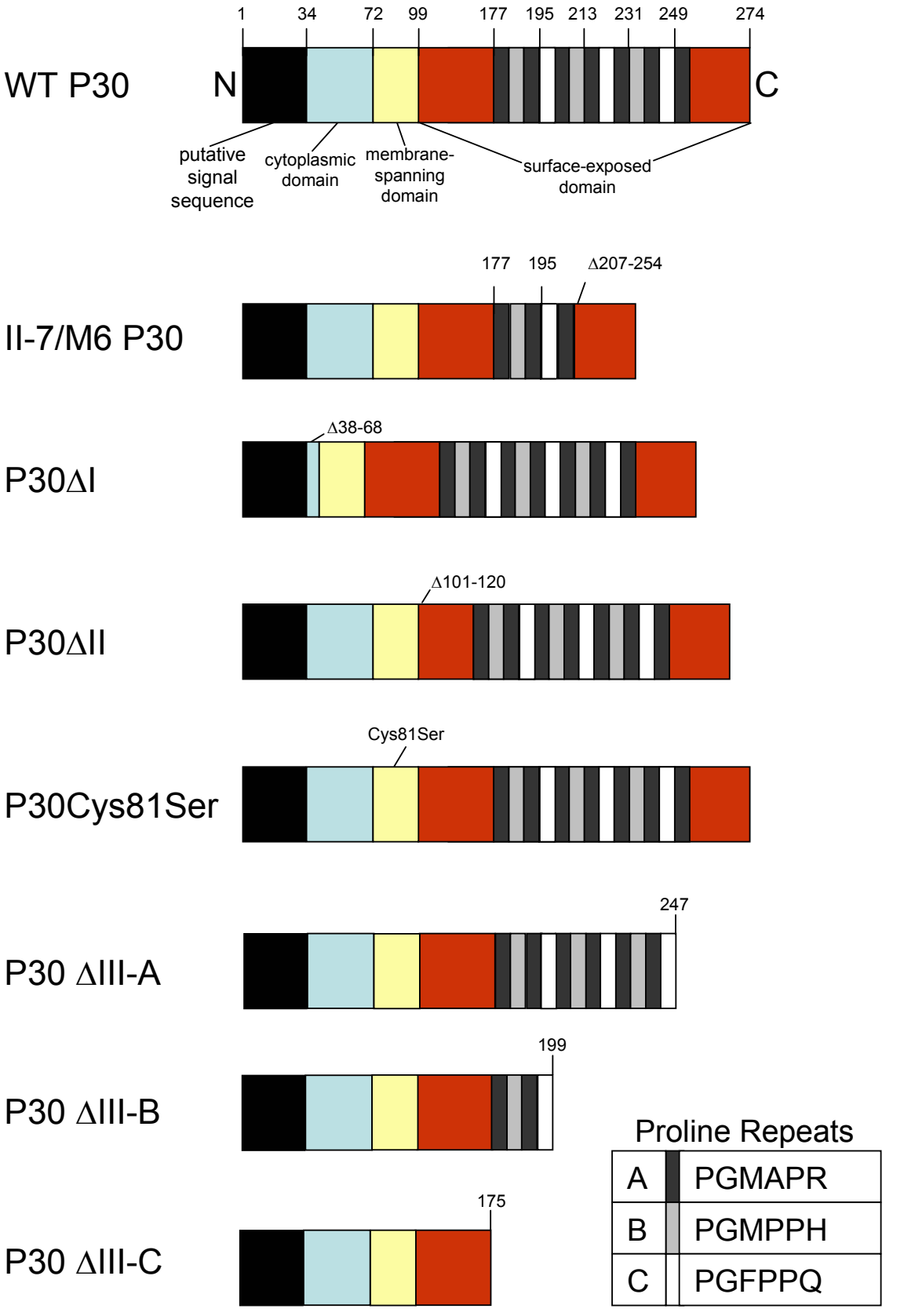
WT P30
N
C
1
34
72
99
177
195
213
231
249
274
putative signal sequence
cytoplasmic domain
membrane-spanning domain
surface-exposed domain
II-7/M6 P30
177
195
Δ207-254
P30ΔI
Δ38-68
P30ΔII
Δ101-120
P30Cys81Ser
Cys81Ser
P30 ΔIII-A
247
P30 ΔIII-B
199
P30 ΔIII-C
175
Proline Repeats
A
PGMAPR
B
PGMPPH
C
PGFPPQ

Figure 22. Immunoblot analysis of P30 production from recombinant *p30* deletion derivatives in P30 null mutant II-3. The 31-kDa molecular mass marker is indicated to the right.

[1] Lack of P30 detection in P30ΔIII-C possibly due to loss of epitope recognized by antibody.

[2] Multimeric P30 in II-3R is not seen as this particular immunoblot was cut in order to probe for protein P65.

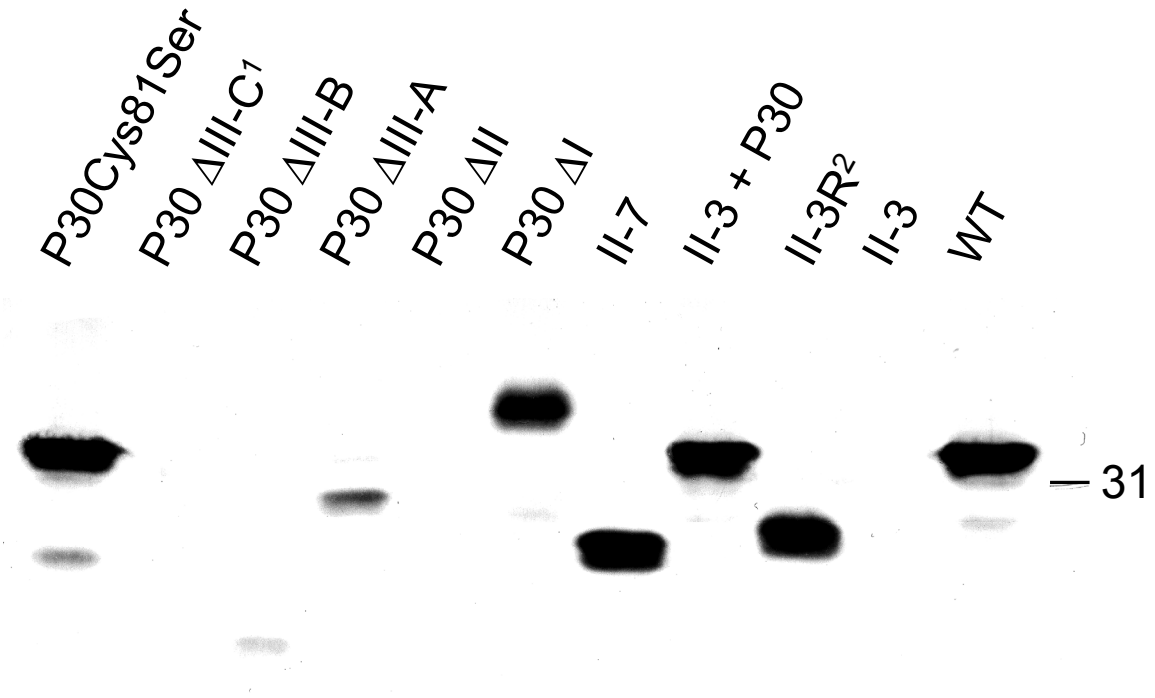
P30Cys81Ser
P30 ΔIII-C1
P30 ΔIII-B
P30 ΔIII-A
P30 ΔII
P30 ΔI
II-7
II-3 + P30
II-3R2
II-3
WT
31

P30ΔI and P30Cys81Ser levels did not appear appreciably dissimilar to those in wild-type and II-3 complemented with recombinant wild-type *p30*.

P65 Levels in P30 Deletion Derivatives- Due to decreased P65 stability in the P30 mutant II-3, the steady-state levels of P65 were also examined in the P30 deletion derivatives to determine if a particular domain is associated with the stabilization of P65. Western immunoblotting using P65-specific antiserum, in conjunction with anti-P40 antiserum (protein C) as a loading control, revealed differences in P65 levels depending on the P30 deletion derivative examined (Figure 23). Deletion of the predicted cytoplasmic domain of P30 (P30ΔI), did not affect the ability of this P30 derivative to stabilize protein P65 (Figure 23B). Loss of the conserved region in the extracellular domain of P30 (P30ΔII), however, resulted in less P65 than was seen in the P30 null mutant II-3 (Figure 23A). The C-terminal deletion derivatives (P30ΔIII-A,-B, and –C) had similar levels of P65 to one another and to mutants II-3, and II-7. Substitution of cysteine 81 to serine (P30Cys81Ser) did not affect the ability of P30 to stabilize P65. As previously demonstrated, mutant II-3 complemented with wild-type recombinant *p30*, and II-3 revertant (II-3R), appeared to fully restore P65 stability to wild-type levels (Figure 23A).

HA Rescue Analysis of P30 Deletion Derivatives- The ability of recombinant *p30* deletion derivates to restore HA in mutant II-3 was examined (Figure 24). P30 deletion-derivatives within the cytoplasmic domain (P30ΔI), conserved extracellular domain (P30ΔII), and C-terminus (P30ΔIII-A, -B, -C) failed to restore HA even to intermediate levels in the II-3 background.

Figure 23. Immunoblot analysis of protein P65 levels in transformants producing P30 deletion derivatives. Protein size standards are indicated in kDa on the left. As a loading control, blots were also probed with anti-P40 antibodies (protein C) as indicated. **(A)** Relative P65 levels of P30ΔII, (P30ΔIII-A, -B, and -C), II-3 complemented with wild-type *p30* (II-3+P30), and P30Cys81Ser. *****Low levels of P65 in P30ΔII were occasionally detected on some blots. **(B)** P65 levels of P30ΔI in relation to wild-type, II-3, and P30 truncation mutants P30ΔIII-A, B, and C.

A

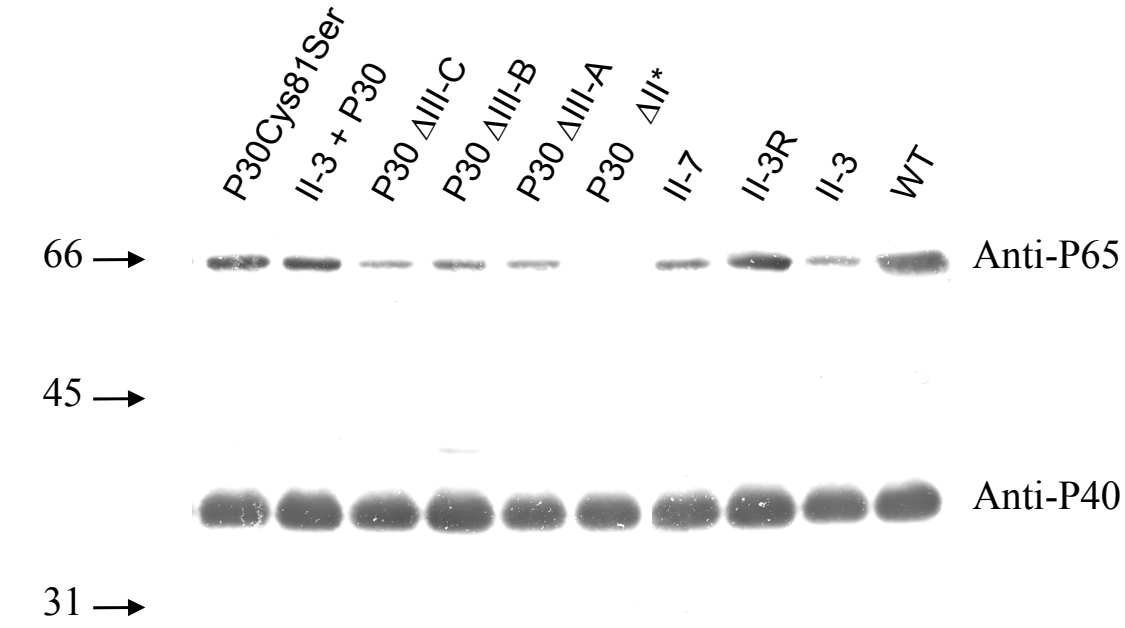
P30Cys81Ser
II-3 + P30
P30 ΔIII-C
P30 ΔIII-B
P30 ΔIII-A
P30 ΔII*
II-7
II-3R
II-3
WT
66
45
31
Anti-P65
Anti-P40

B

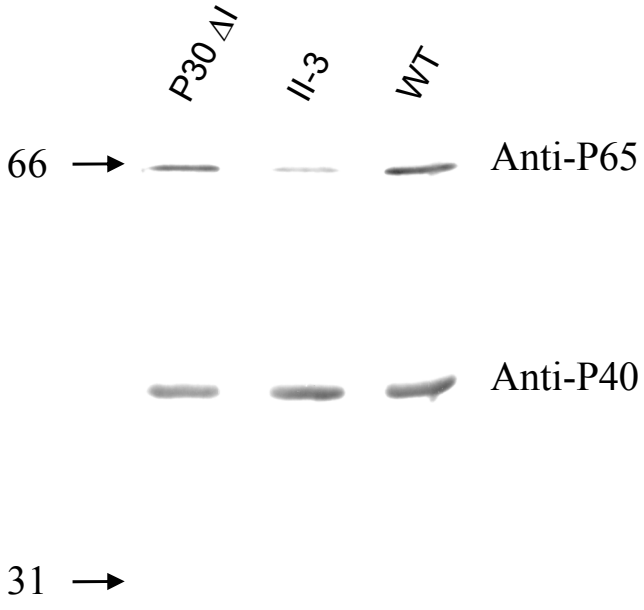
P30 ΔI
II-3
WT
66
31
Anti-P65
Anti-P40

Figure 24. Qualitative hemadsorption analysis in mutant II-3 transformed with P30 deletion derivatives. A 1:100 suspension of sheep erythrocytes in PBS was applied to mycoplasma colonies grown on PPLO agar. Plates were then incubated 30m at 37ºC, washed 3x with PBS, and viewed with an inverted phase-contrast microscope. Scale bars equal 50 μm and are located at the bottom right of each panel.

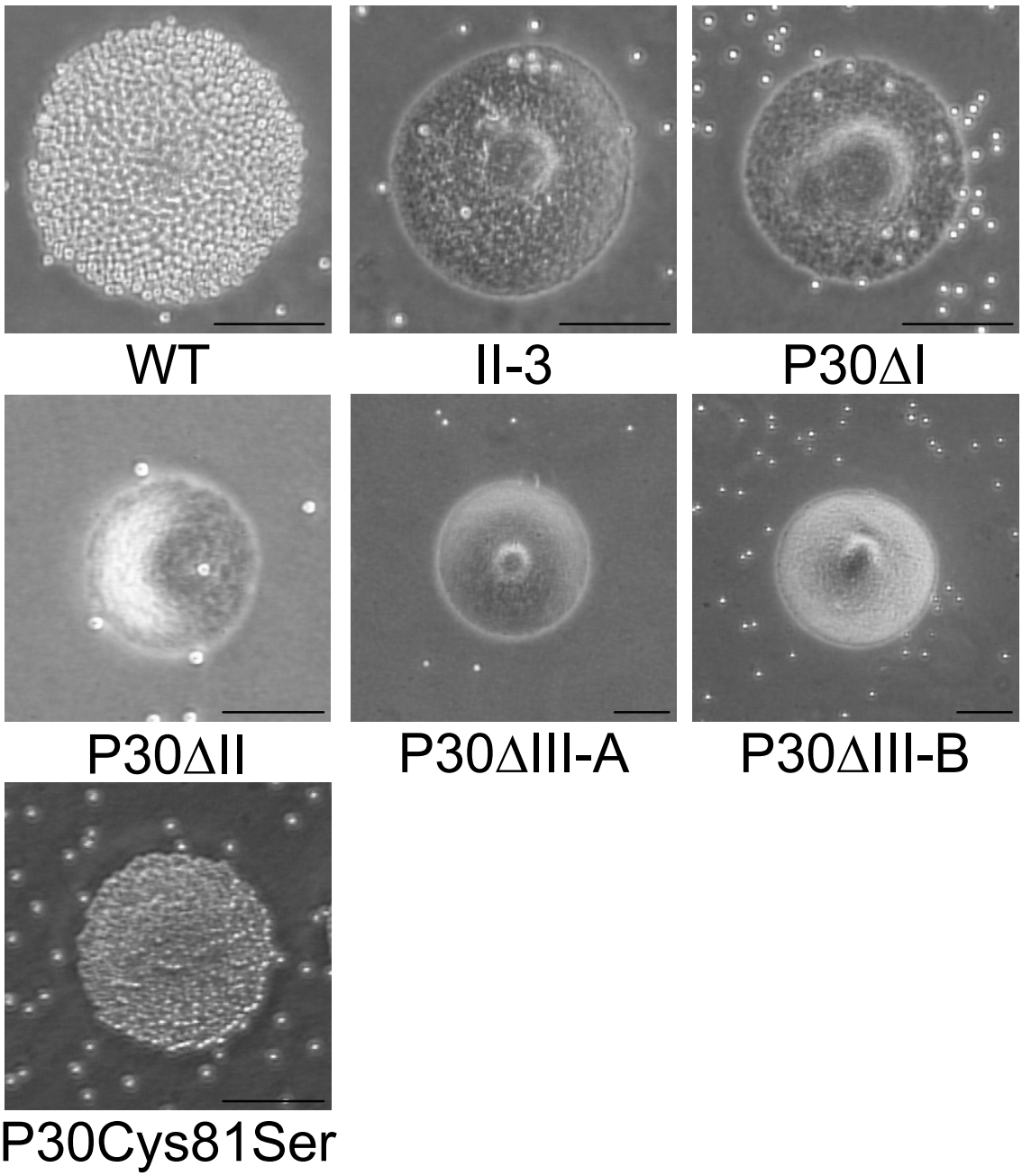
WT
II-3
P30ΔI
P30ΔII
P30ΔIII-A
P30ΔIII-B
P30Cys81Ser

Substitution of the single cysteine in the wild-type *p30* allele (P30Cys81Ser), however, resulted in wild-type HA in this background as determined by qualitative hemadsorption.

Analysis of a P30-GFP Fusion in *M. pneumoniae*

To examine P30 localization and function in vivo, the wild-type *p30* allele was ligated to the enhanced green fluorescent protein gene *egfp*. This C-terminal *p30-gfp* fusion was then transformed into the mutant II-3 background, and transformants were assessed for P30-GFP production and hemadsorption capabilities (Figure 25). Western immunoblots indicated the stable production of the P30-GFP fusion in mutant I-2 and II-3 backgrounds (Figure 25A). P30-GFP has a predicted mass of 57 kDa and migrated at 63 kDa on 12% SDS-PAGE gels. The addition of GFP to the C-terminus of P30 did not inhibit the ability of P30 to restore hemadsorption in mutant II-3, as determined qualitatively (Figure 25B). P30-GFP localization was also determined in living cells (Figure 26). GFP fluorescence at the attachment organelle in II-3 appeared identical to fluorescence from wild-type P30 immunolocalization (Figures 26A and B). Confirmation that the polar GFP localization was indeed at the attachment organelle was achieved by time-lapse microcinematography, where fluorescence was observed at the leading end of motile cells (data not shown). P30-GFP localization in mutant I-2 and M6 backgrounds appeared different from that seen in the II-3 background, being much more diffuse albeit with some polar localization (Figure 26C). Localization of P30-GFP in the wild-type background was identical to that of II-3 transformed with the fusion and likewise did not alter the hemadsorption capability in the wild-type background (data not shown).

Figure 25. Functional analysis of a P30-GFP fusion in *M. pneumoniae*. The *p30-gfp* gene was cloned to the 3'end of the wild-type *p30* gene, creating a C-terminal translational fusion. **(A)** Western immunoblot analysis using P30 specific antisera against wild-type *M. pneumoniae* (WT), and mutants II-3 and I-2 transformed with the P30-GFP fusion. Molecular markers are shown at the right in kDa. P30 and recombinant P30-GFP are indicated. **(B)** Qualitative hemadsorption of II-3 transformed with the wild-type recombinant *p30* allele (positive control), II-3 transformed with *p30* deletion derivative P30ΔIII-A (negative control), and II-3 transformed with the P30-GFP fusion. Scale bars: 50 μm.

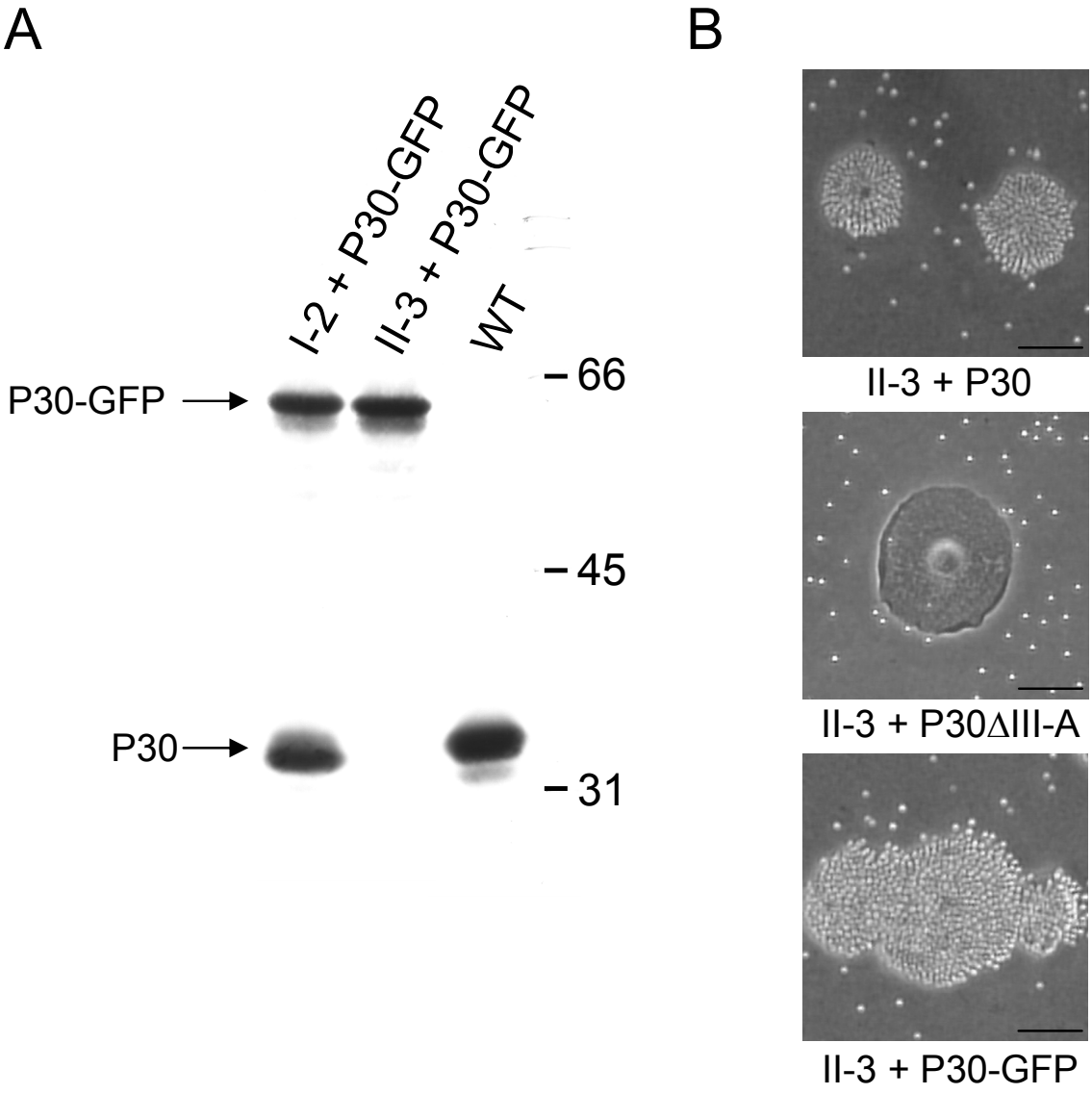
A
I-2 + P30-GFP
II-3 + P30-GFP
WT
P30-GFP
P30
66
45
31
B
II-3 + P30
II-3 + P30ΔIII-A
II-3 + P30-GFP

Figure 26. P30-GFP localization by fluorescent microscopy. Wild-type and mutant *M. pneumoniae*, transformed with recombinant wild-type *p30-gfp* as indicated. Left panel is phase-contrast image, middle panel is fluorescence, and right panel is a composite of the phase-contrast image with the fluorescent image false-colored green for P30-GFP fluorescence or red for P30 immunofluorescence. White arrows indicate cells with nascent attachment organelles. All scale bars: 2.5μm. **(A)** Mutant II-3 transformed with recombinant wild-type *p30-gfp*. **(B)** Comparative image of P30 localized in wild-type *M. pneumoniae* using P30-specific antisera. **(C)** P30-GFP fluorescence in mutant I-2, and M6 backgrounds.

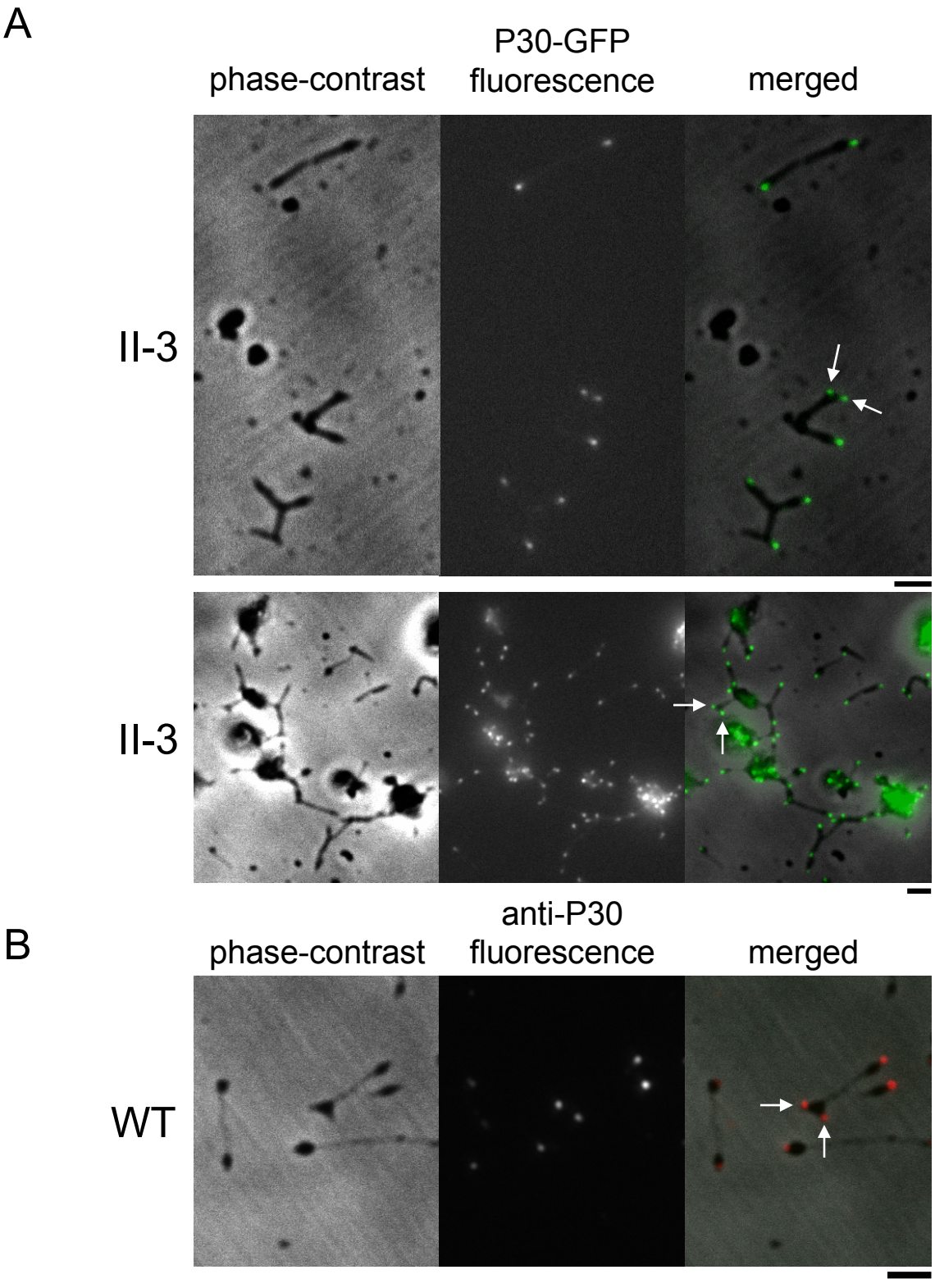
A
phase-contrast
P30-GFP
fluorescence
merged
II-3
II-3
B
phase-contrast
anti-P30
fluorescence
merged
WT

C

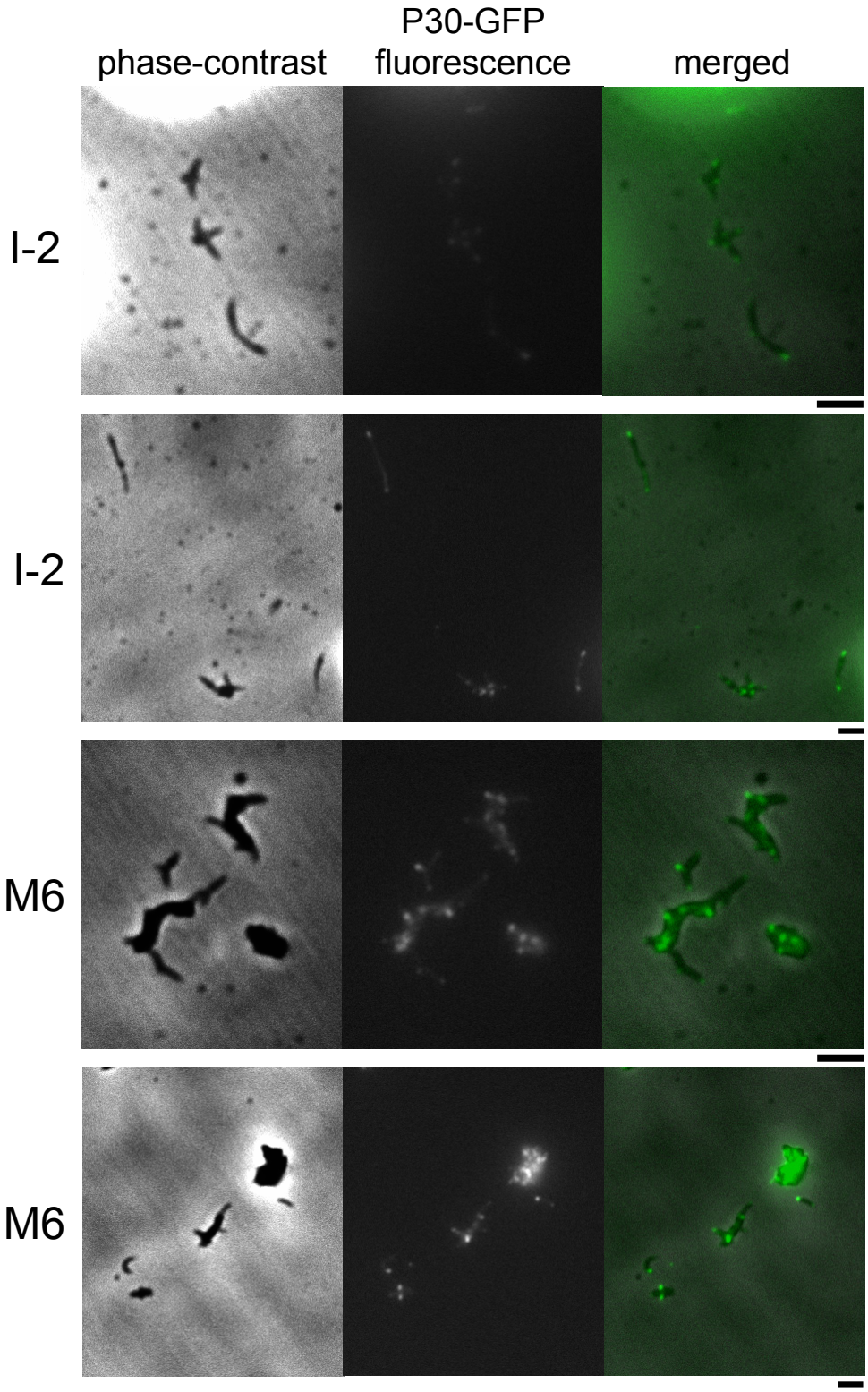

P30 Immunolocalization and Morphology in Cytadherence Mutants

To determine if a particular domain of P30 is needed for its proper localization to the attachment organelle, P30 immunolocalization was investigated in the P30 deletion derivatives. Nucleoid fluorescence generated from the nucleic acid stain DAPI is a general indicator of cellular morphology comparable to the corresponding cellular image seen in phase-contrast microscopy (Seto *et al.*, 2001). Merging of DAPI fluorescent images with the corresponding immunofluorescent images was used to determine protein localization in relation to the mycoplasma cell. As was previously demonstrated, P30 localized to the attachment organelle in wild-type *M. pneumoniae* (Dallo *et al.*, 1990; Seto *et al.*, 2001). Fluorescence from wild-type mycoplasmas probed with anti-sera produced against whole *M. pneumoniae* cells was generally distributed throughout the cell in marked contrast to the condensed polar focus seen when probed with anti-P30 antibodies (Figure 27A). Consistent with P30-GFP fluorescence in mutant I-2, P30 immunofluorescence in this mutant was faint and diffuse, with some indication of polar localization (Figure 27B). In mutant IV-22 bright P30 foci were seen. Due to the highly branched morphology in this mutant, fluorescent localization to a pole using epifluorescent microscopy was unclear. Wild-type *M. pneumoniae* harboring a transposon insertion in the *hmw3* gene (HMW3-) had many variations in P30 localization. In some cells P30 localization and cellular morphology appeared identical to that seen in the wild-type. In other cells there was a complete absence of detectable P30 but a wild-type-like morphology. Branched HMW3- cells either contained diffuse P30 fluorescence, bright foci of P30 fluorescence or a complete absence of detectable P30.

Figure 27. Immunolocalization of P30 in wild-type, mutant, and recombinant *M. pneumoniae* strains by fluorescence microscopy. Merged images are composed of nucleoid fluorescence from DAPI (false-colored cyan) and immunofluorescence from Cy3 (false-colored red) secondary antibody. **(A)** Immunolocalization of P30 and FtsH as a diffuse localization control in wild-type *M. pneumoniae*. **(B)** Immunolocalization of P30 in cytadherence mutants and recombinant *p30* mutants. All scale bars: 2 μm.

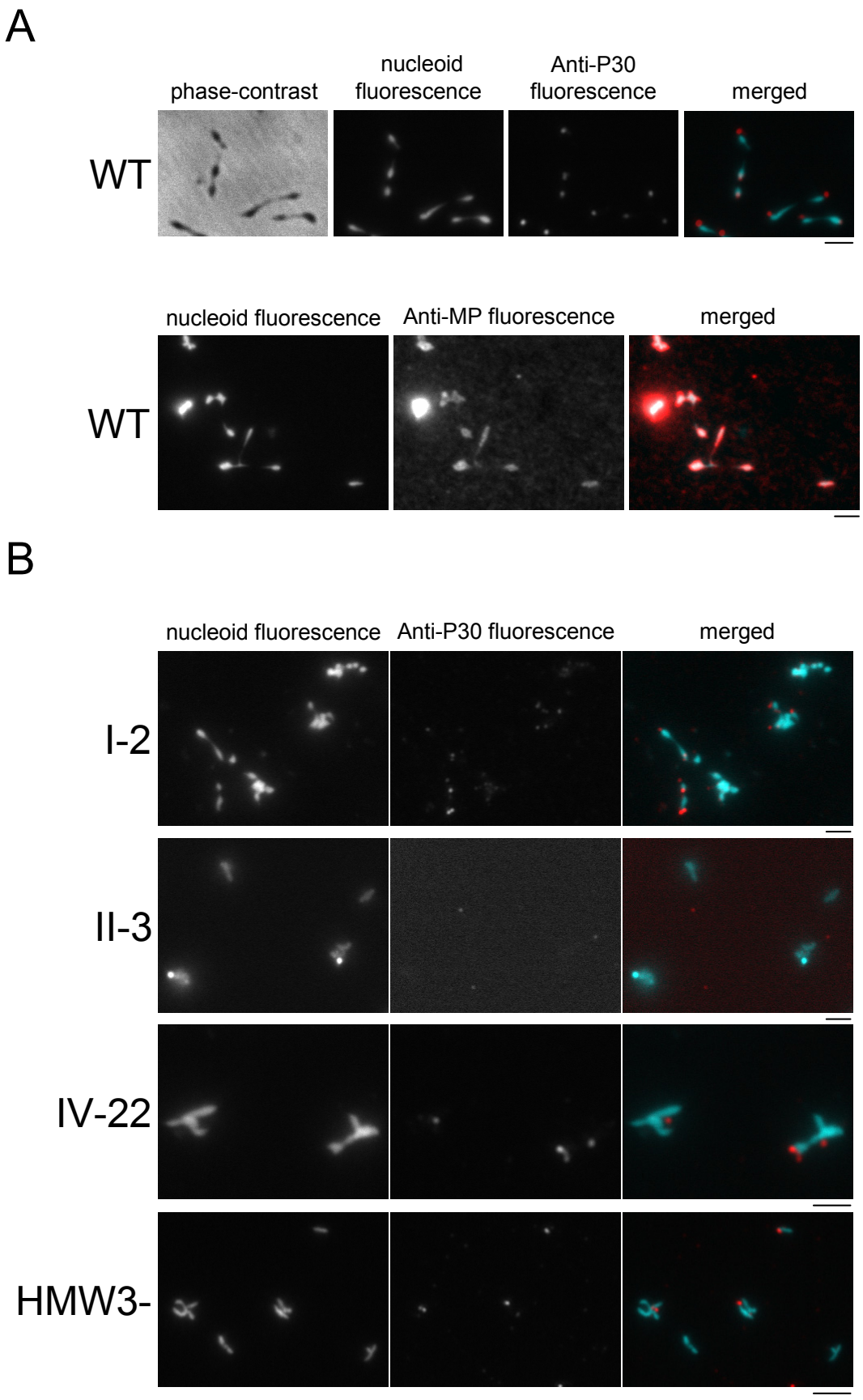
A
phase-contrast
nucleoid fluorescence
Anti-P30 fluorescence
merged
WT
nucleoid fluorescence
Anti-MP fluorescence
merged
WT
B
nucleoid fluorescence
Anti-P30 fluorescence
merged
I-2
II-3
IV-22
HMW3-

C

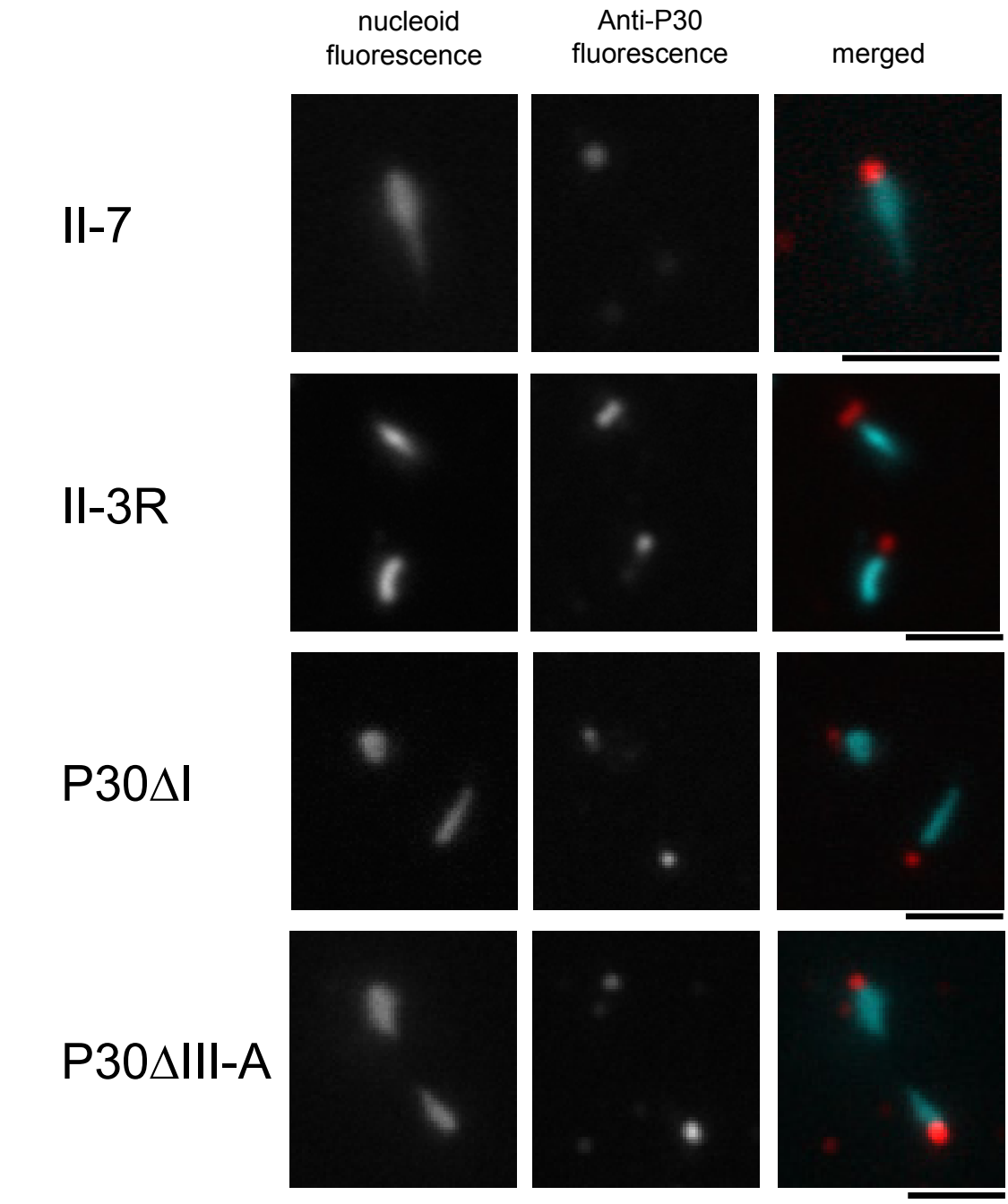
nucleoid fluorescence
Anti-P30 fluorescence
merged
II-7
II-3R
P30ΔI
P30ΔIII-A

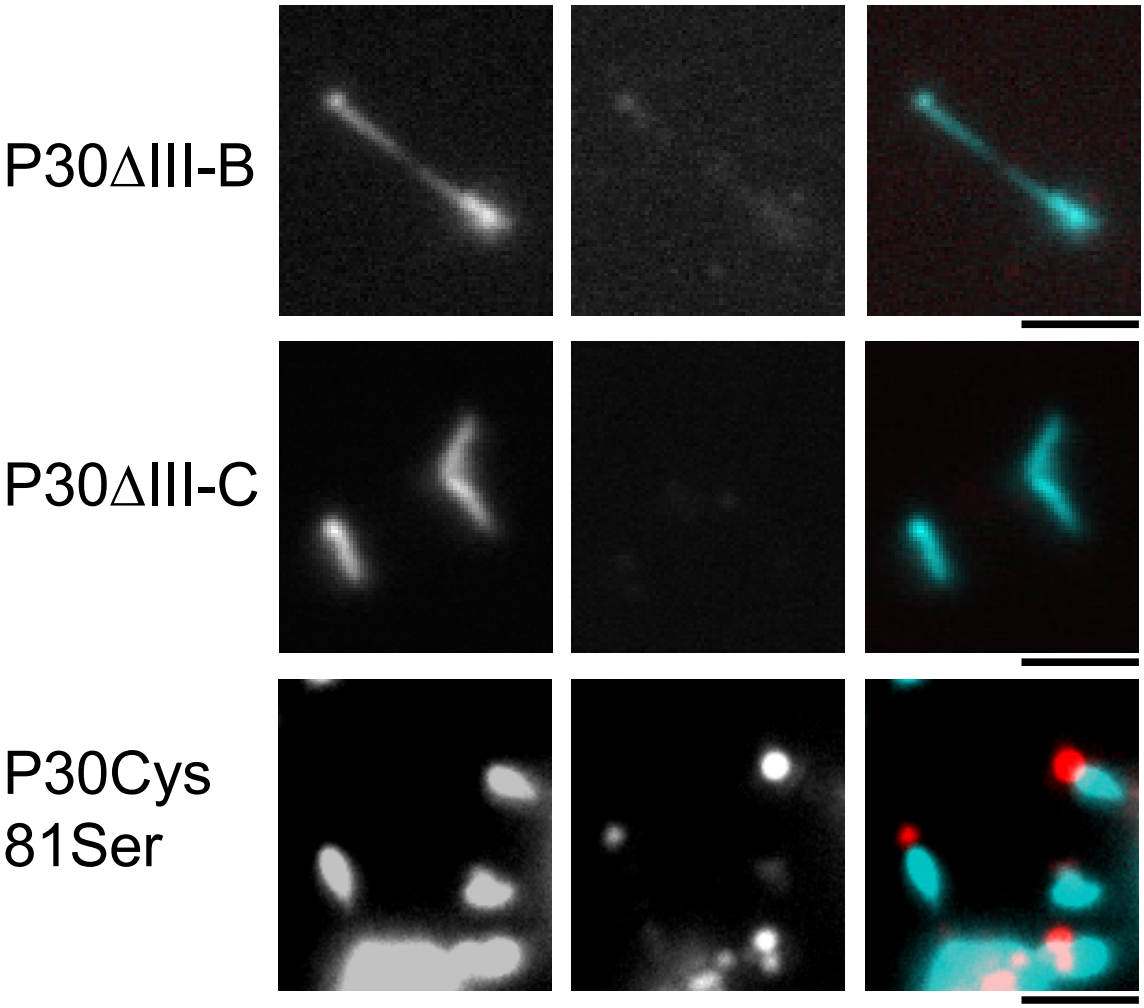
P30ΔIII-B
P30ΔIII-C
P30Cys
81Ser

In P30 mutant II-7, truncated P30 localized similarly to what is seen in wild-type, and cells were likewise morphologically similar to wild-type in the presence of 4% gelatin (Figure 27C). The II-3 P30 revertant (II-3R) localized P30R to the attachment organelle and appeared morphologically similar to wild-type. Deletion of the cytoplasmic domain of P30 (P30ΔI) did not alter its ability to localize to bright foci. This mutant was most morphologically similar to P30 null mutant II-3, having a predominantly branched morphology, although unlike II-3 a small proportion of cells appeared to have wild-type morphology. P30ΔII P30 was undetectable by western immunoblotting and what signal that was seen by immunofluorescence appeared to be distributed throughout the cell and just above background fluorescence seen in mutant II-3. Mutant II-3/P30ΔII was morphologically identical to mutant II-3, within the limits of light microscopy. The C-terminal deletion derivates P30ΔIII-A and –B exhibited a polar localization, and conferred a morphology more filamentous than branched. P30ΔIII-C was not detectable and failed to restore a normal phenotype to mutant II-3 (data not shown). P30 localization and morphology in II-3/P30Cys81Ser was indistinguishable from the wild-type strain.

Examination of P65 Localization in P30 Deletion Derivatives

As previously reported, P65 stability but not localization was affected by the absence of P30 (Jordan *et al.*, 2001). We examined P65 localization in P30 deletion derivatives further using immunofluorescence microscopy. Consistent with recent immunofluorescence co-localization studies (Seto and Miyata, 2003), P65 co-localized with P30-GFP produced in a mutant II-3 background (Figure 28A). With the exception of P30ΔII, where no P65 was detected (data not shown), P65 localized normally in all P30 deletion derivates regardless of the domain affected or extent of deletion (Figure 28B).

Figure 28. Immunolocalization of P65 in wild-type, mutant, and recombinant *M. pneumoniae* strains by fluorescence microscopy. (A) Immunolocalization of P65 in II-3 producing P30-GFP. Cyan indicates nucleoid fluorescence, red is P65 immunofluorescence, and green is P30-GFP fluorescence. **(B)** Immunolocalization of P65 in WT, II-3R, P30ΔI, P30ΔII, (P30ΔIII-A, B, and C), and P30Cys81Ser. Scale bars: 2 μm.

A

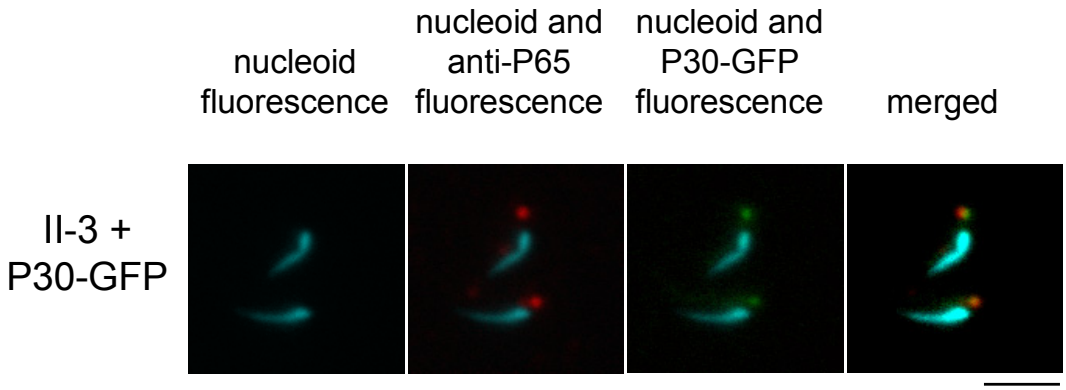
nucleoid fluorescence
nucleoid and anti-P65 fluorescence
nucleoid and P30-GFP fluorescence
merged
II-3 + P30-GFP

B

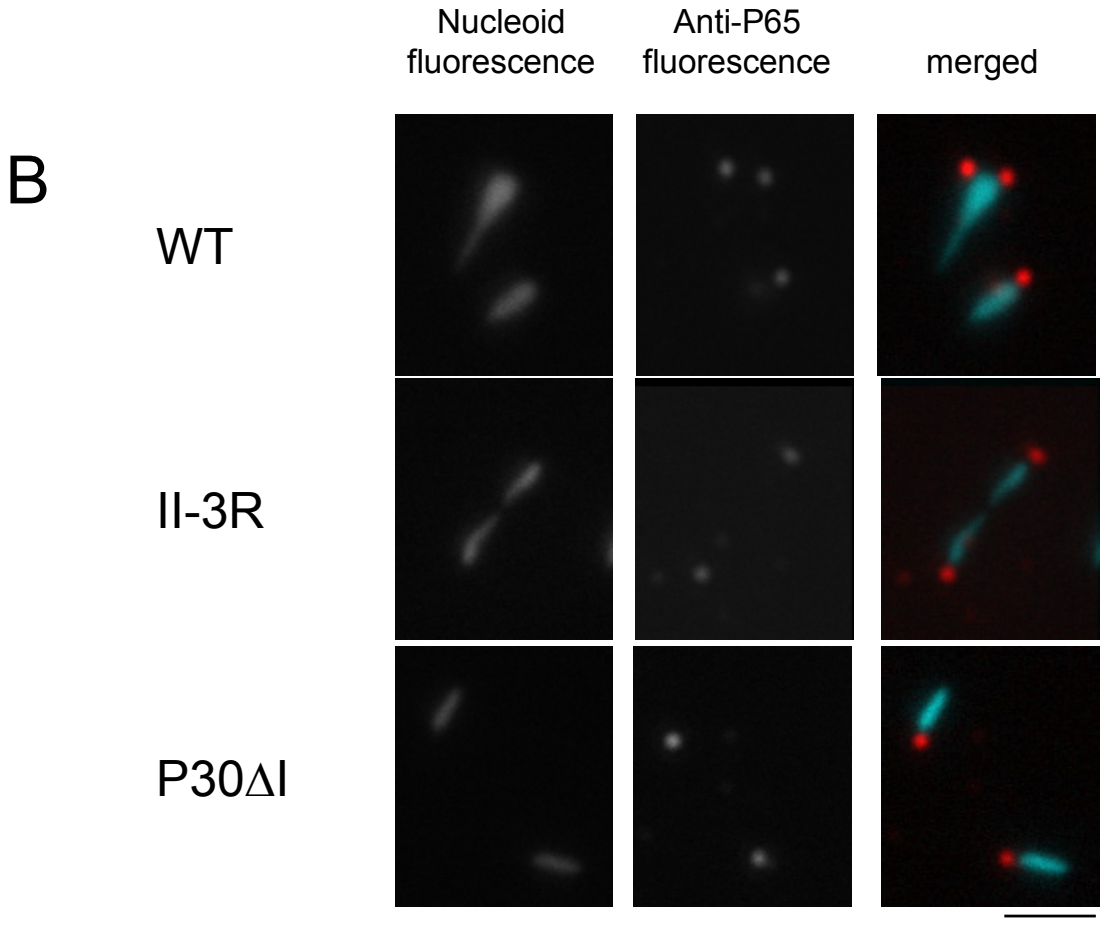
Nucleoid fluorescence
Anti-P65 fluorescence
merged
WT
II-3R
P30ΔI

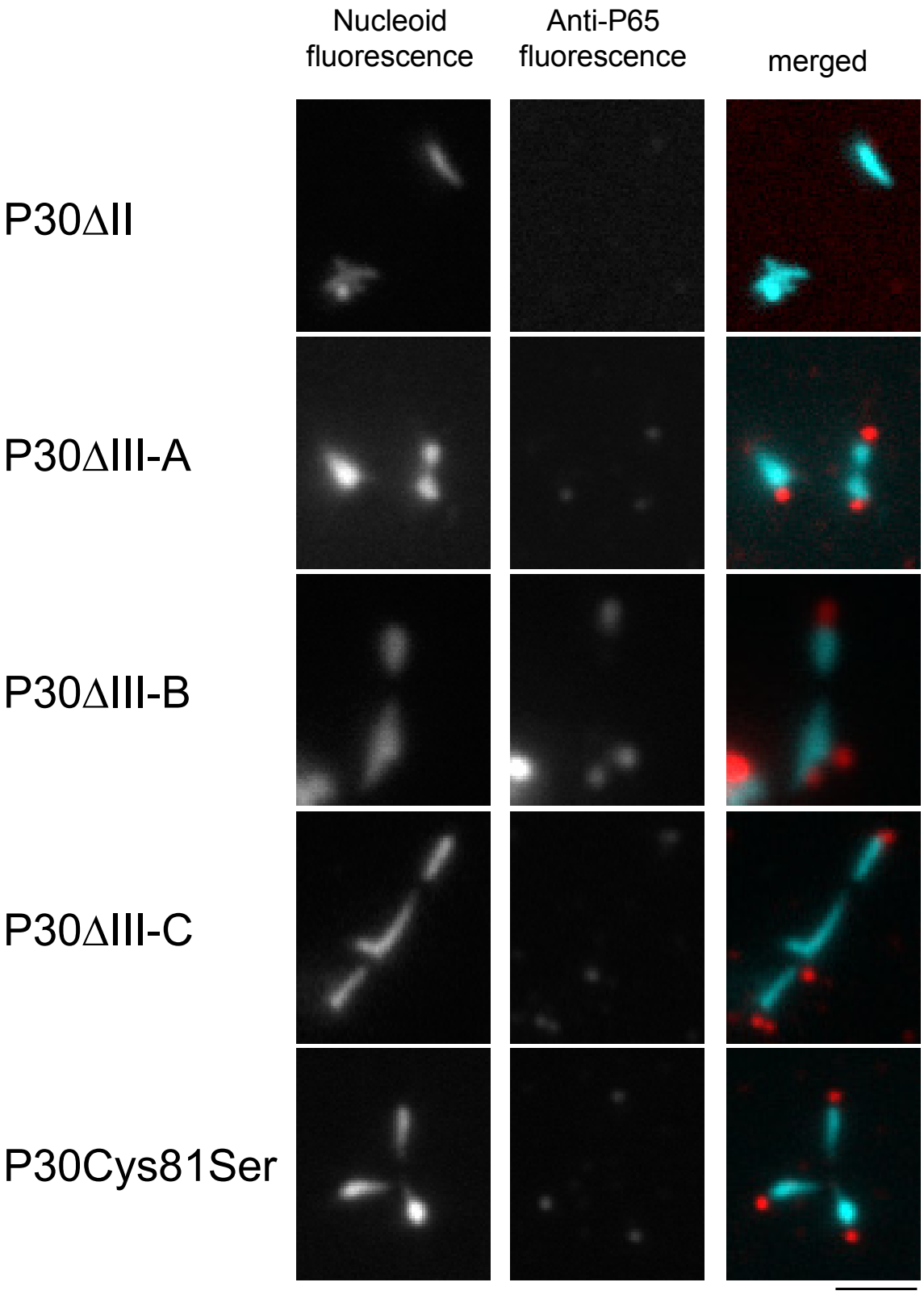
Nucleoid fluorescence
Anti-P65 fluorescence
merged
P30ΔII
P30ΔIII-A
P30ΔIII-B
P30ΔIII-C
P30Cys81Ser

Evaluation of Gliding Motility in Wild-Type and Non-Cytadherent *M. pneumoniae*

Gliding motility in wild-type *M. pneumoniae* is evident at the cellular level by time-lapse microcinematography (Bredt, 1968; Kirchhoff, 1992), revealing movement in linear and circular patterns interrupted by resting periods of various times and frequencies (Radestock and Bredt, 1977). Several bacterial species manifest gliding motility as satellite growth or colony spreading on a solid medium having a low agar concentration, with colonial morphology generally correlating with a gliding-competent phenotype (Burchard, 1981; Jacob *et al.*, 1997; Miyata *et al.*, 2000). We observed satellite growth with wild-type *M. pneumoniae* when incubated on soft (0.5%) agar with a liquid overlay (Figure 29A). While considerably less conspicuous, this satellite growth was also apparent with the standard 1.5% agar concentration provided cultures were incubated with a liquid overlay (data not shown). Cytadherence mutants I-2, III-4, IV-22, and M-6, lacked satellite growth, while complementation of mutant I-2 with recombinant *hmw2* restored satellite growth. The HMW3- mutant appeared to have an intermediate satellite growth, being less uniformly distributed around the entire colony and less prominent than wild-type (Figure 29A). The absence of P30 rendered II-3 unable to form satellite growth, while complementation with the wild-type recombinant *p30* allele restored satellite growth in this background (Figure 29B). Colonies of P30 revertant II-3R exhibited satellite growth but generally taking a few days longer to manifest than in wild-type *M. pneumoniae*. Similar satellite growth was also visualized with mutant II-7. No satellite growth was observed in II-3 transformants with P30 deletion derivatives P30ΔI, P30ΔII, and P30ΔIII-A, -B, or -C. P30Cys81Ser and P30-GFP restored normal satellite growth to mutant II-3 (Figure 29B).

Figure 29. Analysis of wild-type, mutant, and recombinant *M. pneumoniae* for satellite growth. (A) Colonial morphology representative of fields for wild-type (WT) and selected mutant (I-2, I-2+*hmw2*, III-4, IV-22, M6, HMW3-) *M. pneumoniae*. **(B)** Colonial morphology of P30 mutants (II-3, II-3+*p30*, II-3R, II-7, P30ΔI, P30ΔII, [P30ΔIII-A, B, C], P30Cys81Ser, and II-3+*p30-gfp*) as indicated below each frame. Scale bar: 50 μm.

A

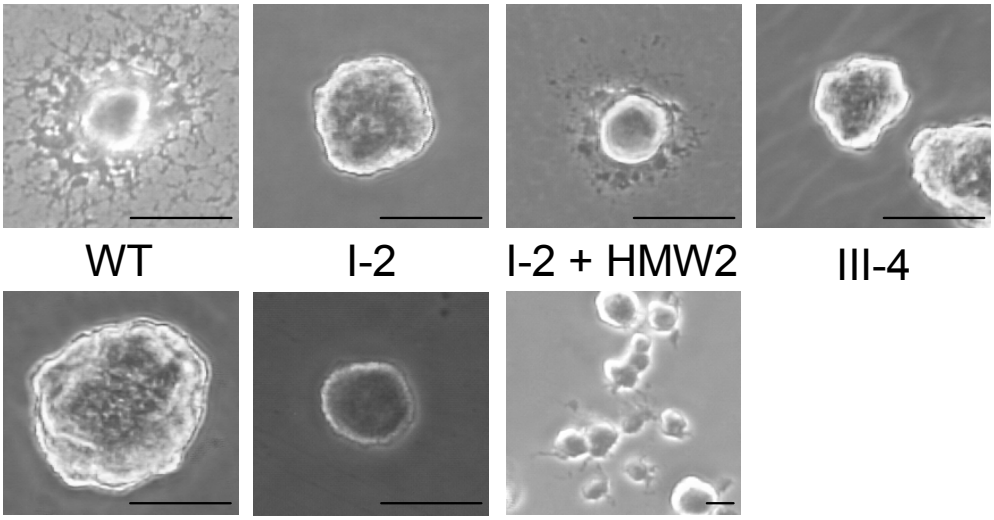
WT
I-2
I-2 + HMW2
III-4
IV-22
M6
HMW3-

B

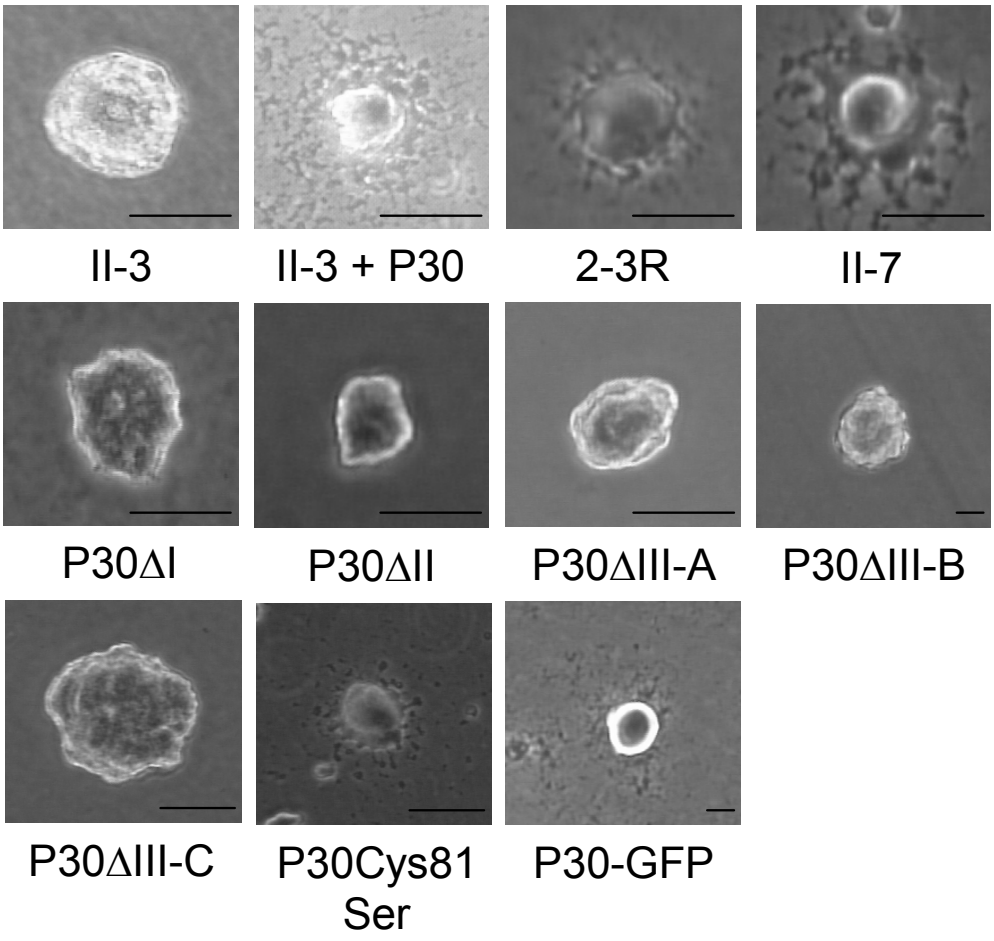
II-3
II-3 + P30
2-3R
II-7
P30ΔI
P30ΔII
P30ΔIII-A
P30ΔIII-B
P30ΔIII-C
P30Cys81 Ser
P30-GFP

Gliding motility in the wild-type FH strain of *M. pneumoniae* was previously characterized by micro-cinematographic studies (Bredt, 1968; Bredt, 1979; Kirchhoff, 1992). Here, phase-contrast images of the same field of strain M129 cells were chronologically recorded while incubating at 37°C in Hayflick medium containing 4% gelatin, confirming gliding motility in this strain (Figure 30). Gliding motility was similarly observed in mutant II-3 complemented with wild-type P30-GFP and P30Cys81Ser (Figure 30C) but was not in cytadherence mutants I-2, II-3, III-4, IV-22, M6, or in P30 deletion derivatives P30ΔII, P30ΔIII-B, and P30ΔIII–C during a period of 2 h (Figure 30B, and C), consistent with the absence of satellite growth with these mutants. Deletion of the cytoplasmic domain of P30 (P30ΔI) resulted in the trace motility of less than one body length in a period of 2 h. Cytadherence mutants HMW3-, II-7, II-3R, and P30ΔIII-A exhibited an intermediate motility as cells glided reproducibly at least one body length within a 2h elapsed time. P30 deletion derivative functionality is summarized in Table 3.

Figure 30. Microcinematography analysis of gliding motility in wild type, mutant, and recombinant *M. pneumoniae* strains. (A) The 3 grayscale panels are consecutive images of wild-type *M. pneumoniae* with 10s intervals between each picture. A black dot pattern surrounds a cell in the 0s frame and marks that cell's initial position in the later time frames. The fourth panel is a RGB composite image of the 0, 10, and 20s images, which were assigned a red, green, or blue channel respectively. After the RGB composite was made the image was processed using the glowing edges command in Adobe Photoshop 7.0 to allow better visualization of differences between each frame. Cells with no motility between all frames are white. **(B)** Each panel is a RGB composite image composed of three separate consecutive images of cytadherence mutants with various time intervals between panels and processed as described above. The time interval between 3 images creating the composite is listed above each panel while the strain is listed below each panel. **(C)** RGB composites of P30 mutants created as described above. Scale bar: 3 μm.

A

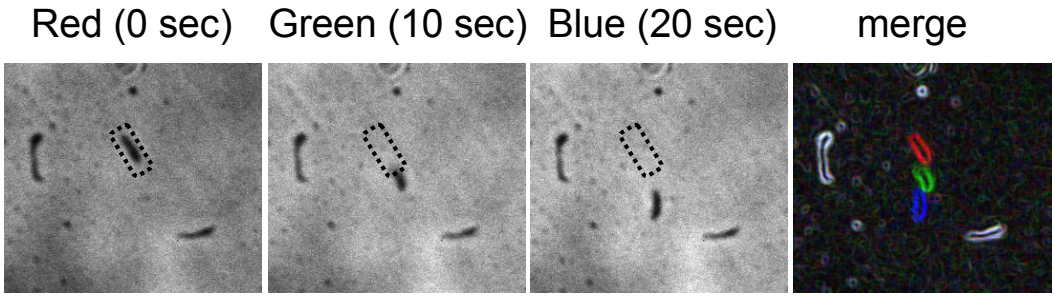
Red (0 sec)
Green (10 sec)
Blue (20 sec)
merge
WT

B

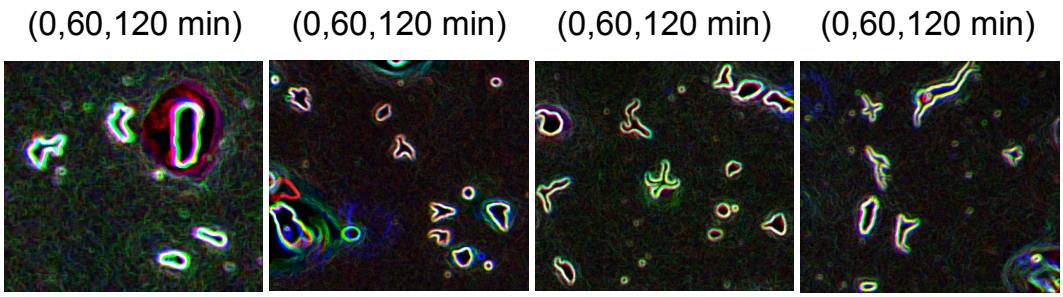
(0,60,120 min)
(0,60,120 min)
(0,60,120 min)
(0,60,120 min)
I-2
III-4
IV-22
M6

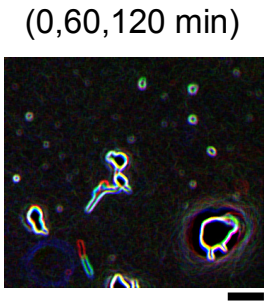
(0,60,120 min)
HMW3-

C

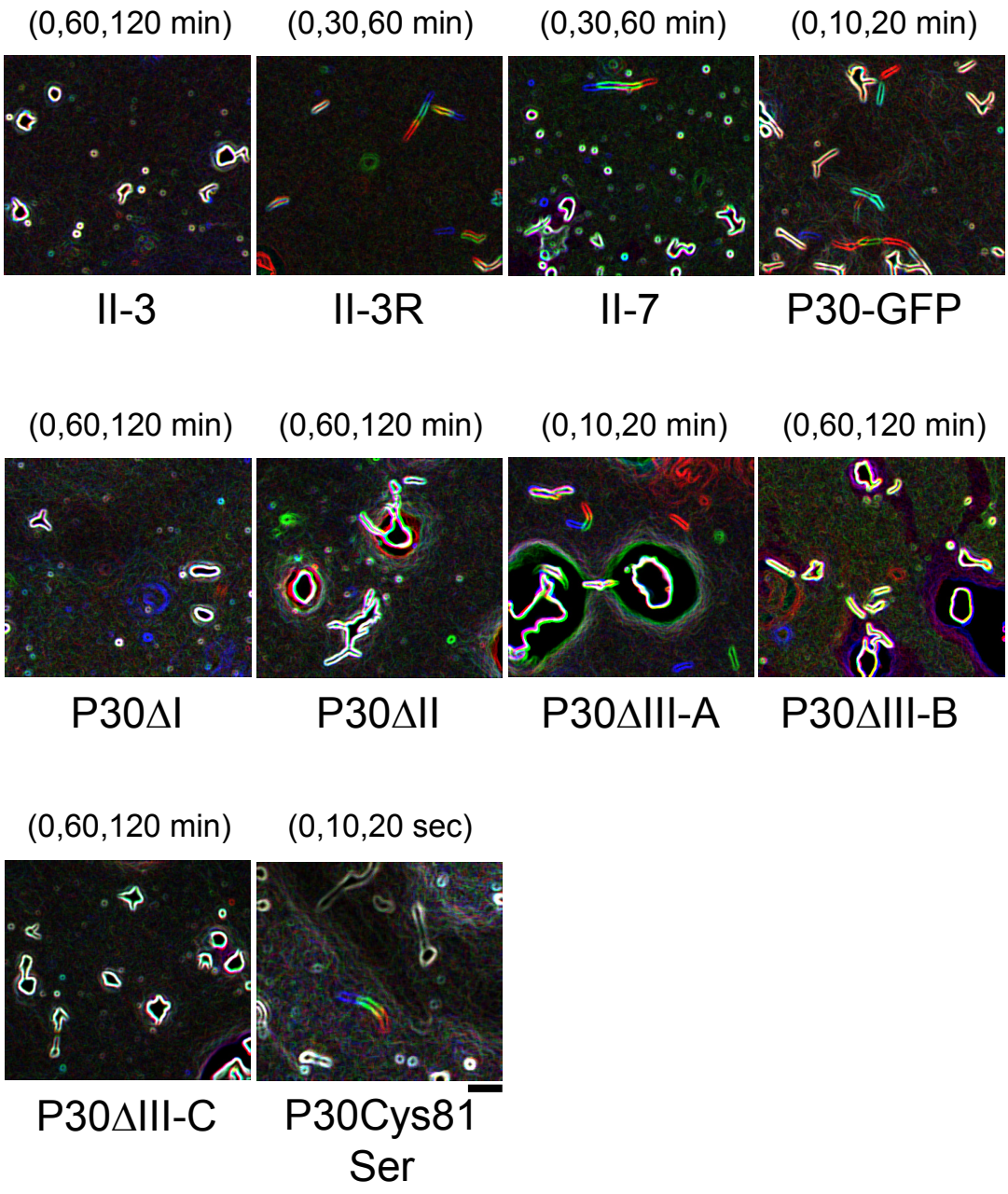
(0,60,120 min)
(0,30,60 min)
(0,30,60 min)
(0,10,20 min)
II-3
II-3R
II-7
P30-GFP
(0,60,120 min)
(0,60,120 min)
(0,10,20 min)
(0,60,120 min)
P30ΔI
P30ΔII
P30ΔIII-A
P30ΔIII-B
(0,60,120 min)
(0,10,20 sec)
P30ΔIII-C
P30Cys81 Ser

Table 3. Phenotypic analysis of P30 Structure-Function Constructs.

	hemadsorption	satellite growth	cellular motility	P30 levels	P65 levels	P30 polar localization	P65 polar localization
WT	++	+	√√	+	++++	+	+
II-3	-	-	**x**	-	++	-	+
II-3 + *p30*	++	+	√√	+	++++	+	+
II-3R	+	+	√	+[1]	++++	+	+
P30Cys 81Ser	++	+	√√	+	++++	+	+
II-7	-	+	√	+	++	+	+
P30 ΔI	-	-	**x**	+[2]	++++	+	+
P30 ΔII	-	-	**x**	-	+/-	-	-[3]
P30 ΔIII-A	-	-	√	+	++	+	+
P30 ΔIII-B	-	-	**x**	+	++	-[3]	+
P30 ΔIII-C	-	-	**x**	-[3]	++	-[3]	+
II-3 + *p30-gfp*	++	+	√√	+	++++	+	+

[1] Migration in monomeric and presumably dimeric and trimeric forms
[2] Migrates larger than predicted
[3] Protein not detected
X no movement seen within a 2h time period
√ full body length of movement within a 30m time period
√√ full body length movement within a 20s time period

CHAPTER 5

DISCUSSION

This discussion of my dissertation research is divided into three sections, the first of which addresses the potential role of gliding motility as a virulence determinant. This section begins by reintroducing the reader to P30 null mutant II-3 and revertant II-3R. This section also describes the development of a novel soft-agar motility assay used in conjunction with time-lapse microcinematography to determine qualitatively the motility phenotype of wild-type *M. pneumoniae* and cytadherence mutants previously uncharacterized with respect to motility. This section closes with a brief summary of what cytadherence proteins appear to be most important in this process. The second part of my discussion analyzes the stability and localization of cytadherence proteins P65 and P30 and their relationship to the other cytadherence proteins. This section closes with a discussion of how these proteins fit in to the assembly of the attachment organelle. The final part of my discussion is a more detailed analysis dissecting protein P30 into separate domains and analyzing the role of each domain in the proper functioning of P30 in hemadsorption, gliding motility and stabilization of protein P65.

P30, Hemadsorption, Host Colonization, and Gliding Motility

For an organism with such a limited genome, *Mycoplasma pneumoniae* is remarkably complex, having a terminal structure involved in adherence, gliding motility and cell development. A key component for the proper functioning of this structure is protein P30. The loss of P30 in mutant class II-3 results in a plethora of phenotypic changes including loss of cytadherence, gliding motility, failure to stabilize protein P65, and morphological changes thought to reflect a cell development defect. The initial finding of the genetic defect in II-3 and the subsequent successful complementation with the wild-type recombinant *p30* allele (Romero-Arroyo *et al.*, 1999) has allowed me to perform a structure-function studies on P30.

Characterization of the Hemadsorption Negative P30 Mutant II-3- Despite a frameshift near the middle of the *p30* gene, the predicted II-3 P30 was predicted to encode a protein actually one residue larger than wild-type P30. Notwithstanding this, I was unable to detect a modified P30 in mutant II-3 with 2 different antisera prepared against peptides corresponding to unique II-3 P30 sequences (Romero-Arroyo *et al.*, 1999). As other mycoplasma cytadherence-related proteins such as HMW1, HMW3 (Popham *et al.*, 1997), and P65 (Jordan *et al.*, 2001) have been shown to be degraded post-translationally, P30 in mutant II-3, although untested, most likely has this same fate. Pulse-chase radioimmunoprecipitation experiments using the P30 antibodies described above or antibodies produced against an N-terminal region of wild-type P30 upstream of where the frameshift occurs would be useful in confirming if II-3 P30 is in fact made and rapidly degraded.

Interestingly, although incapable of hemadsorption, mutant II-3 was able to attach at reduced levels *in vitro* to hamster tracheal epithelium in my studies. The observation of cytadherence in a hemadsorption mutant was unexpected but not unprecedented. A non-hemadsorbing mutant of *M. pneumoniae* that attached normally to lung cells has been previously described (Yayoshi, 1983). *M. pneumoniae* binds sialic acid containing glycoproteins and sulfated glycolipids. Although the proper functioning of the major adhesin P1 appears to be fundamental for successful host colonization by the mycoplasma, the existence of other potential receptor-ligand interactions has recently been described. For example, *M. pneumoniae* proteins elongation factor Tu (EF-Tu) and pyruvate dehydrogenase E1 β subunit (PDH-B) are both reportedly capable of surface translocation and binding to the extracellular matrix constituent fibronectin (Dallo *et al.*, 2002). Most recently, glyceraldehyde-3-phosphate dehydrogenase (GAPDH) was found to be surface-accessible and capable of binding mucin in the human pathogen *M. genitalium,* a close relative of *M. pneumoniae* (Alvarez *et al.*, 2003). GAPDH was found to be randomly distributed on the mycoplasma surface in distinct contrast to the consistent polar localization of the *M. pneumoniae* P30 homolog (P32) in *M. genitalium*. Having an attachment organelle containing protein homologs to *M. pneumoniae* proteins P1, P30, and HMW3, *M. genitalium* could potentially use GAPDH as an independent system from adherence mediated by the attachment organelle to gain an initial foothold, as mucin is a prominent component which the mycoplasma encounters upon entry into the host.

In quantitative tracheal ring attachment studies here, mutant II-3 adherence was greatly reduced in comparison to that seen in wild-type and II-3R. In contrast, LSCM and

TEM images of hamster tracheal epithelium infected with wild-type, II-3, and II-3R were not dissimilar, showing large accumulations of mycoplasmas preferentially located at the base of cilia and at the junction between epithelial cells. LSCM and TEM images of attached mycoplasmas although informative are not quantitative. The discrepancy between the low levels of II-3 adherence compared to wild-type in the quantitative attachment results and the similar number seen in LSCM and TEM images is not alarming. Perhaps the most significant cause for this incongruity is the difference in incubation times between the two assays. Mycoplasmas were incubated with hamster tracheal rings for a period of 3.5 h in the attachment assay, while in the localization experiments, mycoplasmas were incubated with tracheal rings for a minimum of 24 h before fixation. Furthermore, both experiments were conducted in Hayflicks medium, which is permissive for the growth of *M. pneumoniae*, and therefore mycoplasmas increased in numbers. It is feasible that the sheer number of mycoplasmas and their toxic byproducts might compromise the health of the tracheal rings. Indeed, cell-free extracts and purified *M. pneumoniae* membranes have been shown to induce ciliostatic activity in hamster trachea organ culture (Chandler *et al.*, 1987; Gabridge and Polisky, 1977). Remarkably, the cell-free extract used in one study was also capable of inducing a similar lung pathology to that seen after hamsters are infected with virulent *M. pneumoniae* (Chandler *et al.*, 1987). If a ciliostatic effect did result from the extended incubations in my localization studies, then a major obstacle in the colonization of the mycoplasma (mucociliary clearance) was removed. Accordingly, mutant II-3 could have had better access the epithelium without being swept away by the turbulent mucin layer.

In *in vivo* infection studies, mutant II-3 but not other mutants was capable of being recovered from the lungs of intranasally infected hamsters (Krause *et al.*, 1982). In those studies, although mutant II-3 was successfully cultured from lung tissue it was incapable of causing pneumonia in these hamsters. This is consistent with the results of the localization studies described here. TEM images of mutant II-3-infected hamster tracheal epithelium clearly show attachment organelle mediated adhesion, suggesting that P30 is dispensable for adherence to respiratory epithelium in the hamster tracheal ring model. Finally, P1 is localized to the attachment organelle in mutant II-3 (Romero-Arroyo *et al.*, 1999). Thus proper P1 localization is not sufficient for cytadherence, and an attachment competent conformation for P1 probably requires other cytadherence-related proteins.

Why Might Gliding Motility be a Virulence Factor in *M. pneumoniae*?- The absence of P30 results in the complete loss of motility as determined by colonial morphology in soft agar and microcinematography. Perhaps the inability of II-3 to produce pneumonia in hamsters while still capable of maintaining a low level of colonization is due to the lack of motility. Motility may be useful to transport the mycoplasma from the crown to the base of the cilia. If indeed this is the case, mutant II-3 might never reach the base of the cilia and microvilli but be restricted to the crown of the cilia, where its cytotoxic effects may never damage the delicate the host cell epithelium. Although in my study mutant II-3 localized to the base of the cilia and microvilli, I feel that using hamster tracheal rings in organ culture is not the best approach to localize accurately *M. pneumoniae* strains on respiratory epithelium. For example, in the tracheal ring system mycoplasmas can freely access regions that are normally protected by host

defense mechanisms, i.e. immune responses and optimal mucin production. As a result, the mycoplasma could simply settle on the tracheal ring in the pericilliary fluid below the mucin layer without having to penetrate the mucin or withstand the vigorous mucociliary escalator found in an intact trachea. This could presumably account for some of the background seen in the quantitative attachment assays. Although effort was taken during the microscopy preparation to only use sections taken from internal regions of the tracheal ring, this potential artifact cannot be ignored.

Wild-type and mutant mycoplasmas were also found attached to the outside of the trachea or perichondrium, a region normally inaccessible in *M. pneumoniae* infections (data not shown). In lieu of these observations, and in order to properly address mycoplasma adherence and localization in an animal model, ideally the infection should be performed *in vivo*. With this approach, infected hamsters could then be perfused with fixative and the fixed trachea sectioned for localization studies. A promising future approach is to replace the hamster model with a primary culture model of differentiated, polarized human tracheal epithelium. In this methodology the human cells are grown on collagen-treated transwell inserts with a liquid media/air interface. The polarized cells could then be infected with wild-type and mutant strains of *M. pneumoniae* and assessed for attachment as well as localization. This would give a far more accurate picture of mycoplasma host-parasite interactions, as some differences have been found in the localization of mycoplasma receptors between hamster and human respiratory epithelium (Loveless *et al.*, 1992).

Hemadsorption, Host Cell Attachment, and Gliding Motility of II-3R- Protein P30 is absolutely required for hemadsorption. P30 revertant II-3R isolated from the

hemadsorption negative mutant II-3 demonstrated an intermediate hemadsorption phenotype, which was unexpected and might be due to its highly branched morphology. Most branches do not appear to correspond to attachment organelles and might therefore physically limit the efficiency with which mycoplasma adhesins gain access to receptors on the erythrocyte surface. According to this scenario, however, one might predict that all mycoplasma colonies would exhibit a uniform appearance of incomplete coverage by erythrocytes in the qualitative screening. This was not the case, however, as many colonies were uniformly covered by erythrocytes, while others were only partially covered. An intermediate level of hemadsorption was reported in an MsrA mutant of *M. genitalium* (Dhandayuthapani *et al.*, 2001), which is distinct both from the all-or-none hemadsorption phenotype previously observed with *M. pneumoniae*, and from the sectoring seen with hemadsorption patterns for *Mycoplasma gallisepticum* (Athamna *et al.*, 1997) and *Mycoplasma synoviae* (Noormohammadi *et al.*, 1997). The extent of erythrocyte attachment is notably greater on the smaller colonies of the MsrA mutants and tends to be higher around the periphery than the center, suggesting that reduced adherence might reflect more rapid cell death (Dhandayuthapani *et al.*, 2001). However, colony size did not correlate with the extent of hemadsorption in *M. pneumoniae* revertant II-3R. Rather, the patchy pattern suggested a generally lower affinity for erythrocyte binding, and therefore a tendency for incomplete coverage of mycoplasma colonies. This scenario would seem compatible with the observed reduced binding of erythrocytes by revertant II-3R in suspension in quantitative hemadsorption analyses. Conversely, the wild-type level of attachment by revertant II-3R to hamster tracheal rings

suggests a higher affinity for *M. pneumoniae* binding to receptors on respiratory epithelium than erythrocytes.

An alternative explanation for the discrepancy between quantitative hemadsorption and tracheal ring attachment data is that the highly viscous mucin secretions of hamster tracheal epithelium are more conducive for the motility of these cells and the process of motility helps to modulate the morphology of the mycoplasma. This could thereby allow better access between receptors and adhesin proteins on the mycoplasma. The observation that gliding may contribute to the elongated morphology seen in wild-type cells was recently noted by Seto (Seto and Miyata, 2003). Likewise, II-3R cells assumed a more filamentous 'wild-type' morphology with the addition of 4% gelatin to the culture medium. Initially gliding motility of II-3R was also only detected after the addition of gelatin. Indeed, in previous gliding studies of wild-type *M. pneumoniae* gelatin was a required addition to the growth medium for proper attachment (Radestock and Bredt, 1977). Although in my studies, wild-type *M. pneumoniae* appeared to glide with or without gelatin, cells in the presence of gelatin appeared to attach better and remain on the glass surface longer (data not shown).

Perhaps the addition of gelatin to the medium more closely approximates the viscosity of the respiratory epithelium, a surface coated with mucin. This seems reasonable as II-3R although shown to have 50% the hemadsorption capability of wild-type was not significantly different in its ability to colonize hamster tracheal rings. Furthermore, II-3R cells appeared morphologically similar to wild-type in TEM images of infected tracheal rings. Nevertheless, the ability of revertant II-3R to bind to respiratory epithelium at wild-type levels but with impaired gliding makes it a potential

candidate for examining the contribution of gliding motility to the pathogenesis of *M. pneumoniae* infections.

Cytadherence Proteins and Gliding Motility- Gliding motility is the active, flagella-independent movement of cells over a surface (McBride, 2001). *M. pneumoniae* cells glide along their long axis only in the direction of the attachment organelle (Bredt, 1968; Kirchhoff, 1992). The development of satellite growth by colonies of gliding bacteria cultured on soft agar is widely recognized (McBride, 2001). This dissertation provides the first description of satellite growth for *M. pneumoniae*, which is unusual among known gliding bacteria in requiring a liquid overlay in order for this growth pattern to develop. However, this distinction may merely reflect the slow growth rate and extended incubation times (6-9d) required for *M. pneumoniae* culture. Nevertheless, the use of soft-agar with a liquid overlay makes possible a more versatile system for evaluating motility, negating the variability seen with the small window of observation during microcinematography. This development of a means to distinguish non-motile mutants in *M. pneumoniae* by colony screening is significant, making the application of genetic tools to the study of mycoplasma gliding now more feasible.

Previous gliding motility studies with the FH wild-type strain of *M. pneumoniae* demonstrated the requirement of 3-5% gelatin to the medium in order to visualize gliding motility by microcinematography (Radestock and Bredt, 1977). In initial gliding motility studies we found wild-type strain M129 but not mutant *M. pneumoniae* exhibited gliding in the absence of gelatin. Additionally, although not quantitative, cellular motility of wild-type appeared similar with or without the presence of gelatin (data not shown).

Significantly, some cytadherence mutants were only motile with the addition of 4% gelatin to the growth medium.

After analysis of wild-type and cytadherence mutants using the soft-agar assay and time-lapse microcinematography in the presence of 4% gelatin, we were able to detect an intermediate motility phenotype in cells with certain defects in P30 (II-7, II-3R, P30ΔIII-A), and HMW3 (HMW3-). Complete loss of gliding motility was found in cells with defects in HMW1, HMW2, B, C, and P30 (II-3, P30ΔI, P30ΔII, P30ΔIII-B, P30ΔIII-C).

Relationship Between Hemadsorption and Gliding Motility- By definition, attachment to the substratum is required for gliding motility; therefore the observation that many mutants defective in cytadherence could not glide was not surprising. A similar observation was reported with *Mycoplasma mobile*, where loss of gliding motility correlated with the loss of hemadsorption (Miyata *et al.*, 2000). My results agree with this correlation with the exception of mutants II-7, and P30ΔIII-A. These two mutants are completely hemadsorption negative yet exhibit an intermediate level of gliding motility. Other mutants exhibiting an intermediate motility phenotype exhibited intermediate hemadsorption characteristics (II-3R, HMW3-) and all strains with wild-type levels of hemadsorption demonstrated wild-type motility (II-3+P30, II-3 + P30-GFP, P30Cys81Ser).

The observation of gliding motility in any strain lacking hemadsorption was not found in *M. mobile* (Miyata *et al.*, 2000), however, this may reflect the vast differences between these organisms. *M. mobile* and *M. pneumoniae* share no homology between proteins involved in attachment, and proteins required for gliding in *M. mobile* are

likewise absent in *M. pneumoniae*. Interestingly, although unable to hemadsorb, mutant II-7 is able to attach loosely to tissue culture flasks unlike non-motile mutant II-3. It would be useful to analyze attachment of *M. pneumoniae* strains to German borosilicate glass, the actual substrate used for gliding in our microcinematography experiments.

With the exception of P30ΔIII-A, satellite growth correlated with gliding motility as visualized by microcinematography in all strains. Cells with chemotaxis defects have also been observed gliding yet are unable to exhibit satellite growth where the cells move back and forth never achieving significant net movement (Mark McBride, personal communication). Although *M. pneumoniae* is considered to be chemotactic (Kirchhoff, 1992), preliminary microcinematographic visualization of P30ΔIII-A yielded no evidence of unusual cellular movement patterns (data not shown). Given that reacquisition of wild-type P30 restores hemadsorption and gliding motility in mutant II-3, it is plausible that certain mutations in P30 could also alter the ability to attach to different surfaces as attachment to inert surfaces is a property of the wild-type strain. Thus it is conceivable that a strain unable to demonstrate satellite growth could still glide on a glass surface.

It was possible to establish by complementation analysis with mutants II-3 and I-2 that the defect responsible for loss of cytadherence was also directly or indirectly responsible for loss of gliding motility. Not surprisingly, mutant M6 complemented with recombinant wild-type *hmw1* only partially restored motility to M6, as this strain has an additional mutation in *p30* identical to the mutation in II-7, a strain exhibiting intermediate motility (data not shown). We are currently in the process of attempting to complement the defect in mutant III-4, and IV-22. The defect in mutant I-2 is a frameshift mutation in the *hmw2* gene (Fisseha *et al.*, 1999). Loss of HMW2 results in the

accelerated turnover of several proteins associated with the terminal organelle, including HMW1, HMW3, and P65, and therefore a direct requirement for HMW2 in gliding could not be established. Interestingly, an intermediate level of motility was detected in the absence of HMW3. The presence of atypical electron-dense cores in this mutant could either imply that this structure is not absolutely required for motility or perhaps with a more detailed quantitative study of this mutant, the non-motile cells will be found to possess atypical cores. Mutant I-2 and M6 are non-motile and lack electron-dense cores. If in fact the non-motile cells in HMW3- contain atypical cores than this would imply the necessity of the core for gliding motility in *M. pneumoniae*. Certainly, this structure has been hypothesized as being involved in the motility machinery (Brunner *et al.*, 1979; Hegermann *et al.*, 2002; Radestock and Bredt, 1977). The fact that *M. pneumoniae* ceases motility prior to cell division, a process where the electron-dense core is duplicated, also implicates the core in motility. However, like with hemadsorption, the presence of a 'normal' electron-dense core is not the only prerequisite for gliding motility. For instance, non-motile mutants III-4, IV-22, and II-3 were all found to contain electron-dense cores (Seto and Miyata, 2003).

Proteins P65 and P30

P65 and P30 Stability in Mutant Backgrounds- Cytadherence mutants were previously reported as having similar steady-state P65 levels to the wild-type strain (Seto *et al.*, 2001). However, no P65 was detected in these mutants by immunofluorescence microscopy. In contrast to their findings, I found significant differences in P65 steady-state levels between wild-type and several cytadherence mutants of *M. pneumoniae* and detected a signal in all strains by immunofluorescence microscopy (Jordan *et al.*, 2001).

The results of my Western immunoblot experiments indicate that P30, as well as HMW1-HMW2, are necessary for the stabilization of P65, where loss of HMW1 or HMW2 resulted in less steady-state levels of P65 than was seen with the loss of P30. It was later found that HMW3 is also required for P65 stability (Willby and Krause, 2002). Importantly, the absence of proteins P1, B, and C did not affect the steady-state levels of P65. Protein P30 also requires HMW1 and HMW2 but not proteins HMW3, P1, or B and C for stability (Balish and Krause, 2002). Thus P65 depends on P30 and HMW3 for its stability and P30 and P65 both depend on HMW1 and HMW2 for stability. An absolute requirement for stability of these proteins is the presence of an electron dense core.

The studies presented here establish clearly that P65, like HMW1 and HMW3, is unstable in the absence of HMW2. It is not known if P65 turnover requires C-terminal sequences previously suggested to be targeted in HMW1 and HMW3. Specifically, the motif P-X-R-$X_{(0-5)}$-S-S in the HMW1 C-terminal domain, which is necessary for accelerated turnover in *hmw2* mutants, was implicated in protease targeting (Popham *et al.*, 1997). This motif does not occur in P65; hence, P65 might be lost indirectly as a secondary consequence of HMW1/HMW3 turnover, perhaps because of failure to anchor properly with the cytoskeleton or at the mycoplasma surface. Alternatively, additional features in the primary or secondary structure of HMW1, HMW3, and P65 may be targeted in their accelerated turnover. Recent studies with HMW1 deletion derivatives suggest that this may in fact be the case, with HMW1 instability probably resulting from failure to interact with a binding partner, leaving a domain accessible to protease. Indeed, the surface-exposed domain of P30 appears to be essential for P65 stability (as discussed in section 3).

P65 and P30 Localization in Mutant Backgrounds- P65 localization is dependent on proteins HMW1-HMW3, but not P1, B, C, or P30, despite the requirement of P30 for its full stability (Jordan *et al.*, 2001; Seto and Miyata, 2003; Willby and Krause, 2002). Localization of P30 to the attachment organelle is also dependent on HMW1-HMW3, but not proteins B, C, or P1 (Seto and Miyata, 2003). Seto *et al*. were unable to detect P30 in mutant I-2 or mutant M6 complemented with the wild-type recombinant *p30* allele (Seto and Miyata, 2003). My conclusions were similar, although I was able to detect P30 in mutant I-2 by immunofluorescence. P30 immunofluorescence in mutant I-2 was very similar to what was seen in mutant HMW3-, where P30 localization ranged from being completely localized to polar structures, to some cells having partly localized P30, to the complete absence of P30. This was starkly different than the consistently polar localization seen in cytadherence mutants III-4, and IV-22 (Seto and Miyata, 2003).

Consistent with P30 localization in HMW3-, P1 was shown to be localized to the cell pole in some cells, while in the majority of cells P1 was completely scattered throughout the cell surface as determined by immunoelectron microscopy (Willby and Krause, 2002). P30 localization was also monitored by P30-GFP fluorescence in the I-2 and M6 backgrounds. P30-GFP localization in I-2 was vastly different in comparison to the strictly polar localization seen in a wild-type or mutant II-3 background producing P30-GFP. Due to the reduced levels of P30 in M6 in combination with the loss of a large portion of a highly antigenic region of P30 in this strain, P30 localization in mutant M6 was only performed using the P30-GFP reporter. P30-GFP localization in M6 was identical to what was seen in the I-2 background yet strongly dissimilar to the polar

focused fluorescence seen in the II-3 and wild-type backgrounds transformed with P30-GFP. These data again point to the importance of proteins HMW1 and HMW2 for the localization of P30, which is consistent with results from immunofluorescence microscopy (Seto and Miyata, 2003).

P30 localization in HMW3- is unreported and agrees nicely with the localization of adhesin P1 in this strain. P65 was reported as having a patchy localization in HMW3- with some cells exhibiting a polar P65 signal; it is interesting to speculate if the presence of localized P30 in some of the HMW3- cells also correlates with P65 localization. P1 and P65 can localize to a pole in the absence of P30 (Jordan *et al.*, 2001; Romero-Arroyo *et al.*, 1999) Likewise P30 exhibits a polar localization in the absence of P1 (Seto and Miyata, 2003). Interestingly, there is no report of a strain where both P65 and P30 proteins were produced with one localizing differently than the other.

A properly formed electron-dense core is a prerequisite for both P30 and P65 to localize consistently to a cell pole (Dallo *et al.*, 1990; Jordan *et al.*, 2001; Seto *et al.*, 2001; Seto and Miyata, 2003; Willby and Krause, 2002). Thus in the absence of cores mutants (I-2, M6) or in the presence of atypical cores (HMW3-) both proteins are largely delocalized. Surprisingly, loss of HMW3- affected the steady-state levels of P65 but not P30. Due to the dependency on HMW3 for the stability of P65 it is thought that a physical interaction between the two proteins might occur within the attachment organelle (Willby and Krause, 2002).

P30 and P65 are Components of the Nascent Attachment Organelle- At some point during cell division, *M. pneumoniae* ceases to move and coordinates DNA replication with attachment organelle duplication while eventually condensing mother

and daughter nucleoids and septating, ultimately moving off again by gliding motility (Bredt, 1968; Seto *et al.*, 2001). Besides the major adhesin protein P1 and HMW2, it is not known which cytadherence proteins are components of the nascent organelle (Balish *et al.*, 2003; Seto *et al.*, 2001). For example, it is not known if these proteins incorporate at the opposite pole or arrive there by way of the nascent tip.

In this study, two adjacent P30 foci were seen in many P30 immunofluorescent images and fluorescent images of II-3 transformed with P30-GFP suggesting that P30 is a component of the nascent organelle. Additionally, fixed wild-type cells probed with P65 anti-serum also revealed similar adjacent foci in some cells (data not shown). This is the first description of P30 and P65 as components of the nascent organelle. Interestingly, some cells expressing P30-GFP contained bipolar P30 fluorescence in motile cells, with the attachment organelle focus being much brighter than the trailing end focus, indicating that some P30 might also assemble at the new pole before the nascent organelle is formed. A similar observation was also previously made by visualization of fixed wild-type *M. pneumoniae* cells probed with anti-P30 antisera, but with a less intense focus at the site of cytokinesis (Jason Cloward, unpublished data).

One of the major utilities of the P30-GFP fusion is its functionality in complementing mutant II-3. Thus II-3 transformed with P30-GFP makes a convenient 'wild-type' strain to perform double-labeling experiments when an attachment organelle marker is required. The ultimate use of the P30-GFP fusion is to follow individual mycoplasmas during a life cycle. Although we have had some success following initial nascent tip migration, we have been largely unsuccessful at following the nascent tip to maturation. One of the obstacles has been the limited number or images obtainable before

the loss of GFP fluorescence. Additionally, challenges maintaining a constant temperature throughout the process of microcinematography, and inconsistencies in some of the components in our growth medium, have no doubt hindered time-lapse recording of this process with GFP. Nevertheless, the P30-GFP fusion is a useful tool to study cell-division, assembly of the attachment organelle and P30 function.

Functional Domain Analysis of P30

Putative Role of the Cytoplasmic Domain of P30- P30 is a membrane protein with an N-terminal domain predicted to be located in the cytoplasm and the C-terminus exposed externally. Deletion of 30 out of 38 residues within the predicted cytoplasmic domain (P30ΔI) yielded a derivative which failed to restore either hemadsorption or gliding motility but was capable of restoring P65 stability in the mutant II-3 background. As P30 and P65 are produced at wild type levels and are localized in these transformants, intracytoplasmic protein interactions to P30 are likely required for both hemadsorption and gliding motility to occur. Perhaps in the case of the loss of gliding, P30 could be a link between the internal gliding motor and the external substrate for attachment. Following this logic, deletion of much of the cytoplasmic domain of P30 would result in the uncoupling of the motor from the external adhesive components. In a car analogy, the cytoplasmic domain of P30 could be similar to the clutch in a manual transmission. Although highly speculative, perhaps an interaction with HMW3 occurs with this domain. This internal coupling, however, is not necessary for P30 stability or localization, suggesting a dependence on interactions with a surface exposed protein for this function. Failure to restore hemadsorption to mutant II-3 upon complementation with P30ΔI also suggests that P30 intracytoplasmic interactions are required for

hemadsorption to occur. The construction of a P30 strain containing a hexahistadine tag followed by a unique proteolytic cleavage site such as factor Xa incorporated into the *p30* sequence just before the internal portion of the membrane-spanning domain might be useful in coprecipitation experiments to identify these internal interactions.

Putative Role of the Conserved Domain of P30- A region predicted to be surface exposed and highly conserved between *M. pneumoniae* P30, *M genitalium* P32, and *M. gallisepticum* MGC2, was deleted, and this recombinant P30 derivative (P30ΔII) was transformed into mutant II-3. I was unable to detect P30ΔII. Not surprisingly, hemadsorption, and gliding motility were absent in these transformants. Unexpectedly, P65 levels appeared even lower than what is seen in P30 null mutant II-3. Interestingly, a coiled coil is predicted between residues 100-150 in P30 where residues 101-120 are absent in P30ΔII. Furthermore, the region absent in P30ΔII is predicted to have the highest surface probability in P30. Perhaps this region of P30 is involved in protein-protein interactions which in their absence ultimately result in the rapid degradation of P30. This region may also be crucial for the proper external conformation of P30, as it is part of a region beginning at the end of the membrane spanning region to the beginning of the proline repeat region thus serving as a spacer conceivably permitting the proper spatial constraints for the proline repeats to interact with potential binding partners. Pulse-chase radioimmunoprecipitation experiments with P30ΔII using P30 and P65 specific antiserum would be useful to determine if P30 and P65 are made in this background. Furthermore, TX-100 fractionation of radiolabeled P30ΔII, and wild-type P30 might also reveal differences in P30 and P65 partitioning between these strains. For example, initially wild-type HMW1 exists as a TX-100-soluble pool. In time the level of

TX-100 soluble HMW1 decreases, accompanied by a greater proportion of cytoskeletal-associated HMW1. In the absence of HMW2 (mutant I-2), HMW1 is not efficiently associated with the TX-100-insoluble fraction with time and ultimately is degraded.

P30 Surface-Exposed Domain and Hemadsorption- Deletion of any P30 region predicted to be outside of the membrane results in the complete loss of hemadsorption. Despite the altered P30 sequence (135-151), II-3R is capable of an intermediate level of hemadsorption. As defects in this domain also destabilize P65, one cannot rule out a possible role for P65 in hemadsorption. Indeed the only P30 surface-exposed domain mutant capable of at least intermediate levels of hemadsorption (II-3R) is the only one producing wild-type levels of P65. Interestingly, absence of HMW3 results in destabilized P65 and localization defects in both P30 and P65 yet is still capable of an intermediate level of hemadsorption. However because some cells appear to have normal P1, P30, and P65 localization and there is also evidence of motility in some of the cells, one cannot discount that the intermediate hemadsorption phenotype is a reflection of this 'normal' population of cells. Quantitative analysis of this mutant in regards to the number of cells localizing P1, P30 and P65, the frequency of motile cells, and the frequency of cells containing abnormal cores would shed light on the relationship of these phenotypes. Unfortunately, no mutant lacking only P65 has been reported, making it impossible for now to know the exact role of P65 in this process.

P30 Surface-Exposed Domain and Gliding Motility- Absence of P30 (II-3) results in the loss of gliding motility. In my studies, mycoplasma cells were capable of exhibiting an intermediate level of gliding motility in the absence of 8 out of 12 proline repeats (II-7). Likewise, loss of one repeat in addition to the remaining 20 residues of the

C-terminus of P30 also resulted in an intermediate gliding phenotype. However, P30 C-terminal truncation mutants P30ΔIII-B, and -C, were incapable of even partial restoration of gliding motility to mutant II-3. Mutant II-7 and P30ΔIII-A, the two deletion derivatives exhibiting intermediate levels of motility, contain 227, and 247 residues respectively. P30ΔIII-B, and –C contain 199 and 175 residues respectively and because they both differ from P30ΔIII-A only in proline repeats, and partial motility was seen after the loss of 8 proline repeats in II-7, the loss of gliding motility in P30ΔIII-B, and –C might simply be due to the shortened length of this surface-exposed region. Back to the car analogy, the proline repeat region could be similar to the tread on tires whereas loss of a substantial amount of the tread will result in less traction with the road, or in the case of a gliding mycoplasma with the substratum. If this domain needs to be a certain length to be accessible to a potential binding partner or receptor, progressive shortening of this domain might disrupt these interactions. If this is the case, construction of a P30 derivative by swapping out the portion of sequence deleted in II-7 with a non-remarkable spacer sequence might be useful to further test the role of length surface-exposed domain in gliding motility.

An alternative explanation for the inability of P30ΔIII-B, and –C, to restore gliding even partially to II-3 might be simply the decreased P30 production in these derivatives. However, failure to detect P30ΔIII-C and the barely detectable P30ΔIII-B may be a product of a major loss of epitope as 9 or 13 proline repeats, respectively, were deleted in these recombinants. Layh-Schmitt reported identical P30 levels in a P30 mutant (M7) missing 12 of the 13 total repeats (but having a normal C-terminus) in comparison to the wild-type strain using anti-sera prepared against an N-terminal region

of P30 (Layh-Schmitt *et al.*, 1997). P30ΔIII-A is only missing one proline repeat, and although its detection is much more prominent in P30-immunoblots than P30ΔIII-B, it is substantially decreased in comparison to wild-type P30 and other P30-derivatives, including P30ΔI and II-7. This suggests that the extreme C-terminal region of P30 might in fact be important for its stability. However, until P30 levels in these strains are tested with an antibody produced against an N-terminal region of P30, one cannot be sure as to whether there is a lack of total P30 or just a lack of epitopes recognized by the antiserum.

Interestingly, the alteration of the surface-exposed region of P30 (135-151) in II-3R also changed the electrophoretic mobility of the protein by SDS-PAGE and yielded likely multimeric forms of the protein. SDS-PAGE analysis of WT *M. pneumoniae* indicates the presence of only monomeric P30, although overexpression of wild-type P30 in *E. coli* reveals mature and unprocessed P30 (Kannan and Baseman, 2000), and in some cases dimeric forms detected with P30 specific antiserum (S. Dhandayuthapani, personal communication and data not shown). Perhaps the multimeric P30 in II-3R is non-functional and is therefore responsible for the intermediate levels of hemadsorption and motility seen in this strain. Wild-type P30 contains a single cys at residue 81, in the predicted membrane-spanning region of the protein, while the revertant P30 has additional cys residues at positions 140 and 144, in the surface-exposed domain of the protein. P30 is predicted to have a coiled-coil domain spanning from residues 100-150, and additional cys residues in this region might promote multimerization in the oxidizing environment of the cell exterior. However, the putative multimers of revertant P30 were resistant to the reducing agents dithiothreitol and β-mercaptoethanol, with and without

alkylation with iodoacetamide (data not shown), suggesting that nondisulfide covalent or strong hydrophobic interactions may contribute to multimerization.

Although only monomeric P30 was detected in wild-type *M. pneumoniae*, the single cysteine in P30 (Cys 81) was mutagenized to a serine (P30Cys81Ser) to determine if it is needed in proper P30 function. This substitution did not affect the ability of this P30-derivative to restore cytadherence, gliding motility, morphology, and stability of P30 in the mutant II-3 background. Furthermore, recombinant P30Cys81Ser P30 migrated identically to wild-type P30 and only as a monomer on SDS-PAGE gels.

P30 in II-3R was found to localize at the attachment organelle as determined by immunofluorescence microscopy, indicating that the intermediate motility and hemadsorption phenotype was not a result of the improper localization of P30 in this strain. Interestingly, the fluorescent signal from II-3R probed with anti-P30 was generally lower in comparison to wild-type and strains with similar levels of P30, i.e. P30ΔI, indicating that some of the P30 in II-3R could be antibody inaccessible (data not shown). It is tempting to speculate that the formation of stable multimers by the revertant P30 may interfere with normal function in cell development and gliding motility, while having a reduced impact on cytadherence function. If indeed the case, this would represent an important first step in dissecting the mechanism by which *M. pneumoniae* gliding is achieved.

The Surface-Exposed Domain and P65 Stability- In this study, the loss of 1, 9, or all 13 of the proline repeats in addition to 20 residues at the extreme C-terminus of P30 (P30ΔIII-A, -B, and –C respectively) each resulted in identical P65 levels as the P30 null mutant II-3. Furthermore, P65 levels in a P30 mutant with a deletion in the conserved

portion of the surface-exposed domain (P30ΔII) resulted in less steady-state P65 than in mutant II-3. However, deletion of the cytoplasmic domain (P30ΔI), alteration of the wild-type sequence from residues 135-151 (II-3R), or substitution of cysteine (81) for serine (P30Cys81Ser), did not reduce the ability of these P30 derivatives to stabilize P65 to wild-type levels. These results suggest a direct or indirect role for the surface-exposed domain of P30 in P65 stability.

Colocalization studies of wild-type *M. pneumoniae* probed for P30 and P65 showed a distinct co-localized pattern at the very end of the attachment organelle (Seto and Miyata, 2003). These colocalized foci were distally located from the fluorescence of HMW1 and HMW3, which also colocalized and are thought to be important components of the electron dense core. Due to the spatial differences in the colocalization of P30 and P65 compared to HMW1 and HMW3, it was postulated that P30 and P65 may correspond to the terminal button of the attachment organelle (Seto and Miyata, 2003). Extensive analysis of TEM thin sections of mutant II-3 and wild-type *M. pneumoniae* might reveal differences in the terminal button further supporting this hypothesis. The conserved-domain deletion mutant (P30ΔII) would be particular useful for these studies as this strain has less P65 than mutant II-3 and has no detectable P30.

At least some P65 has been shown to be surface accessible as partial cleavage of a small population of P65 in whole cells was found after α-chymotrypsin or proteinase K treatment (Proft *et al.*, 1995). Based on these findings, it was thought that either a subpopulation of P65 was localized internally or alternatively all P65 is surface-exposed but is masked by another component or by the conformation of P65 itself making it

incompletely susceptible to proteolytic cleavage (Proft *et al.*, 1995). In these experiments the stability of the cytosolic protein Elongation Factor G (EF-G) was monitored to insure structural integrity of the membrane and was only degraded upon addition of 0.1% TX-100 prior to proteolytic treatment. Significantly, protease treatment of cells pretreated with TX-100 also resulted in complete cleavage of P65.

Although greater than what is seen in the absence of HMW1, and HMW2, the amount of steady-state P65 is drastically reduced in the absence of P30. Perhaps this P30 independent population of P65 is the population inaccessible to proteolytic cleavage in the absence of TX-100 pretreatment. Thus the surface-exposed P65 would interact with the surface-exposed domain of P30 and the internal P65 be stable in the presence of a normal electron dense core. Along these lines it is possible that the surface-exposed domain of P30 is responsible for anchoring P65 to the cell where, in its absence, the P65 that is surface accessible would be lost into the media. Examination of protein precipitations of spent culture medium from wild-type and mutant II-3 *M. pneumoniae* for P65 might yield data to support or challenge this hypothesis.

In conclusion, this structure-function analysis of P30 has given us insight into potential protein-protein interactions with protein P30 which gives us a starting point for future experiments. Based on our knowledge of P30 topology this study also shows us which side of the membrane these interactions are most likely to take place for a given phenotype. A graphical summary of P30 structure-function is provided in Figure 31.

Figure 31. Overview of P30 structure-function analysis results. Each phenotype examined is indicated to the left of each topology figure of P30. Each line above the diagram corresponds to the region of the deletion or substitution and mutant strain is indicated adjacent to each line. Star indicates the P30Cys81Ser substitution. Green, yellow or red line color indicates that mutation has no affect, an intermediate affect, or that the phenotype is indifferent from the P30 null mutant II-3 respectively. Data from M7 was inferred from previous characterization (Layh-Schmitt *et al.*, 1997).

[1] Strains with altered but not deleted sequence

[2] P30ΔIII-B was detected and localized to the attachment organelle in some experiments. The C-terminus of M7 is surface exposed based on proteolysis experiments (Layh-Schmitt *et al.*, 1997).

[*] Strains with a lack of detectable P30 as determined by Western immunoblotting with P30 specific antiserum.

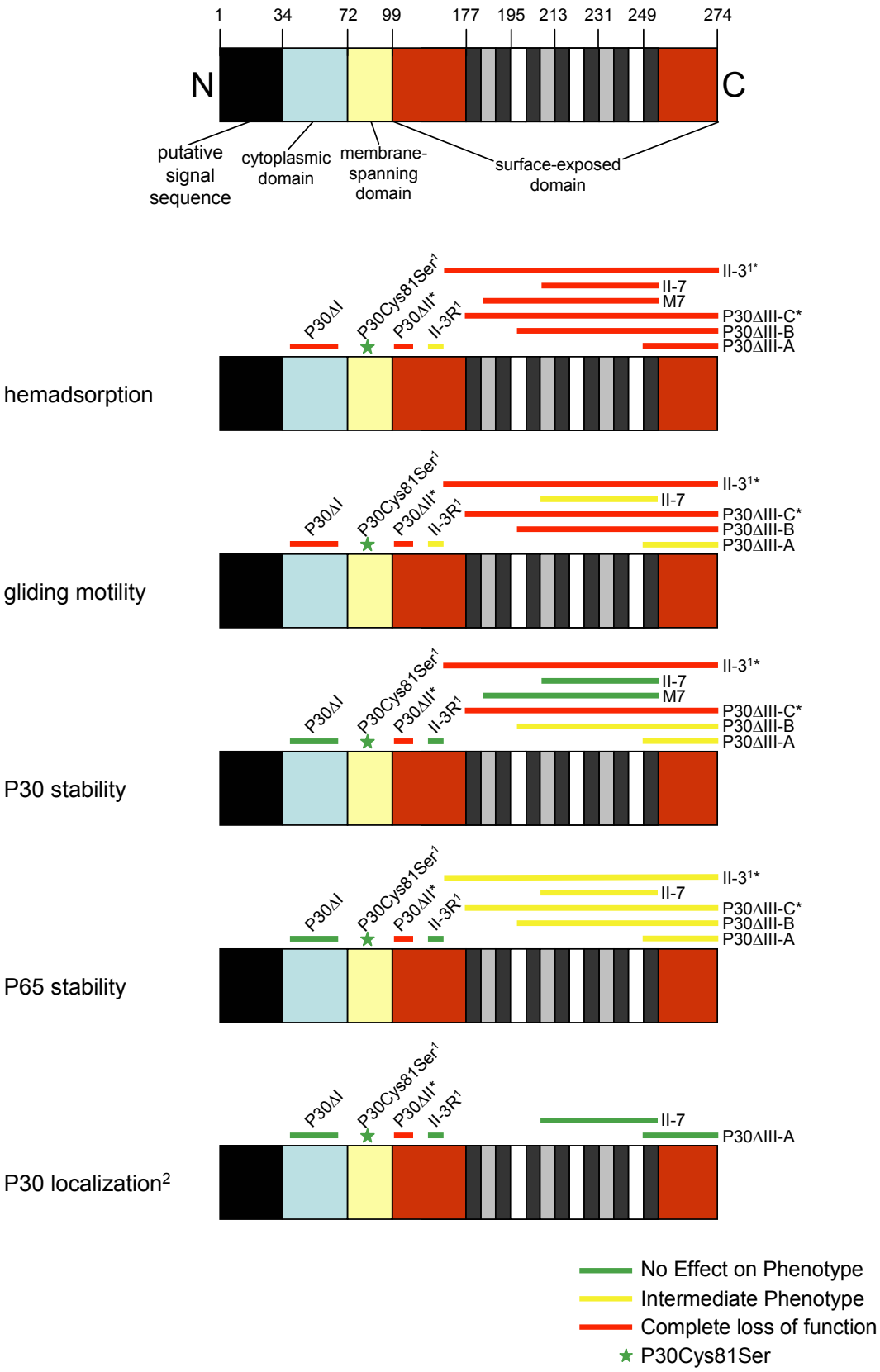
1
34
72
99
177
195
213
231
249
274
N
C
putative signal sequence
cytoplasmic domain
membrane-spanning domain
surface-exposed domain
hemadsorption
gliding motility
P30 stability
P65 stability
P30 localization2
P30ΔI
P30Cys81Ser1
P30ΔII*
II-3R1
II-31*
II-7
M7
P30ΔIII-C*
P30ΔIII-B
P30ΔIII-A
No Effect on Phenotype
Intermediate Phenotype
Complete loss of function
P30Cys81Ser

REFERENCES

Alvarez, R.A., Blaylock, M.W., and Baseman, J.B. (2003) Surface localized glyceraldehyde-3-phosphate dehydrogenase of *Mycoplasma genitalium* binds mucin. *Mol Microbiol* **48**: 1417-1425.

Ang, C.W., Tio-Gillen, A.P., Groen, J., Herbrink, P., Jacobs, B.C., Van Koningsveld, R., Osterhaus, A.D., Van der Meche, F.G., and van Doorn, P.A. (2002) Cross-reactive anti-galactocerebroside antibodies and *Mycoplasma pneumoniae* infections in Guillain-Barre syndrome. *J Neuroimmunol* **130**: 179-183.

Athamna, A., Rosengarten, R., Levisohn, S., Kahane, I., and Yogev, D. (1997) Adherence of *Mycoplasma gallisepticum* involves variable surface membrane proteins. *Infect Immun* **65**: 2468-2471.

Balish, M.F., Hahn, T.W., Popham, P.L., and Krause, D.C. (2001) Stability of *Mycoplasma pneumoniae* cytadherence-accessory protein HMW1 correlates with its association with the triton shell. *J Bacteriol* **183**: 3680-3688.

Balish, M.F., and Krause, D.C. (2002) Cytadherence and the Cytoskeleton. In *Molecular Biology and Pathogenecity of Mycoplasmas*. Razin, S. and Herrmann, R. (eds). New York: Kluwer Academic/Plenum Publishers, pp. 491-518.

Balish, M.F., Santurri, R.T., Ricci, A.M., Lee, K.K., and Krause, D.C. (2003) Localization of *Mycoplasma pneumoniae* cytadherence-associated protein HMW2

by fusion with green fluorescent protein: implications for attachment organelle structure. *Mol Microbiol* **47**: 49-60.

Baseman, J.B., Cole, R.M., Krause, D.C., and Leith, D.K. (1982) Molecular basis for cytadsorption of *Mycoplasma pneumoniae*. *J Bacteriol* **151**: 1514-1522.

Baseman, J.B., Morrison-Plummer, J., Drouillard, D., Puleo-Scheppke, B., Tryon, V.V., and Holt, S.C. (1987) Identification of a 32-kilodalton protein of *Mycoplasma pneumoniae* associated with hemadsorption. *Isr J Med Sci* **23**: 474-479.

Baseman, J.B., and Tully, J.G. (1997) Mycoplasmas: sophisticated, reemerging, and burdened by their notoriety. *Emerg Infect Dis* **3**: 21-32.

Becci, P.J., McDowell, E.M., and Trump, B.F. (1978) The respiratory epithelium. II. Hamster trachea, bronchus, and bronchioles. *J Natl Cancer Inst* **61**: 551-561.

Biberfield, G., and Biberfield, P. (1970) Ultrastructural Features of *Mycoplasma pneumoniae*. *J Bacteriol* **102**: 855-861.

Boatman, E.S. (1979) Morphology and Ultrastructure of the *Mycoplasmatales*. In *The Mycoplasmas: Cell Biology*. Vol. 1. Barile, M.F. and Razin, S. (eds): Academic Press, pp. 63-102.

Boguslavsky, S., Menaker, D., Lysnyansky, I., Liu, T., Levisohn, S., Rosengarten, R., Garcia, M., and Yogev, D. (2000) Molecular characterization of the *Mycoplasma gallisepticum pvpA* gene which encodes a putative variable cytadhesin protein. *Infect Immun* **68**: 3956-3964.

Bredt, W. (1968) Motility and multiplication of *Mycoplasma pneumoniae*. A phase contrast study. *Pathol Microbiol* **32**: 321-326.

Bredt, W. (1979) Motility. In *The Mycoplasmas*. Vol. 1: Academic Press.

Brunner, H., Krauss, H., Schaar, H., and Schiefer, H.G. (1979) Electron microscopic studies on the attachment of *Mycoplasma pneumoniae* to guinea pig erythrocytes. *Infect Immun* **24**: 906-911.

Burchard, R.P. (1981) Gliding motility of prokaryotes: ultrastructure, physiology, and genetics. *Annu Rev Microbiol* **35**: 497-529.

CDC (2002) *Mycoplasma pneumoniae* disease information. Centers for Disease Control and Prevention.

Chalfie, M., Tu, Y., Euskirchen, G., Ward, W.W., and Prasher, D.C. (1994) Green fluorescent protein as a marker for gene expression. *Science* **263**: 802-805.

Chambaud, I., Heilig, R., Ferris, S., Barbe, V., Samson, D., Galisson, F., Moszer, I., Dybvig, K., Wroblewski, H., Viari, A., Rocha, E.P., and Blanchard, A. (2001) The complete genome sequence of the murine respiratory pathogen *Mycoplasma pulmonis*. *Nucleic Acids Res* **29**: 2145-2153.

Chandler, D.K., Grabowski, M.W., Rabson, A.S., and Barile, M.F. (1987) Further studies on the *Mycoplasma pneumoniae* extract: ciliostatic and cell recruitment activities. *Isr J Med Sci* **23**: 580-584.

Chanock, R.M., Hayflick, L., and Barile, M.F. (1962) Growth on artificial medium of an agent associated with atypical pneumonia and its identification as a PPLO. *Proc Natl Acad Sci U S A* **48**: 41-49.

Chanock, R.M., Dienes, L., Eaton, M.D., Edward, D.G., Freunt, E.A., Hayflick, L., Hers, J.F., Jensen, K.E., Liu, C., Marmion, B.P., Morton, H.E., Mufson, M.A., Smith, P.F., Somerson, N.L., and Taylor-Robinson, D. (1963) *Mycoplasma pneumoniae*:

Proposed Nomenclature for Atypical Pneumonia Organism (Eaton Agent). *Science* **140**: 662.

Cimolai, N., Taylor, G.P., Mah, D., and Morrison, B.J. (1992) Definition and application of a histopathological scoring scheme for an animal model of acute *Mycoplasma pneumoniae* pulmonary infection. *Microbiol Immunol* **36**: 465-478.

Collier, A.M., and Clyde, W.A. (1971) Relationships Between *Mycoplasma pneumoniae* and Human Respiratory Epithelium. *Infection and Immunity* **3**: 694-701.

Collier, A.M., Clyde, W.A., Jr., and Denny, F.W. (1971) *Mycoplasma pneumoniae* in hamster tracheal organ culture: immunofluorescent and electron microscopic studies. *Proc Soc Exp Biol Med* **136**: 569-573.

Collier, A.M., and Baseman, J.B. (1973) Organ Culture Techniques with Mycoplasmas. *Annals of the New York Academy of Sciences* **225**: 277-289.

Collier, A.M., and Clyde, W.A., Jr. (1974) Appearance of *Mycoplasma pneumoniae* in lungs of experimentally infected hamsters and sputum from patients with natural disease. *Am Rev Respir Dis* **110**: 765-773.

Dallo, S.F., Chavoya, A., and Baseman, J.B. (1990) Characterization of the gene for a 30-kilodalton adhesion-related protein of *Mycoplasma pneumoniae*. *Infect Immun* **58**: 4163-4165.

Dallo, S.F., Lazzell, A.L., Chavoya, A., Reddy, S.P., and Baseman, J.B. (1996) Biofunctional domains of the *Mycoplasma pneumoniae* P30 adhesin. *Infect Immun* **64**: 2595-2601.

Dallo, S.F., Kannan, T.R., Blaylock, M.W., and Baseman, J.B. (2002) Elongation factor Tu and E1 beta subunit of pyruvate dehydrogenase complex act as fibronectin binding proteins in *Mycoplasma pneumoniae*. *Mol Microbiol* **46**: 1041-1051.

Dhandayuthapani, S., Rasmussen, W.G., and Baseman, J.B. (1999) Disruption of gene *mg218* of *Mycoplasma genitalium* through homologous recombination leads to an adherence-deficient phenotype. *Proc Natl Acad Sci U S A* **96**: 5227-5232.

Dhandayuthapani, S., Blaylock, M.W., Bebear, C.M., Rasmussen, W.G., and Baseman, J.B. (2001) Peptide methionine sulfoxide reductase (MsrA) is a virulence determinant in *Mycoplasma genitalium*. *J Bacteriol* **183**: 5645-5650.

Dirksen, L.B., Proft, T., Hilbert, H., Plagens, H., Herrmann, R., and Krause, D.C. (1996) Sequence analysis and characterization of the *hmw* gene cluster of *Mycoplasma pneumoniae*. *Gene* **171**: 19-25.

Dykstra, M.J., Levisohn, S., Fletcher, O.J., and Kleven, S.H. (1985) Evaluation of cytopathologic changes induced in chicken tracheal epithelium by *Mycoplasma gallisepticum in vivo* and *in vitro*. *Am J Vet Res* **46**: 116-122.

Feldner, J., Gobel, U., and Bredt, W. (1982) *Mycoplasma pneumoniae* adhesin localized to tip structure by monoclonal antibody. *Nature* **298**: 765-767.

Fisseha, M., Gohlmann, H.W., Herrmann, R., and Krause, D.C. (1999) Identification and complementation of frameshift mutations associated with loss of cytadherence in *Mycoplasma pneumoniae*. *J Bacteriol* **181**: 4404-4410.

Foy, H.M. (1999) *Mycoplasma pneumoniae* pneumonia: current perspectives. *Clin Infect Dis* **28**: 237.

Fraser, C.M., Gocayne, J.D., White, O., Adams, M.D., Clayton, R.A., Fleischmann, R.D., Bult, C.J., Kerlavage, A.R., Sutton, G., Kelley, J.M., and et al. (1995) The minimal gene complement of *Mycoplasma genitalium*. *Science* **270**: 397-403.

Furness, G. (1970) The growth and morphology of Mycoplasmas replicating in synchrony. *J Infect Dis* **122**: 146-158.

Gabridge, M.G., and Polisky, R.B. (1977) Intracellular levels of adenosine triphosphate in hamster trachea organ cultures exposed to *Mycoplasma pneumoniae* cells or membranes. *In Vitro* **13**: 510-516.

Gabridge, M.G., and Stahl, Y.D. (1978) Role of adenine in pathogenesis of *Mycoplasma pneumoniae* infections of tracheal epithelium. *Med Microbiol Immunol (Berl)* **165**: 43-55.

Gabridge, M.G. (1979) Hamster tracheal organ cultures as models for infection and toxicology studies. *Prog Exp Tumor Res* **24**: 85-95.

Gabridge, M.G. (1983) Attachment of *Mycoplasma pneumoniae* to tracheal monolayer outgrowths. *Yale J Biol Med* **56**: 657-663.

Gabridge, M.G. (1986) Differentiated Respiratory Epithelium as an *In Vitro* Model for Mycoplasma Infections. In *In Viro Models of Respiratory Epithelium*. Schiff, L.J. (ed). Boca Raton: CRC Press, Inc., pp. 85-102.

Gerstenecker, B., and Jacobs, E. (1990) Topological mapping of the P1-adhesin of *Mycoplasma pneumoniae* with adherence-inhibiting antibodies. *Journal of General Microbiology* **136**: 471-476.

Glass, J.I., Lefkowitz, E.J., Glass, J.S., Heiner, C.R., Chen, E.Y., and Cassell, G.H. (2000) The complete sequence of the mucosal pathogen *Ureaplasma urealyticum*. *Nature* **407**: 757-762.

Gobel, U., Speth, V., and Bredt, W. (1981) Filamentous structures in adherent *Mycoplasma pneumoniae* cells treated with nonionic detergents. *J Cell Biol* **91**: 537-543.

Haas, J., Park, E.C., and Seed, B. (1996) Codon usage limitation in the expression of HIV-1 envelope glycoprotein. *Curr Biol* **6**: 315-324.

Hahn, T.W., Willby, M.J., and Krause, D.C. (1998) HMW1 is required for cytadhesin P1 trafficking to the attachment organelle in *Mycoplasma pneumoniae*. *J Bacteriol* **180**: 1270-1276.

Hahn, T.W., Mothershed, E.A., Waldo, R.H., 3rd, and Krause, D.C. (1999) Construction and analysis of a modified Tn*4001* conferring chloramphenicol resistance in *Mycoplasma pneumoniae*. *Plasmid* **41**: 120-124.

Hayflick, L. (1965) Tissue cultures and mycoplasmas. *Tex Rep Biol Med* **23**.

Hedreyda, C.T., Lee, K.K., and Krause, D.C. (1993) Transformation of *Mycoplasma pneumoniae* with Tn*4001* by electroporation. *Plasmid* **30**: 170-175.

Hegermann, J., Herrmann, R., and Mayer, F. (2002) Cytoskeletal elements in the bacterium *Mycoplasma pneumoniae*. *Naturwissenschaften* **89**: 453-458.

Himmelreich, R., Hilbert, H., Plagens, H., Pirkl, E., Li, B.C., and Herrmann, R. (1996) Complete sequence analysis of the genome of the bacterium *Mycoplasma pneumoniae*. *Nucleic Acids Res* **24**: 4420-4449.

Hnatow, L.L., Keeler, C.L., Jr., Tessmer, L.L., Czymmek, K., and Dohms, J.E. (1998) Characterization of MGC2, a *Mycoplasma gallisepticum* cytadhesin with homology to the Mycoplasma pneumoniae 30-kilodalton protein P30 and *Mycoplasma genitalium* P32. *Infect Immun* **66**: 3436-3442.

Hu, P.C., Collier, A.M., and Baseman, J.B. (1976) Interaction of virulent *Mycoplasma pneumoniae* with hamster tracheal organ cultures. *Infect Immun* **14**: 217-224.

Hu, P.C., Collier, A.M., and Baseman, J.B. (1977) Surface parasitism by *Mycoplasma pneumoniae* of respiratory epithelium. *J Exp Med* **145**: 1328-1343.

Hu, P.C., Cole, R.M., Huang, Y.S., Graham, J.A., Gardner, D.E., Collier, A.M., and Clyde, W.A., Jr. (1982) *Mycoplasma pneumoniae* infection: role of a surface protein in the attachment organelle. *Science* **216**: 313-315.

Jacob, C., Nouzieres, F., Duret, S., Bove, J.M., and Renaudin, J. (1997) Isolation, characterization, and complementation of a motility mutant of *Spiroplasma citri*. *J Bacteriol* **179**: 4802-4810.

Jacobs, E., Bartl, A., Oberle, K., and Schiltz, E. (1995) Molecular mimicry by *Mycoplasma pneumoniae* to evade the induction of adherence inhibiting antibodies. *J Med Microbiol* **43**: 422-429.

Jordan, J.L., Berry, K.M., Balish, M.F., and Krause, D.C. (2001) Stability and subcellular localization of cytadherence-associated protein P65 in *Mycoplasma pneumoniae*. *J Bacteriol* **183**: 7387-7391.

Kahane, I., Tucker, S., Leith, D.K., Morrison-Plummer, J., and Baseman, J.B. (1985) Detection of the major adhesin P1 in triton shells of virulent *Mycoplasma pneumoniae*. *Infect Immun* **50**: 944-946.

Kannan, T.R., and Baseman, J.B. (2000) Expression of UGA-containing Mycoplasma genes in *Bacillus subtilis*. *J Bacteriol* **182**: 2664-2667.

Kempf, M.J., and McBride, M.J. (2000) Transposon insertions in the *Flavobacterium johnsoniae ftsX* gene disrupt gliding motility and cell division. *J Bacteriol* **182**: 1671-1679.

Kirchhoff, H., Rosengarten, R., Lotz, W., Fischer, M., and Lopatta, D. (1984) Flask-shaped mycoplasmas: properties and pathogenicity for man and animals. *Isr J Med Sci* **20**: 848-853.

Kirchhoff, H. (1992) Motility. In *Mycoplasmas- Molecular Biology and Pathogenesis*. J. Maniloff, R.N.M., L. R. Finch & J. B. Baseman. (ed). Washington, D.C.: American Society for Microbiology, pp. 289-306.

Krause, D.C., Leith, D.K., Wilson, R.M., and Baseman, J.B. (1982) Identification of *Mycoplasma pneumoniae* proteins associated with hemadsorption and virulence. *Infect Immun* **35**: 809-817.

Krause, D.C., and Baseman, J.B. (1983) Inhibition of *Mycoplasma pneumoniae* hemadsorption and adherence to respiratory epithelium by antibodies to a membrane protein. *Infect Immun* **39**: 1180-1186.

Krause, D.C., and Taylor-Robinson, D. (1992) Mycoplasmas Which Infect Humans. In *In Mycoplasmas- Molecular Biology and Pathogenesis*. J. Maniloff, R.N.M., L. R. Finch & J. B. Baseman. (ed). Washington, D.C.: American Society for Microbiology, pp. 417-444.

Krause, D.C., Proft, T., Hedreyda, C.T., Hilbert, H., Plagens, H., and Herrmann, R. (1997) Transposon mutagenesis reinforces the correlation between *Mycoplasma*

pneumoniae cytoskeletal protein HMW2 and cytadherence. *J Bacteriol* **179**: 2668-2677.

Krause, D.C. (1998) *Mycoplasma pneumoniae* cytadherence: organization and assembly of the attachment organelle. *Trends Microbiol* **6**: 15-18.

Krause, D.C., and Balish, M.F. (2001) Structure, function, and assembly of the terminal organelle of *Mycoplasma pneumoniae*. *FEMS Microbiol Lett* **198**: 1-7.

Kusunoki, S., Shiina, M., and Kanazawa, I. (2001) Anti-Gal-C antibodies in GBS subsequent to mycoplasma infection: Evidence of molecular mimicry. *Neurology* **57**: 736-738.

Labarere, J. (1992) DNA Replication and Repair. In *In Mycoplasmas- Molecular Biology and Pathogenesis*. J. Maniloff, R.N.M., L. R. Finch & J. B. Baseman. (ed). Washington, D.C.: American Society for Microbiology, pp. 309-323.

Laemmli, U.K. (1970) Cleavage of structural proteins during the assembly of the head of bacteriophage T4. *Nature* **227**: 680-685.

Layh-Schmitt, G., and Herrmann, R. (1992) Localization and biochemical characterization of the ORF6 gene product of the *Mycoplasma pneumoniae* P1 operon. *Infect Immun* **60**: 2906-2913.

Layh-Schmitt, G., and Herrmann, R. (1994) Spatial arrangement of gene products of the P1 operon in the membrane of *Mycoplasma pneumoniae*. *Infect Immun* **62**: 974-979.

Layh-Schmitt, G., Hilbert, H., and Pirkl, E. (1995) A spontaneous hemadsorption-negative mutant of *Mycoplasma pneumoniae* exhibits a truncated adhesin-related

30-kilodalton protein and lacks the cytadherence-accessory protein HMW1. *J Bacteriol* **177**: 843-846.

Layh-Schmitt, G., Himmelreich, R., and Leibfried, U. (1997) The adhesin related 30-kDa protein of *Mycoplasma pneumoniae* exhibits size and antigen variability. *FEMS Microbiol Lett* **152**: 101-108.

Layh-Schmitt, G., and Harkenthal, M. (1999) The 40- and 90-kDa membrane proteins (ORF6 gene product) of *Mycoplasma pneumoniae* are responsible for the tip structure formation and P1 (adhesin) association with the Triton shell. *FEMS Microbiol Lett* **174**: 143-149.

Lipman, R.P., and Clyde, W.A., Jr. (1969) The interrelationship of virulence, cytadsorption, and peroxide formation in *Mycoplasma pneumoniae*. *Proc Soc Exp Biol Med* **131**: 1163-1167.

Loveless, R.W., Griffiths, S., Fryer, P.R., Blauth, C., and Feizi, T. (1992) Immunoelectron Microscopic Studies Reveal Differences in Distribution of Sialo-Oligosaccharide Receptors for *Mycoplasma pneumoniae* on the Epithelium of Human and Hamster Bronchi. *Infection and Immunity* **60**: 4015-4023.

Luby, J.P. (1991) Pneumonia Caused by *Mycoplasma pneumoniae* Infection. In *Clinics in Chest Medicine: Atypical Pneumonia Syndromes*. Vol. 12(2). Winterbauer, R.H. (ed). Philadelphia: W.B. Saunders Company, pp. 237-244.

Maniloff, J., and Quinlan, D.C. (1974) Partial Purification of a Membrane-Associated Deoxyribonucleic Acid Complex from *Mycoplasma gallisepticum*. *J Bacteriol* **120**: 495-501.

Maniloff, J. (2002) Phylogeny and Evolution. In *Molecular Biology and Pathogenicity of Mycoplasmas*. Razin, S. and Herrmann, R. (eds). New York: Kluwer Academic/Plenum, pp. 31-43.

Margolin, W. (2000) Green fluorescent protein as a reporter for macromolecular localization in bacterial cells. *Methods* **20**: 62-72.

McBride, M.J. (2001) BACTERIAL GLIDING MOTILITY: Multiple Mechanisms for Cell Movement over Surfaces. *Annu Rev Microbiol* **55**: 49-75.

Meng, K.E., and Pfister, R.M. (1980) Intracellular structures of *Mycoplasma pneumoniae* revealed after membrane removal. *J Bacteriol* **144**: 390-399.

Miyata, M., Yamamoto, H., Shimizu, T., Uenoyama, A., Citti, C., and Rosengarten, R. (2000) Gliding mutants of *Mycoplasma mobile*: relationships between motility and cell morphology, cell adhesion and microcolony formation. *Microbiology* **146**: 1311-1320.

Miyata, M. (2002) Cell Division. In *Molecular Biology and Pathogenicity of Mycoplasmas*. Razin, S. and Herrmann, R. (eds). New York, Boston, Dordrecht, London, Moscow: Kluwer Acedemic/Plenum Publishers, pp. 117-130.

Miyata, M., Ryu, W.S., and Berg, H.C. (2002) Force and Velocity of *Mycoplasma mobile* Gliding. *J Bacteriol* **184**: 1827-1831.

Muse, K.E., Powell, D.A., and Collier, A.M. (1976) *Mycoplasma pneumoniae* in hamster tracheal organ culture studied by scanning electron microscopy. *Infect Immun* **13**: 229-237.

Muto, A., and Ushida, C. (2002) Transcription and Translation. In *Molecular Biology and Pathogenicity of Mycoplasmas*. Razin, S. and Herrmann, R. (eds). New York: Kluwer Academic / Plenum Publishers, pp. 323-345.

Noormohammadi, A.H., Markham, P.F., Whithear, K.G., Walker, I.D., Gurevich, V.A., Ley, D.H., and Browning, G.F. (1997) *Mycoplasma synoviae* has two distinct phase-variable major membrane antigens, one of which is a putative hemagglutinin. *Infect Immun* **65**: 2542-2547.

Ogle, K.F., Lee, K.K., and Krause, D.C. (1992) Nucleotide sequence analysis reveals novel features of the phase-variable cytadherence accessory protein HMW3 of *Mycoplasma pneumoniae*. *Infect Immun* **60**: 1633-1641.

Popham, P.L., Hahn, T.W., Krebes, K.A., and Krause, D.C. (1997) Loss of HMW1 and HMW3 in noncytadhering mutants of *Mycoplasma pneumoniae* occurs post-translationally. *Proc Natl Acad Sci U S A* **94**: 13979-13984.

Powell, D.A., Hu, P.C., Wilson, M., Collier, A.M., and Baseman, J.B. (1976) Attachment of *Mycoplasma pneumoniae* to respiratory epithelium. *Infect Immun* **13**: 959-966.

Proft, T., and Herrmann, R. (1994) Identification and characterization of hitherto unknown *Mycoplasma pneumoniae* proteins. *Mol Microbiol* **13**: 337-348.

Proft, T., Hilbert, H., Layh-Schmitt, G., and Herrmann, R. (1995) The proline-rich P65 protein of *Mycoplasma pneumoniae* is a component of the Triton X-100-insoluble fraction and exhibits size polymorphism in the strains M129 and FH. *J Bacteriol* **177**: 3370-3378.

Proft, T., Hilbert, H., Plagens, H., and Herrmann, R. (1996) The P200 protein of *Mycoplasma pneumoniae* shows common features with the cytadherence-associated proteins HMW1 and HMW3. *Gene* **171**: 79-82.

Radestock, U., and Bredt, W. (1977) Motility of *Mycoplasma pneumoniae*. *J Bacteriol* **129**: 1495-1501.

Razin, S., and Jacobs, E. (1992) Mycoplasma adhesion. *J Gen Microbiol* **138**: 407-422.

Razin, S., Yogev, D., and Naot, Y. (1998) Molecular biology and pathogenicity of mycoplasmas. *Microbiol Mol Biol Rev* **62**: 1094-1156.

Reddy, S.P., Rasmussen, W.G., and Baseman, J.B. (1995) Molecular cloning and characterization of an adherence-related operon of *Mycoplasma genitalium*. *J Bacteriol* **177**: 5943-5951.

Regula, J.T., Ueberle, B., Boguth, G., Gorg, A., Schnolzer, M., Herrmann, R., and Frank, R. (2000) Towards a two-dimensional proteome map of *Mycoplasma pneumoniae*. *Electrophoresis* **21**: 3765-3780.

Regula, J.T., Boguth, G., Gorg, A., Hegermann, J., Mayer, F., Frank, R., and Herrmann, R. (2001) Defining the mycoplasma 'cytoskeleton': the protein composition of the Triton X-100 insoluble fraction of the bacterium *Mycoplasma pneumoniae* determined by 2-D gel electrophoresis and mass spectrometry. *Microbiology* **147**: 1045-1057.

Renaudin, J. (2002) Extrachromosomal Elements and Gene Transfer. In *Molecular Biology and Pathogenicity of Mycoplasmas*. Razin, S. and Herrmann, R. (eds). New York: Kluwer Academic / Plenum Publishers, pp. 347-370.

Rhodin, J.A.G. (1966) The Ciliated Cell: Ultrastructure and Function of the Human Tracheal Mucosa. *The American Review of Respiratory Diseases* **93**: 1-15.

Ricci, A.M., and University of Georgia. (1999) Use of recombinant green fluorescent protein in *Mycoplasma pneumoniae*. pp. ix, 107 leaves.

Romero-Arroyo, C.E., Jordan, J., Peacock, S.J., Willby, M.J., Farmer, M.A., and Krause, D.C. (1999) *Mycoplasma pneumoniae* protein P30 is required for cytadherence and associated with proper cell development. *J Bacteriol* **181**: 1079-1087.

Rosengarten, R., and Kirchhoff, H. (1987) Gliding motility of *Mycoplasma* sp. nov. strain 163K. *J Bacteriol* **169**: 1891-1898.

Rosengarten, R., and Kirchhoff, H. (1988) Energetic Aspects of the Gliding Motility of Mycoplasmas. *Current Microbiology* **16**: 247-252.

Sasaki, Y., Ishikawa, J., Yamashita, A., Oshima, K., Kenri, T., Furuya, K., Yoshino, C., Horino, A., Shiba, T., Sasaki, T., and Hattori, M. (2002) The complete genomic sequence of *Mycoplasma penetrans*, an intracellular bacterial pathogen in humans. *Nucleic Acids Res* **30**: 5293-5300.

Seto, S., Layh-Schmitt, G., Kenri, T., and Miyata, M. (2001) Visualization of the attachment organelle and cytadherence proteins of *Mycoplasma pneumoniae* by immunofluorescence microscopy. *J Bacteriol* **183**: 1621-1630.

Seto, S., and Miyata, M. (2003) Attachment Organelle Formation Represented by Localization of Cytadherence Proteins and Formation of the Electron-Dense Core in Wild-Type and Mutant Strains of *Mycoplasma pneumoniae*. *J Bacteriol* **185**: 1082-1091.

Shimizu, T., and Miyata, M. (2002) Electron Microscopic Studies of Three Gliding Mycoplamas, *Mycoplasma mobile*, *M. pneumoniae*, and *M. gallisepticum*, by using the Freeze-Substitution Technique. *Current Microbiology* **44**: 431-434.

Sleigh, M.A. (1981) Ciliary function in mucus transport. *Chest* **80**: 791-795.

Smith, P.F. (1967) The physiology of mycoplasma. In *Mycoplasma and bacterial L-forms*. Panos, C. (ed). New York: World Publishing Company.

Sobeslavsky, O., Prescott, B., and Chanock, R. (1968) Adsorption of *Mycoplasma pneumoniae* to neuraminic acid receptors of various cells and possible role in virulence. *J Bacteriol* **96**: 695-705.

Stevens, M.K., and Krause, D.C. (1991) Localization of the *Mycoplasma pneumoniae* cytadherence-accessory proteins HMW1 and HMW4 in the cytoskeletonlike Triton shell. *J Bacteriol* **173**: 1041-1050.

Stevens, M.K., and Krause, D.C. (1992) *Mycoplasma pneumoniae* cytadherence phase-variable protein HMW3 is a component of the attachment organelle. *J Bacteriol* **174**: 4265-4274.

Su, C.J., Chavoya, A., and Baseman, J.B. (1989) Spontaneous mutation results in loss of the cytadhesin (P1) of *Mycoplasma pneumoniae*. *Infect Immun* **57**: 3237-3239.

Sullivan, K.F., and Kay, S.A. (1998) *Green fluorescent proteins.* San Diego, Calif.; London: Academic Press.

Taylor-Robinson, D., and Bredt, W. (1983) Motility of *Mycoplasma* strain G37. *Yale Journal of Biological Medicine* **56**: 910.

Towbin, H., Staehelin, T., and Gordon, J. (1979) Electrophoretic transfer of proteins from polyacrylamide gels to nitrocellulose sheets: procedure and some applications. *Proc Natl Acad Sci U S A* **76**: 4350-4354.

Waldo, R.H., 3rd, Popham, P.L., Romero-Arroyo, C.E., Mothershed, E.A., Lee, K.K., and Krause, D.C. (1999) Transcriptional analysis of the *hmw* gene cluster of *Mycoplasma pneumoniae*. *J Bacteriol* **181**: 4978-4985.

Waldo, R.H., 3rd, Balish, M.F., Willby, M.J., Ross, S.M., and Krause, D.C. (2002) Triton X-100-Insolubility Determinants in Cytadherence-Associated Proteins of *Mycoplasma pneumoniae*. In *14th International Congress of the International Organization for Mycoplasmology (IOM)* Vienna, Austria, pp. 69.

Willby, M.J., and Krause, D.C. (2002) Characterization of a *Mycoplasma pneumoniae hmw3* mutant: implications for attachment organelle assembly. *J Bacteriol* **184**: 3061-3068.

Yayoshi, M. (1983) Association between *Mycoplasma pneumoniae* hemolysis, attachment, and pulmonary pathogenicity. *Yale J Biol Med* **56**: 685-689.